UNIVERSIDADE D
COIMBRA

Daniela Filipa de Figueiredo Marques Metello

MODELING, SIMULATION AND EXPERIMENTAL VALIDATION OF A PVDF-BASED ELECTROACTIVE ACTUATOR

Dissertação no âmbito do Mestrado Integrado em Engenharia Biomédica – especialização em Instrumentação Biomédica orientada pela Professora Doutora Ana Paula Bettencourt Martins Amaro e pela Professora Doutora Raffaella Carloni e apresentada à Faculdade de Ciências e Tecnologia da Universidade de Coimbra no Departamento de Engenharia Mecânica

Outubro de 2020

1 2 9 0

FACULDADE DE CIÊNCIAS E TECNOLOGIA
UNIVERSIDADE D COIMBRA

Modeling, Simulation and Experimental Validation of a PVDF-based Electroactive Actuator

Dissertation to obtain the Master Degree in Biomedical Engineering – specialization in Biomedical Instrumentation

Author

Daniela Filipa de Figueiredo Marques Metello

Advisors

Professora Doutora Ana Paula Bettencourt Martins Amaro

Professora Doutora Raffaella Carloni

Jury

President	**Professor Maria Augusta Neto** **Assistant Professor at the University of Coimbra**
Vowel(s)	**Professor Fernando Jorge Ventura Antunes** **Assistant Professor at the University of Coimbra**
	PhD. Riccardo D'Anniballe **Researcher at the University of Groningen**
Advisor	**Professor Raffaella Carloni** **Associate Professor at the University of Groningen**

Institutional Collaboration

university of groningen
faculty of science and engineering

Robotics Laboratory – Faculty of Science and Engineering, University of Groningen - RUG

Coimbra, October, 2020

"Life will knock you down, but it is your choice whether or not you get back up."
Mr. Han, Karate Kid

"Never forget why you started. Motivation comes from working on things we care about."
Sheryl Sandberg

Acknowledgments

Este trabalho representa não só o culminar de 5 anos de trabalho árduo, mas é também o resultado de um crescimento de 23 anos. Dessa forma quero agradecer a todos os que contribuiram para o meu crescimento pessoal e profissional, sem eles, não seria a pessoa que sou hoje.

Embora já não seja parte ativa da minha vida, quero agradecer a todos os meus treinadores de natação, os meus "segundos pais", que me viram crescer, me acompanharam, aconselharam e moldaram, a eles devo o meu carácter, integridade, resiliência e organização... Cortesão, Marques, Tsukagoshi e Fausto, a minha gratidão é eterna.

A título profissional, um enorme obrigado à professora Amaro, por aceitar o desafio, por enfrentar comigo todos os obstáculos e me mostrar que há sempre uma solução. O seu profissionalismo e dedicação são incomparáveis, a professora é, e será, para mim, uma fonte de inspiração e motivação. In English, with the importance it deserves, I would also like to express my deepest appreciation for professor Carloni for kindly accepting me in her project, and to Riccardo for making me feel welcomed from the very start, being an anchor throughout the pandemic, always present, and going beyond everything to make this project come to light.

Ao BEST, por me mostrar que somos capazes de tudo o que quisermos, que a recompensa é tanto maior quanto mais trabalhamos, e que essa recompensa extende-se em experiências inimagináveis e sensações inexplicáveis. Ao Bilboard Baggins, por me dar o maior desafio da minha vida estudantil, e o quinteto mais improvável e o mais divertido... Farinha, Faria, Beja e Louro, não o desejaria de outra forma. A ti José Teodoro, por estares sempre presente, por me fazeres rir e chorar e por seres um amigo que levo para vida, espero retribuir tudo o que fizeste por mim.

À minha família adotada, os Lokos, por todas as aventuras que já vivemos e ainda vamos viver e às Babes Lokas, por serem a surpresa mais agradável, pelo vosso apoio e amizade, seguimos juntas.

Um agradecimento a quem tornou tudo isto possível, a minha família, ao meu irmão, aos meus tios e aos meus avós. Em especial aos meus pais, por moverem mundos e fundos para que conseguisse viver todos os meus sonhos, por serem os meus maiores fãs e por estarem sempre presentes, na mesma casa ou a milhares de kilómetros de distância. Espero no futuro ser como vocês, e conseguir transmitir todos os valores que me transmitiram a mim.

Por último, mas não menos importante, ao meu namorado, António "Mike" Louro, por seres o meu porto de abrigo, por me entenderes melhor que ninguém, por me fazeres viver a vida ao máximo, por acreditares em mim mesmo quando eu não acredito, por me inspirares a fazer sempre mais e melhor e por seres o meu melhor amigo. O futuro é nosso!

Resumo

Nos últimos 20 anos, os polímeros electroactivos (EAPs) têm recebido mais atenção no mundo dos mecanismos de actuação. O termo "electroactivo" significa que o polímero é electricamente activo ou reactivo, ou seja, que terá uma resposta mecânica a um estímulo eléctrico. Como qualquer polímero, este é conhecido por ser leve e fácil de processar. Para além disso, os EAPs são resistentes e capazes de produzir grandes tensões de actuação, quando comparados com actuadores convencionais. Portanto, a sua importância está a aumentar em várias aplicações, nomeadamente biomédicas, tais como instrumentos médicos, implantes biónicos, próteses e "músculos artificiais". Os EAPs dividem-se em iónicos e electrónicos, sendo a principal diferença o transporte físico: os EAPs iónicos utilizam cargas iónicas, enquanto os EAPs electrónicos utilizam cargas eléctricas. O P(VDF-TrFE-CTFE) é um polímero *ferrorelaxor* pertencente aos EAPs electrónicos e é considerado um material promissor pela sua elevada constante dieléctrica (≈ 50), bem como pela elevada resposta electromecânica e densidade de energia elástica.

Neste trabalho, três actuadores (cinco camadas) foram caracterizados electromecanicamente para estudar a influência de dois parâmetros geométricos: a espessura da camada do P(VDF-TrFE-CTFE), e a largura total do actuador. A defleção, a força de bloqueio e a rigidez à flexão de cada actuador foram obtidas através de testes mecânicos sob três valores de campo eléctrico. Subsequentemente, foi executada uma análise MEF em COMSOL Multiphysics®. Realizou-se um estudo estacionário de cada actuador para avaliar o comportamento electromecânico sob três valores de campo eléctrico. A defleção em cada simulação foi comparada com os testes experimentais.

A partir dos resultados dos testes, concluiu-se que a largura não influencia o desempenho do actuador. Além disso, um aumento da espessura do P(VDF-TrFE-CTFE) provocou um aumento da defleção, força de bloqueio e rigidez de flexão. Mais ainda, a simulação foi validada, pois o comportamento observado revelou-se semelhante nos testes experimentais, ou seja, a defleção aumentava linearmente com o aumento do campo eléctrico aplicado.

Finalmente, comparando os três actuadores com outras tecnologias electroactivas, é possível afirmar que as defleções observadas são mais elevadas, mas a força de bloqueio exercida por estes actuadores é significativamente inferior a outras tecnologias de actuação já estabelecidas.

Palavras Chave: Polímero Electroactivo, Músculos Artificiais, Atuadores, Biomateriais, P(VDF-TrFE-CTFE), COMSOL Multiphysics

Abstract

In the last 20 years, Electroactive Polymers (EAPs) have gained attention in the world of actuation mechanisms. *"Electroactive"* means that the polymer is electrically active or responsive, i.e. that it will have a mechanical response to an electric stimulus. As any polymer, they are known for being lightweight and easy to process. Adding to this, EAPs are resilient and able to produce large actuation strains, when compared to conventional actuators. Therefore, their importance is increasing in several applications, namely biomedical applications such as surgery-assisting tools, bionic implants, prosthetics and "artificial muscles". EAPs are divided into ionic and electronic, with the major different being the physic transport: ionic EAPs use ionic charges, while electronic EAPs use electric charges. P(VDF-TrFE-CTFE) is a ferrorelaxor polymer that belongs to electronic EAPs and it is considered one of the most promising materials for its high dielectric constant (≈ 50), as well as its high electromechanical response and elastic energy density.

In this work, three cantilever-like multilayered actuators (five layers) were electromechanically characterized to study the influence of two geometry parameters: the thickness of the active layer, P(VDF-TrFE-CTFE), and the total width of the actuator. The tip displacement, blocking force and bending stiffness of each actuator were obtained through mechanical testing under three values of electric field. Subsequently, a FEM analysis was executed on COMSOL Multiphysics®. A stationary study was performed for each actuator, to evaluate the electromechanical behavior under the three values of electric field. The tip displacement in each simulation was also obtained and compared with the experimental tests.

From the tests' results, it was concluded that the width of the actuator does not play a major influence in the performance of the actuator. Moreover, an increase in the thickness of the active layer translated in an increase of the tip displacement, blocking force and bending stiffness. On the other hand, the simulation was validated as the tip displacement increased linearly with the electric field, which was a behavior already observed in the experimental tests.

Finally, comparing these three actuators with other electroactive technologies, it is possible to state the displacements observed are higher, but the blocking force exerted by these actuators is significantly lower than other existing actuation technologies.

Keywords: Electroactive Polymer, Artificial Muscles, Soft Actuator, Biomaterials, P(VDF-TrFE-CTFE), COMSOL Multiphysics

Contents

List of Figures

List of Tables

List of Acronyms

3D 3-dimensional

ABS Acrylonitrile Butadiene Styrene

AgNW Silver Nanowires

AlN Aluminum Nitride

DEAs Dielectric Elastomer Actuators

EAPs Electroactive Polymers

EPAM Electroactive Polymer Artificial Muscles

FIB Focused Ion Beam

IPMCs Ionic Polymer Metal Composites

JPL Jet Propulsion Lab

MEMS Microelectromechanical Systems

MIS Minimally Invasive Surgery

Mo Molybdenum

Ppy Polypyrrole

PVDF Polyvinylidene Difluoride

P(VDF-TrFE) Poli(vinylidene fluoride-co-trifluoroethylene

P(VDF-TrFE-CTFE) Poli(vinylidene-fluoride-trifluoroethylene-chlorotrifluoroethylene)

RMIC Reconfigurable MRI Surface-Imaging Coil

1 Introduction

Mankind and its incessant desire for more has led to great accomplishments that allowed, among other aspects, to improve the general quality of life of human beings. Not that long ago, what today we consider ordinary and granted, was deemed impossible. In all fairness, the majority, if not all, of these developments came to be out of necessity, especially, the ones concerning our human body. This premise gave room to an evolution of Healthcare, with a constant defiance of the human boundaries.

For decades now, artificial muscles are seen as the utopia of motion-generating devices, however, considerable progress has been made by research groups all around the world.

For this, EAPs seem to have the most relevant position in the fabrication of such mechanisms, earning, over the last decades, a privileged spot when talking about "artificial muscles". EAPs are essentially recognized for their reaction to an electric stimulation, altering their size or shape, enabling them to mimic biological muscles (1). Generally, EAPs can be divided in two big types, ionic EAPs and electronic EAPs, by their physical behavior, and each one is comprised by a group of EAPs that are different themselves, therefore as suitable for different applications.

Because of their biocompatibility, easy processability in various sizes, compliance and, in most cases, low energy consumption, several mechanisms have been built with EAPs. Examples range from a 4-finger gripper similar to a miniature robotic arm, developed at the Jet Propulsion Lab (JPL) (Figure 1.1) to new Microelectromechanical Systems (MEMS) devices, consumer electronics or haptics, but the most relevant applications in this case, are in biomedical devices and robotics.

Usage of EAPs as soft actuators for the development of new biomedical applications resulted in active medical tools like catheters, endoscopes, micro-pumps or micro-chips for analysis. Moreover, the incorporation of EAP soft actuators, once again due to the similar actuation mechanism to the human muscle, can originate a whole new generation of biologically inspired soft robots, giving room for safe interactions with

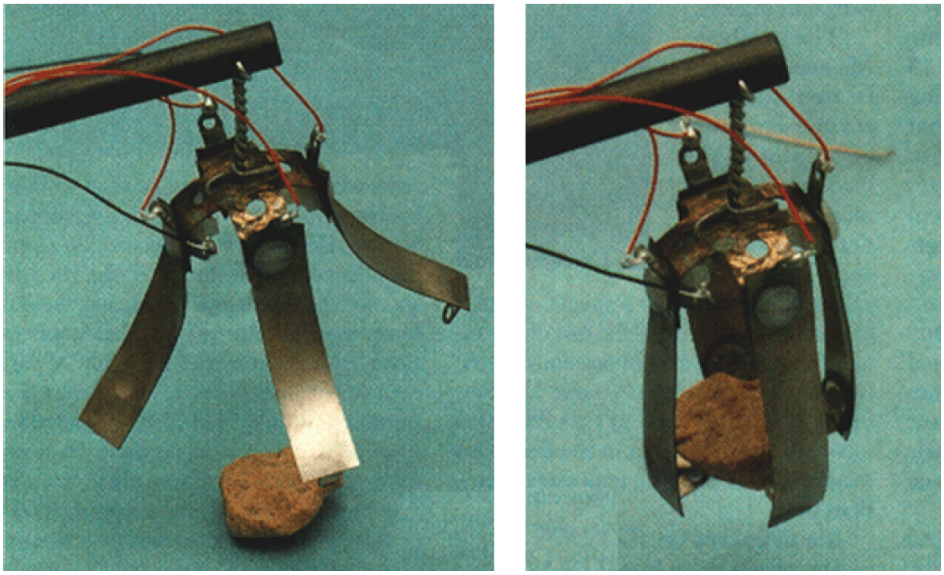

Figure 1.1: 4-finger EAP gripper lifting a rock. Retrieved from:(2).

humans and adaptability (3). Soft wearable robotics or exoskeletons for daily use or rehabilitation are some examples (4; 5). More detailed examples of each application will be given in Chapter 2 of this dissertation.

There is no discussion that the biological muscle is essential in fulfilling basic actions of the human body whether they are conscious, like walking or grabbing something, or unconsciously, such as breathing or allowing our heart to beat. Therefore, muscle can be viewed as an optimized system and its infinite capabilities make it a desirable tissue to replicate for medical reasons (6). The successful development of a muscle-like technology would amount to great benefits, from muscle-repair or assistance, to medical implants and more compliant tools for minimally invasive surgeries or diagnostics (7).

The biological muscle has been studied for long and considerable effort has been made to fully comprehend it. Not every biological muscle is the same, with their composition and organization varying according to the specific function they appear to be designed for (8), however, their properties can be summarized, as in Table 1.1.

Although its characteristics and properties are surpassed by artificial actuators, such as strain, stress, or work density, it is the design itself that becomes difficult to emulate. Some of these features are: the graded control of fibers activated in a movement, optimizing the efficiency of the action; and the ability to constantly convert chemical energy into mechanical work, allowing it to provide endless fuel energy density that is two orders of magnitude greater than that of batteries (7).

Table 1.1: Mammalian Skeletal Muscle properties. Adapted from: (7).

Property	Typical	Maximum
Strain (%)	20	>40
Stress (MPa)	0.1 (sustainable)	0.35
Work Density (kJ m^{-3})	8	40
Density (kg m^{-3})	1037	-
Strain Rate (% s^{-3})	-	>50
Specific Power (W kg^{-1})	50	284
Efficiency (%)	-	50
Cycle Life	-	$>10^9$
Modulus (MPa)	10 - 60	-

The assessment of the physical, mechanical and electrical properties of an actuator, is of major importance. Moreover, in the same way soft EAP actuators seem to be best suited for "artificial muscles", a type of material can be a better match than others, due to its properties.

Since the muscle is stimulated through an electric pulse that runs through it and it is mechanically translated into a contraction or strain of the muscle, the chosen material will have to possess that characteristic as well.

While a detailed explanation will be given in Chapter 2, the Poli(vinylidene-fluoride-trifluoroethylene-chlorotrifluoroethylene) (P(VDF-TrFE-CTFE)) terpolymer, a relaxor ferroelectric polymer from the electronic EAPs family, was chosen to integrate a soft EAP actuator. The actuation properties under an electric potential and the relevant values of strain of Polyvinylidene Difluoride (PVDF) have gained the attention of the scientific community (8), which led to the development of a copolymer and, consequently, a terpolymer, with the intent of improving even further, the electromechanical properties that made this material interesting in the first place.

The assessment of an actuator can be done with the experimental evaluation, which is the classical approach in the laboratory. On the other hand, using a simulation program to execute the same tests can eliminate time and resource waste, making it much more practical to precisely assess every parameter and exhaust all possible

outcomes without exhausting the budget.

With this in mind, this work focuses on the evaluation and electromechanical characterization of a new PVDF-based actuator, via experimental tests; by simulation method, with a simulation software called COMSOL Multiphysics®, and also with an analytical model of the mechanic behavior of the actuator, comparing and interpreting all the results obtained.

1.1. Author's Contribution

With the present work, the author intends to experimentally evaluate the maximum deflection, the bending stiffness and blocking force of a PVDF-based electroactive polymer when under an applied electric field.

To validate and compare the results, a simulation of the same experiment is built, using COMSOL Multiphysics, and also an analytical mechanical model recurring to a beam theory-based model.

Furthermore, using the simulation, a study is also performed, focused on the evaluation and influence of the following parameters on the displacement produced by the actuator:

- The thickness of the active layer;
- The Young's Modulus of the passive layers chosen.
- The width of each layer, and consequently, of the actuator itself.

The structure of the actuator used is explained, in detail, in the following chapter.

The ultimate goal of this work is to study and conclude on the influence of the parameters mentioned above, and its consequences on the overall performance, resorting to the data given by the experimental tests and validated through the constructed simulation.

1.2. Dissertation's Structure

For the sake of understanding, the author displays here the chapter organization of this dissertation and its respective content:

- Chapter 1 - In the Introduction chapter, the motivation and scientific content of the dissertation's theme is presented, as well as the proposed study and its main focus.;
- Chapter 2 – The chapter of Literature Review provides a context of all scientific concepts needed to understand the carried-out work. Therefore, a review of the development of EAP actuators is given. A brief presentation of the active material used is also present, as well as an explanation of the phenomena involved. Then, a research on the composition and structure of actuators nowadays is presented, both unimorph and bimorph. Finally, an overview of the current state of the art of EAP actuators and main applications is provided;
- Chapter 3 – The chapter of Methods and Methodology is focused on the brief explanation of the methods used, namely, an explanation of the experimental test and every step taken to execute it.A mechanical analytical model, based on the beam-theory is also presented to validate the actuator as a multilayered cantilever beam;
- Chapter 4 – In the Results and Discussion chapter, all the results obtained are presented, as well as the respective analysis of the parameters of interest, with the use of EXCEL® and MATLAB®.
- Chapter 5 – A detailed description of how simulation was contructed, the parameters chosen and the type of analysis used is given in this chapter. Furthermore, it is in this chapter that a comparative analysis between the simulation and the real experimental test data is developed;
- Chapter 6 – In this final chapter, Conclusions and Future Suggestions, all the reached conclusions about the work developed are laid out, followed by possible suggestions for next steps.

Finally, as required, all bibliographic references used for writing this dissertation are listed at the end.

2 Literature Review

This chapter comprises a contextualization of the main concepts, experimental and theoretical, needed for the development and understanding of this work.

Firstly, an overview on EAPs is presented, starting with a description, historical development and how they are classified. The material used for this work is a ferroelectric polymer called P(VDF-TrFE-CTFE), so a short description of its properties will also be given.

The composition and structure of actuators is crucial for their performance, therefore an assessment was made on the several types of structure, namely bimorph and unimorph, their respective characteristics and common applications. A summary table is presented for comprehension purposes.

Finally, as the actuator is stimulated by an electric field, there are two effects present that contribute to the strain of the actuator: Electrostriction and the Maxwell Stress. With this in mind, a detailed explanation of these two effects is given for a better understanding of the consequent behavior of the actuator.

2.1. Electroactive Polymer Actuators

Polymers have a wide range of properties, depending on their constitution, but in general, they are lightweight, easy to process and mass-produce, which makes them highly attractive for several purposes. Adding to this, EAPs are known for their resilience, toughness, large actuation strain and inherent vibration damping (9; 10), emulating biological muscles, therefore, they are commonly considered, among other "smart" materials, for biologically-inspired devices (Figure 2.1). *"Electroactive"* means that the polymer is electrically active or responsive, i.e. that it will have a mechanical response to an electric stimulus. They are the common choice for elastic deformation in polymers, due to the practicality of the electric stimulation and rapid response im-

provements, when compared to other activation mechanisms like chemical, pneumatic, optical or magnetic (11) (Figure 2.2).

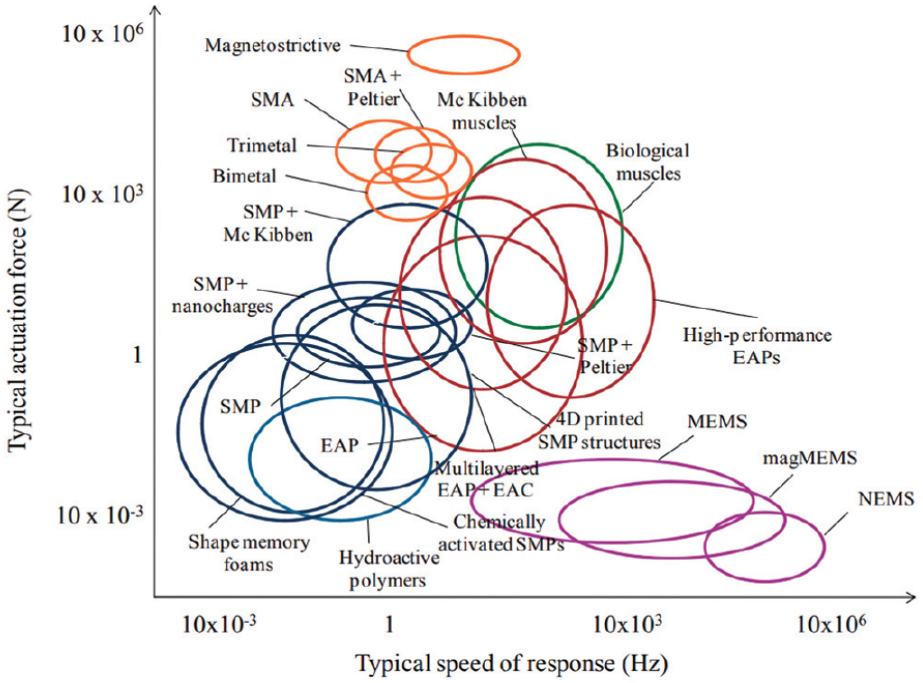

Figure 2.1: Typical actuation force vs. speed of response comparison between several actuators based on "smart" materials. Retrieved from: (12).

However, a lot of progress is still needed so these materials can be properly exploited, namely, a comprehensive knowledge of the materials' behavior to establish a database with documented material properties, which in turn, entails new and refined electromechanical analytic tools and material processing techniques to maximize the EAPs' capabilities and performance (13). Some of the obstacles to overcome are related with the characterization of the properties of EAPs, including:

- Nonlinearity – unpredictability in the behavior;
- Large compliance - large mismatch with metal electrodes;
- Non-homogeneity - formed during the processing (9).

2.1.1. Historical Background and Development

From the first documented study conducted by *Roentgen et al.* (15), in which a rubber band was used and subjected to an electric field across the fixed end and a

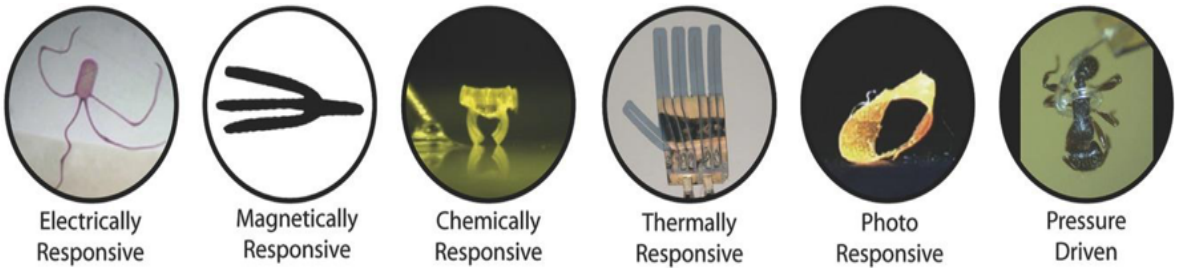

Figure 2.2: Examples of small soft robotic systems actuated with various stimuli. Retrieved from: (14).

mass attached to the free end, knowledge of EAPs has evolved a great deal. The formulation of the strain response to electric field activation by Sacerdote in 1899 (ref), the discovery of a piezoelectric polymer called electret (16), and perhaps one of the most notable, the detection of a substantially high piezoelectric activity in PVDF when stress/strain-tested by *Kawai et al.* (17), after Fukada's work on piezoelectric biopolymers (18), are all great examples of this development. Naturally, several researches were developed to test PVDF copolymers, in order to discover combinations, mainly with non-crystalline polymers with dielectric relaxations (19; 20) that would enhance this property. While it was already recognized the EAPs' capability of inducing small strains, a more intense development was realized mostly in the 1990's, with reports of new actuator mechanisms through conducting polymers (21), ferroelectric polymers that also exhibit piezoelectricity as is PVDF (22), single-walled carbon nanotubes that required a low voltage to generate large strains (23), and, undoubtedly, the creation of the dielectric elastomer actuator (DEA) demonstrating strains over 100% with a fast response speed of less than 0.1 s (24), increasing their potential exponentially and opening doors to new possible applications (25).

2.1.2. Types of EAPs (26)

Currently, EAPs divide into electrochemical (wet or ionic) EAPs and field activated (dry or electronic) EAPs, and each group is subdivided in different types that are enumerated in Figure 2.3 .

In ionic EAPs the actuation process involves mass transport and diffusion of ions or other electrically charged species, while in field-activated EAPs involves electronic

charge transport.

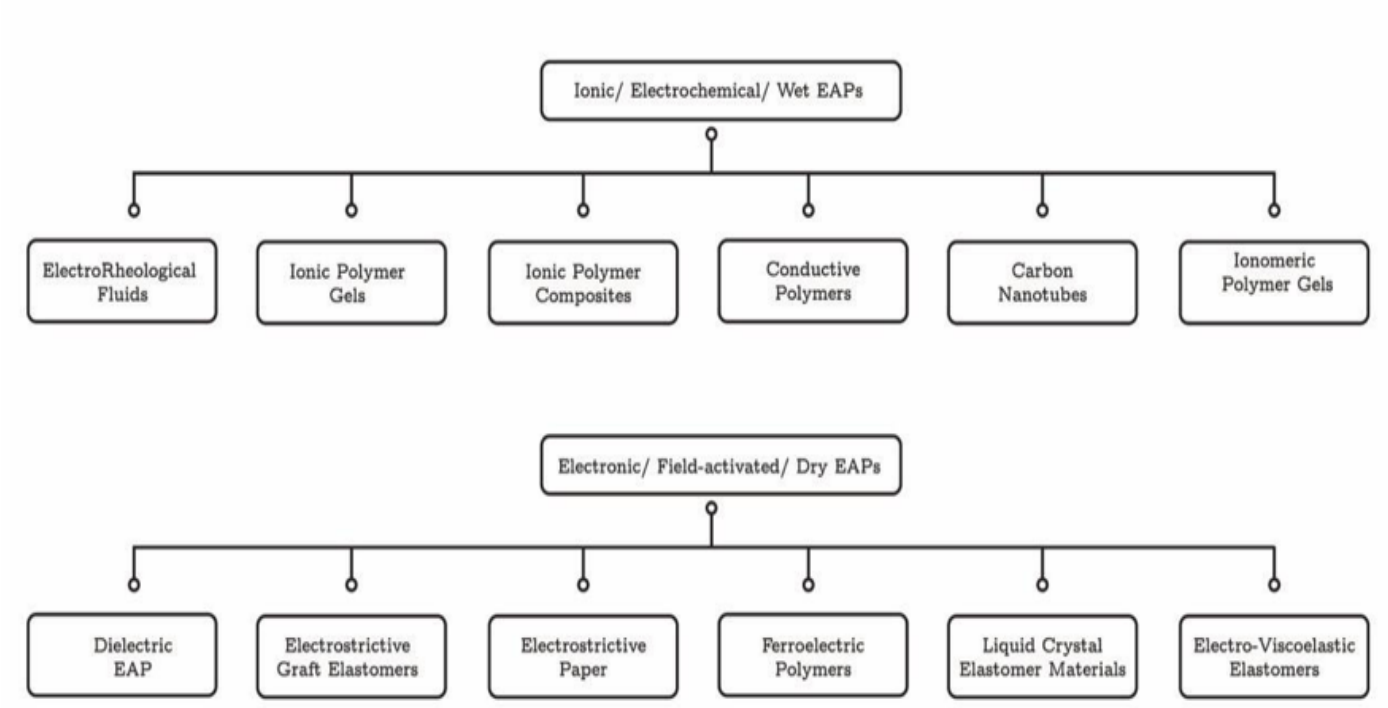

Figure 2.3: Scheme of EAP classification. Adapted from: (13).

Table 2.1 summarizes the main characteristics of both types of EAPs, highlighting the advantages and disadvantages of each one.

Among EAPs, electrostrictive polymers are mainly used for actuators and the piezoelectric ones are the main choice for sensors or transducers. They are driven by the electrostrictive strain and Maxwell stress effect, which require high activation with voltage levels in the ranges of > 10 V/μm, which often matches the breakdown level. To avoid reaching this level, the two main alternatives are (10):

- Developing a polymeric material that increases the dielectric constant, without affecting the strain and or force;
- Combining thin films stacked, shaping multilayered structures to achieve the required thickness.

Unlike ionic EAPs, electronic EAPs materials can hold an induced displacement under a DC voltage, making them important for robotic applications which would require high efficiency. It is important to note that, in this context, **to strain can mean to bend, to stretch or to contract.**

The scope of this work focuses on electrostrictive polymers, namely, ferroelectric polymers, in which an intrinsic field-induced molecular conformational change to the polymer, causes the electrostriction.

Table 2.1: Summary of the advantages and disadvantages of the two basic EAP groups. Adapted from (27; 10; 25; 28; 26).

EAP Type	Advantages	Disadvantages
Electronic EAP	-Can operate in room conditions for a long time; -Rapid response (mSec levels); -Can hold strain under DC voltage activation; -Induces relatively large actuation forces; -Higher levels of efficiency; -Insensitive to temperature and humidity specifications.	-Requires high voltages: ∼150 MV/m for DEs, and ∼20 MV/m for composite DEs; -Requires compromise between strain and stress; -Glass transition temperature is inadequate for low temperature actuation tasks; -Electrostriction dictates monopolar actuation that is independent of the voltage polarity.
Ionic EAP	-Requires low voltage (1 - 2 V); -Provides mostly bending actuation (longitudinal mechanisms can be constructed); -Exhibit large bending displacements; -Sustain hydrolysis at >1.23 V; -Natural bi-directional actuation that depends on the voltage polarity.	-Do not hold strain under DC voltage (except CPs and NTs); -Slow response (fraction of a second); -Bending EAPs induce a relatively low actuation force; -Difficult to produce a consistent material, particularly IPMC (except CPs and CNTs); -Low electromechanical coupling efficiency; -To operate in air requires attention to the electrolyte.

2.1.3. P(VDF-TrFE-CTFE) : A Ferroelectric Polymer

Ferroelectricity happens when a non-conducting crystal or dielectric material displays spontaneous electric polarization, meaning they can transition from polar to nonpolar states, producing a strain and dimensional change under electric fields (14). Piezoelectricity occurs in non-centrosymmetric materials. The reverse effect was dis-

covered, meaning that when an electric field was applied, the materials would sustain a strain (28).

Even though the ceramics and crystals are the most common type of materials to exhibit this characteristic, ferroelectric polymers are also able adding that they can be operated as actuators in air, vacuum or water. They are partly crystalline, with an inactive amorphous phase, with a Young's modulus near 1-10 GPa, providing a high mechanical energy density (28).

Among many ferroelectric polymers PVDF is the most notorious displaying interesting properties under an electric potential, namely being capable of muscle-like contraction (8), exemplified in Figure 2.4. However, its copolymers and, even more, its terpolymers, present an improvement for actuation mechanisms.

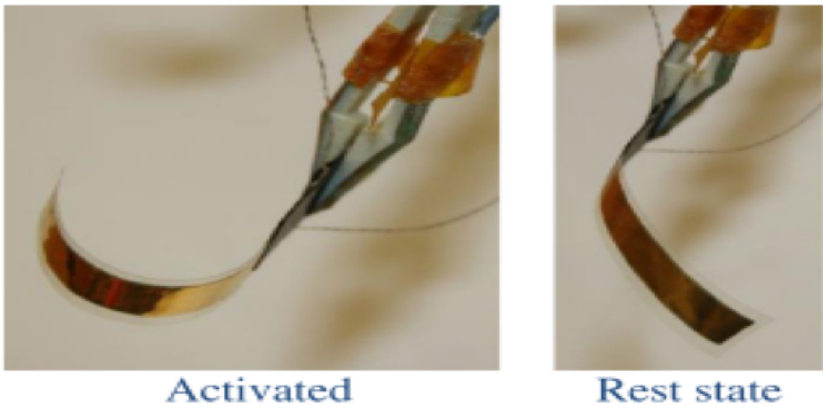

Figure 2.4: Composite ferroelectric EAP in passive (right) and activated states (left). Retrieved from (29).

While PVDF reaches strain levels of just 0.1%, its copolymers can go up to 2%, under an electric field of $\sim$200 V/μm, which as stated before is extremely close to dielectric breakdown. Operating in the ferroelectric-paraelectric (F-P) transition area can enhance performance, but it generally involves large hysteresis, preventing its practical use.

A first attempt to improve the strain was made in (30), producing the copolymer P(VDF-TrFE) using electron radiation to increase the dielectric constant, and the results were strains of $\sim$ 5%, with 45 MPa of pressure, under around 150 V/μm, however, some unwanted defects arose, calling for a need to further improve the material (8).

The following experiments (31; 32) comprised the production of a terpolymer via molecular design, enhancing the degree of conformational changes at the molecular level in the polymer, enabling the generation of a higher electro-mechanical response (33). This converts the polymer from a normal ferroelectric to a relaxor ferroelectric, due to the significant decrease in the hysteresis effect. Table 2.2 sums up the main characteristics of this group of polymers.

Table 2.2: General properties of ferroelectric polymers. Adapted from: (7).

Property	**Typical**	**Maximum**
Strain (%)	3.5	7
Stress (MPa)	20	45
Work Density (kJ/m^3) (based on internal strain)	320	>1000
Density (kg/m^3)	1870	2000
Strain Rate (% s^{-1})		>2000 (10 kHz, -0.1% strain)
Bandwidth (Hz)	<100	>10,000 (for ∼0.1% strain)
EM Coupling S3 (at optimal temperature)	0.1 - 0.2	
EM Coupling S1 (at optimal temperature)	0.4	
Modulus (MPa) (Composition dependent)	400	1200
Voltage (V) (Geometry dependent)		>1000
Max. Field (MV/m)	13	150
Dielectric Constant (4 - 60)	55	Temp. dependent
Temperature Range	△T ∼60°C	

P(VDF-TrFE-CTFE) or P(VDF-TrFE-CFE) terpolymers differ from the P(VDF-TrFE) copolymer in the sense that the defect introduced is a third monomer rather than

electron radiation, which, modifying the molecular structure, eliminates the adverse effects of the F-P transition, at the same time maintaining high material responses. When this third bulky monomer is a chemical one, such as 1,1-chlorofluoroethylene (CFE) or chlorotrifluoroethylene (CTFE), copolymerized with the VDF-TrFE, this triggers a change in conformation, the normal ferroelectric phase is eliminated, giving space for the relaxor ferroelectric with higher polarization, which in turn leads to an electromechanical strain greater than 7%, with an elastic energy density of 0.7 J/cm^3 under an electrical field of 150 MV/m. Naturally, with this in mind, one can assume that the amount of CFE or CTFE should also affect these properties, and to the best of the author's knowledge, there is an optimized percentage of CFE/CTFE of 8.5% for a VDF-TrFE composition of about 65/35 (34). In Table 2.3 a comparison is made to highlight the improvement in the values of the electromechanical properties. Moreover, they have a relatively high modulus of $>$ 0.3 GPa and a (room temperature) dielectric constant higher than 50 (35)(François Bauer, 2012).

Table 2.3: Comparison of electromechanical properties between PVDF, PVDF-TrFE and P(VDF-TrFE-CTFE). Adapted from (31; 36; 37).

	PVDF Polymer	**PVDF-TrFE Copolymer**	**P(VDF-TrFE-CTFE/CFE) Terpolymer**
Strain (%)	∼0.1	∼2	>7
Electric Field Supported (MV/m)	150		
Energy Density (J/cm³)	0.002	0.5	0.7
Young's Modulus (GPa)	2	0.5 - 1	>0.3
Dielectric Constant	8.4	35	∼50

Figure 2.5 graphically expresses the relation and improvement of these electrostrictive polymers by plotting the maximum thickness strain at different electric fields. It confirms the dominance of the terpolymer, being the one with the highest thickness strain and greater electric field operating range, even though the copolymer can be a better fit when using lower electric fields.

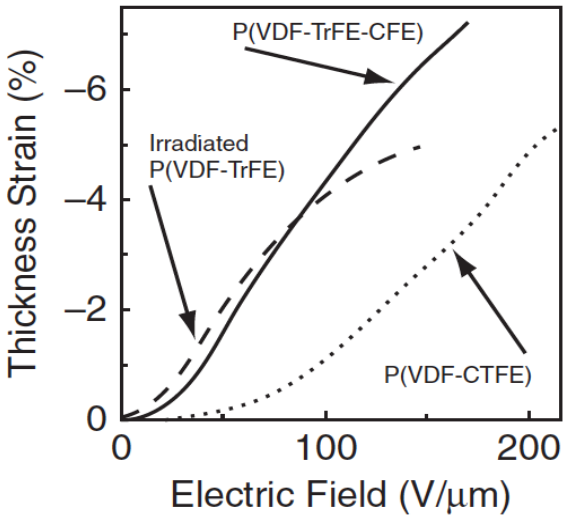

Figure 2.5: Relation of maximum thickness strain of P(VDF-TrFE-CTFE), irradiated P(VDF-TrFE) and P(VDF-CTFE). Retrieved from: (38).

2.2. Electromechanical Properties

2.2.1. Piezoelectricity vs. Electrostriction

Concerning the electromechanical properties of P(VDF-TrFE-CTFE) and though the effect is not yet fully understood, the electrostriction effect is the name given to the quadratic coupling between strain and electric polarization ($S = P^2$), so reversing the electric field does not change the strain Figure 2.6. This means that at moderate electric fields, the electroactive response is due to electrostriction, contracting perpendicularly to the electric field and independently of the field direction (14). It can be present in all materials, even amorphous' ones (39) Moreover, this is why the terpolymer is an interesting choice, its high polarization enables a greater strain of the actuator.

Electrostriction, unlike piezoelectricity, is not affected by hysteresis or aging, therefore it sets a great improvement in applications such as small motors, optical instruments, etc. Moreover, electrostriction is a property inherent to all dielectric material and can more accurately be expressed by:

$$S = QP^2 \tag{2.1}$$

where S is the material strain, Q is the electrostrictive coefficient, and P is the electric polarization. This electrostrictive coefficient can vary as it depends on the prepara-

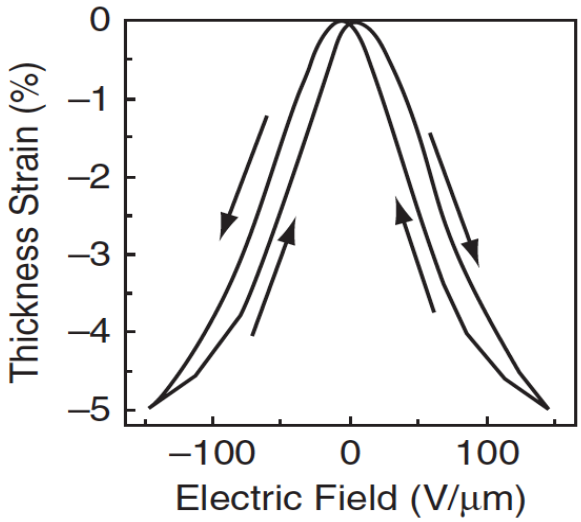

Figure 2.6: Relation between the strain response and the electric field applied for a typical electrostrictive polymer. Retrieved from: (38).

tion procedure, the presence of impurities, among other factors hard to control in the manufacturing process (39).

Figure 2.7 represents the graphic relation between the electrostriction effect and piezoelectric effect.

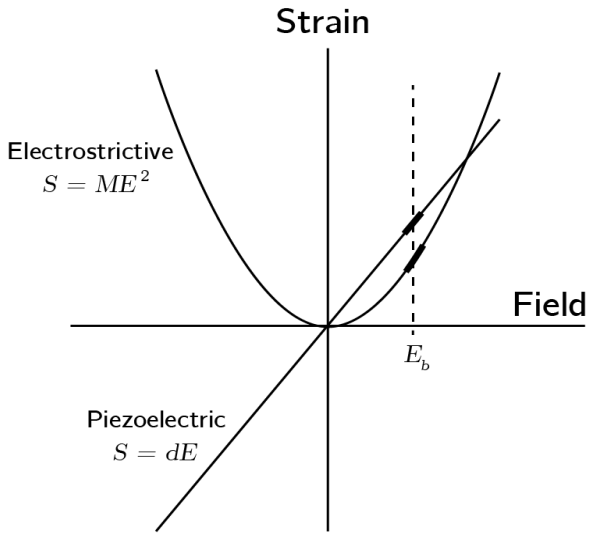

Figure 2.7: Relation between the strain response and the electric field applied for a typical electrostrictive polymer. Adapted from: (38).

2.2.2. Electrostriction and Maxwell Stress (40)

As stated before, the electrostrictive effect occurs due to variations in the dielectric properties of the material under strain. However, this is not the only electromechanical effect present in dielectric materials. When the active material as electrodes attached to it, another phenomenon known as the Maxwell Stress effect is also present, but instead it occurs due to variations in the electric field distribution under strain, and describes the Coulomb forces between the positive and negative charges in the material's surfaces. It is represented as:

$$S = -\frac{\varepsilon_0 \varepsilon_r E^2}{Y} \tag{2.2}$$

with Y being the Young's Modulus, ε_r being the dielectric constant of the material and ε_0 as the dielectric permittivity of vacuum. In dielectric materials with a high Young's Modulus, the electrostriction effect is the predominant one as the cause for the strain, however for materials with a low Young's Modulus, the Maxwell Stress effect quickly increases its contribution. A relevant example is the P(VDF-TrFE) copolymer with a Young's Modulus around 1 GPa and the P(VDF-TrFE-CTFE)) terpolymer with a modulus 10% lower than the copolymer.

Quiao et al. (40) details an experiment to clarify the roles of these two effects on P(VDF-TrFE-CTFE) terpolymers – stretched and unstretched - with different percentages of CTFE units, revealing the changes in the contribution of electrostriction or Maxwell Stress for the produced strain.

2.3. Structural Characterization of EAP Actuators

Actuators are devices built to convert some kind of energy into mechanical energy, producing movement – as it is graphically explained in (Figure 2.8) - therefore, often used as a component of motion-driven mechanisms. Over the years, the progression of these devices is notable and we are presented with many actuators and consequently many classifications, each of them based on a different component, whether it is the material used, the type of structure built, the source of energy, or even the type of movement produced. Even more, in terms of movement, they can be classified as

rotary, if there is a circular motion caused, or as linear, if they cause movement in a straight line.

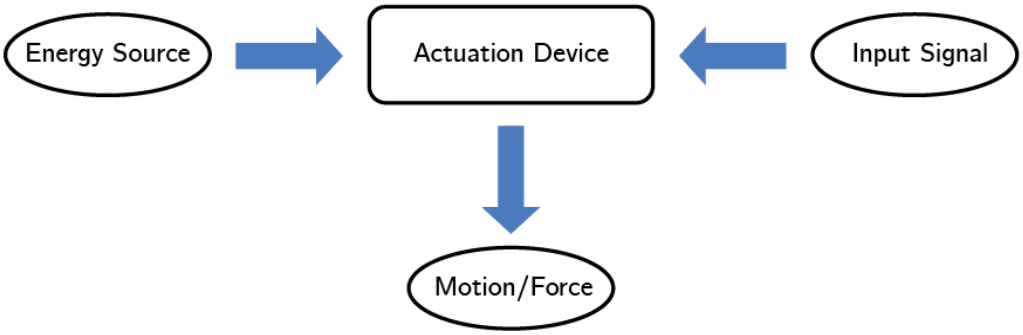

Figure 2.8: General scheme of the working mechanism of an actuator.

2.3.1. Unimorph vs. Bimorph

Another important aspect of actuators' characterization is their structure. The way an actuator is built is directly linked to the application and function they are supposed to perform.

It is of crucial importance to focus on unimorph and bimorph actuators, since here a unimorph actuator is used. Simply put, a unimorph structure has one active layer and at least one passive layer. On the other hand, a bimorph actuator consists of two active layers and, generally, at least one passive layer (41). Figure 2.9 illustrates some examples of structural schemes of unimorph and bimorph actuators.

So, the next subsections will be focused on reporting examples of each type of actuator. The purpose is to highlight current developments in this field and to compare them in terms of performance, essentially in metrics such as strain (%), block force (N), etc.

Frecker et al. (42) idealize an actuator with the intent of using it in Minimally Invasive Surgery (MIS). A segmented unimorph actuator is realized using P(VDF-TrFE) as the active EAP, and consists of several independent actuators linked alongside one another as depicted in (Figure 2.10). Although it seems a bimorph configuration, because these actuators have each one an independent pair of electrodes attached, it

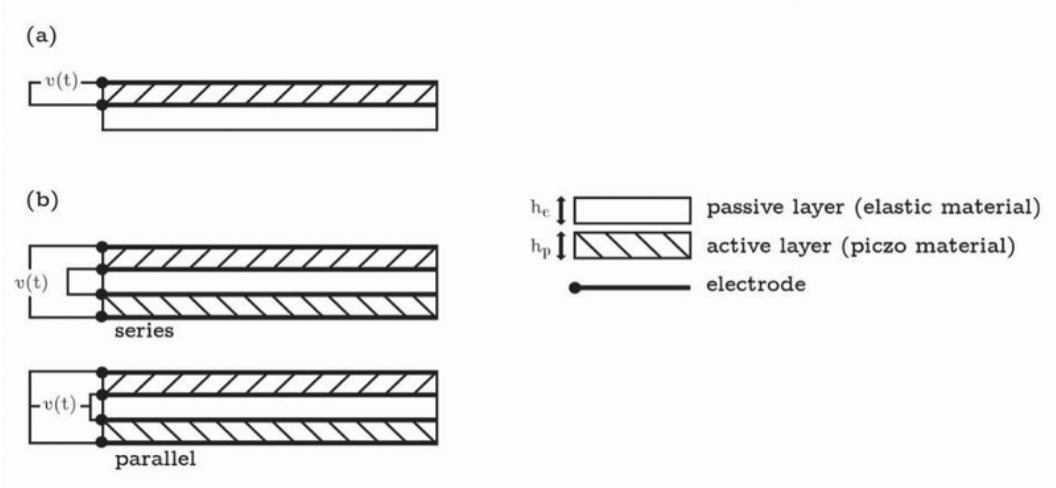

Figure 2.9: Examples of unimorph and bimorph actuators. a) unimorph actuator; b) bimorph series and parallel actuator with no passive layer; c) bimorph series and parallel actuator with one passive layer.

enables the activation of only one layer in each segment at a time. It is important to refer that this activation can be controlled through the voltage value applied.

The full picture is an indefinite-length steerable device with varying curvature. A great application of this actuator, although not limited to, is the medical field, namely the minimally invasive surgery and other surgery procedures where improved dexterity is still needed and the options available are still a bit limited in terms of degrees of freedom and movement.

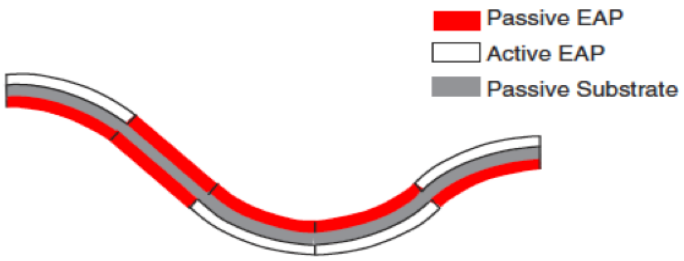

Figure 2.10: Simplified scheme of the activation method of the segmented actuator. Retrieved from: (42).

Zarif et al. (43) detail a new method for estimating the tip displacement of a piezoelectric bimorph actuator, employing two resistive strain gauges within the electrodes. A bimorph actuator is used for this purpose. Figure 2.11 shows the graphic model of the actuator, highlighting the multilayered structure, the neutral axis (dashed-line

in the orange layer), the electric potential applied (V_u) and the resulting movement direction of the actuator (y_{tip}). The values of displacement and force are displayed in Table 2.4.

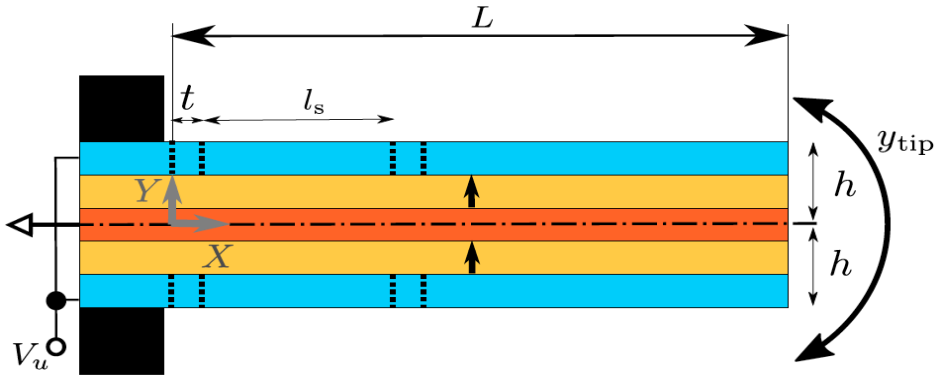

Figure 2.11: Electromechanical model of the actuator. Retrieved from: (43).

To enhance the output force of an actuator, *Fook et al.* (44) propose the introduction of a highly conductive nanolayer, made of Silver Nanowires (AgNW) between two P(VDF-TrFE-CTFE) layers, therefore enhancing the dielectric constant, without compromising the electrical breakdown field and holding the strength, flexibility and transparency of the film matrix. The results concerning the dielectric constant in function of Frequency (Hz) are displayed in Figure 2.12, demonstrating the clear improvement, while Figure 2.13 shows the plotted results of Force (mN) in function of Electric Field (V/μm) with significant higher values of Force for the actuator with a greater nanowire layer present.

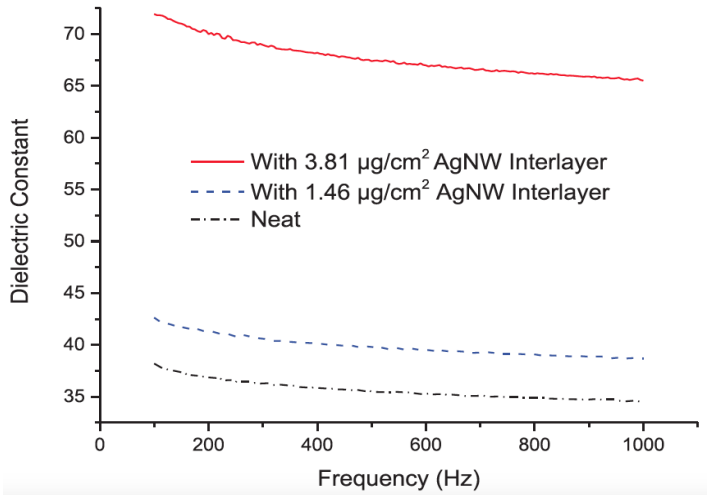

Figure 2.12: Dielectric constant of neat P(VDF-TrFE-CTFE) films and films with AgNW interlayer. Retrieved from: (44).

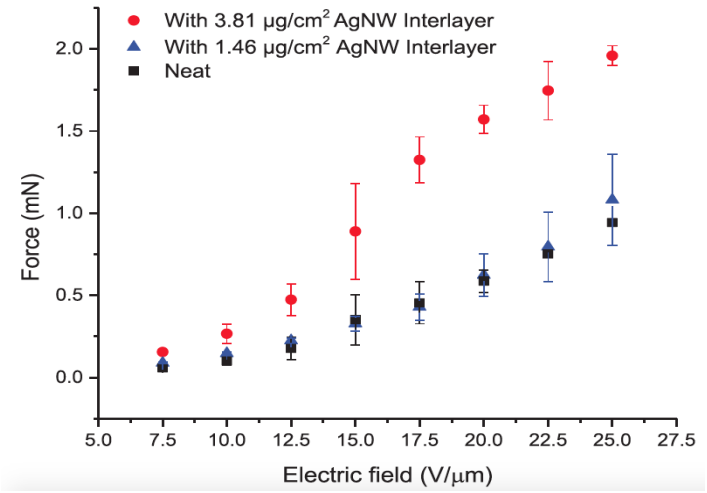

Figure 2.13: Output force of P(VDF-TrFE-CTFE) actuators with and without AgNW interlayer. Retrieved from: (44).

Bauer et al. (45) after analysing the developments of the relaxor ferroelectric terpolymer, give the example of a unimorph actuator made of a P(VDF-TrFE-CTFE) layer onto a stainless-steel electrode layer, whose purpose is to be integrated as a microsensor attached to a projectile that can react to pressure, adjusting the trajectory and improving the accuracy of the flight. Figure 2.14 shows the actuator in action, with the tip changing direction when actuated.

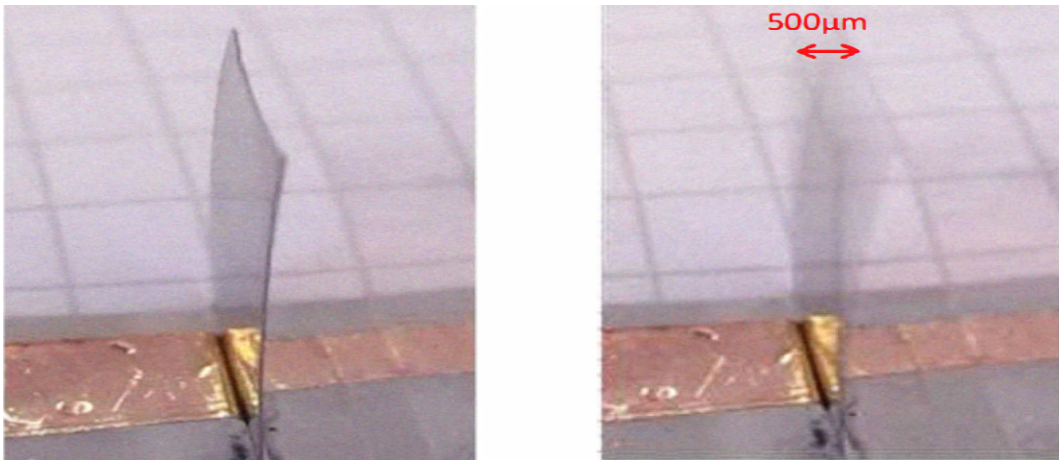

Figure 2.14: Motion of the unimorph actuator when under an applied electric field of 50 MV/m (300 Hz). Retrieved from: (45).

Xia et al. (46) test a valveless microfluidic pump realized with a unimorph diaphragm actuator configuration. Incorporating a nozzle/diffuser structure (Figure 2.15) in the micropump resulted in an efficiency of 11,7% and 16%, since two sizes

of the diffuser structure were experimented. However, the high voltage required for functioning presents a common issue among other EAP solutions.

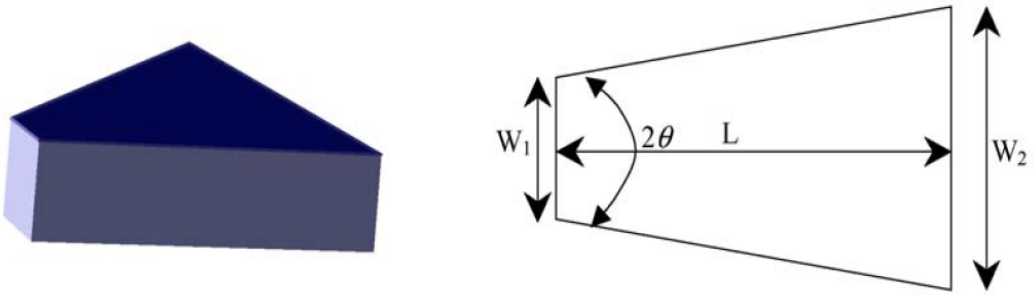

Figure 2.15: Nozzle/Diffuser type structure incorporated in the micropump. Retrieved from: (46).

Ahmed et el. (47) developed a multilayer unimorph actuator and studied the influence of geometry and design parameters such as the Young's Modulus of the passive layers and the number of layers (Figure 2.16. Through a self-constructed analytical model, it was possible to conclude that the curvature, tip displacement and blocking force are influenced by these parameters, and that, for example, the curvature reaches a peak for a two-active-layered actuator.

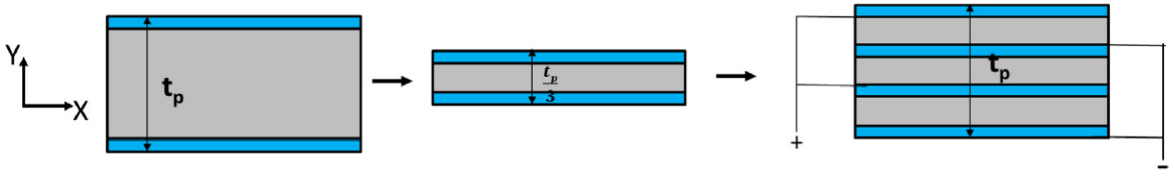

Figure 2.16: Graphic explanation of the multilayer hypothesis. Retrieved from: (47).

Poncet et al. (48) study a vibrotactile button based on a printed piezoelectric polymer actuator. The electromechanical characterization of the electroactive unimorph actuator - used as the basis for the construction of the vibrotactile button - was realized through an actuation of the mechanisms, that resulted in 4.9 μm of displacement under 100 V. Moreover, similar to the work done in this dissertation, an analytical model and a FEM analysis simulation are created to compare with the experimental results 2.17, and the increase of displacement along with the increase of voltage applied was clear.

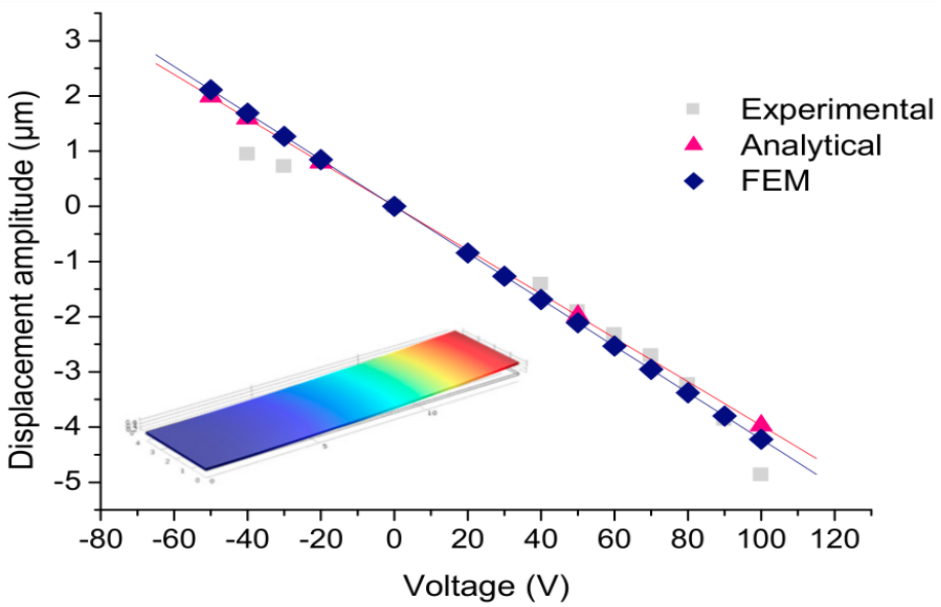

Figure 2.17: Concordance between experimental, analytical and FEM analysis measurements, in terms of maximal displacement as function of applied voltage, on a cantilever unimorph actuator. Retrieved from: (48).

Panda et al. (49) focus on a Polypyrrole (Ppy) bimorph actuator to develop a tadpole-like robot for underwater motion (Figure 2.18), which means the actuator is composed by two layers of Ppy with another layer in between. In this case, the actuator is stimulated with AC voltage, through a sine wave, to mimic the lateral motion of the tadpole (Figure 2.19), and it achieves displacements, with low voltage, significantly higher than some unimorph examples already described.

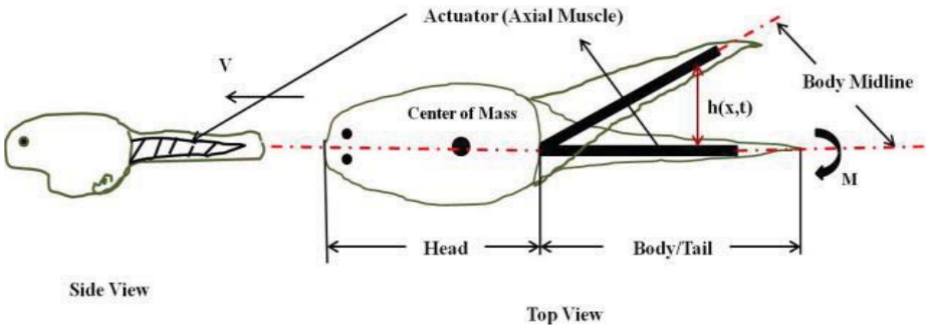

Figure 2.18: Schematic diagram of a tadpole. Retrieved from: (49).

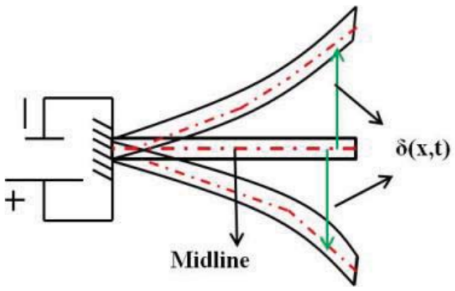

Figure 2.19: Schematic diagram of a Ppy actuator bending on applying electric voltage. Retrieved from: (49).

Xiao et al. (50) studies another approach for a fish-like robot, instead using PVDF and flexible graphene paper in a bimorph actuator. Again, the results were great displacements using low voltage stimulus, achieving 14 mm under 13 V. Figure 2.20 shows a schematic of the experimental setup, displaying that when the electric field is on, the actuator bends down, when it is turned off, the actuator returns to the original position.

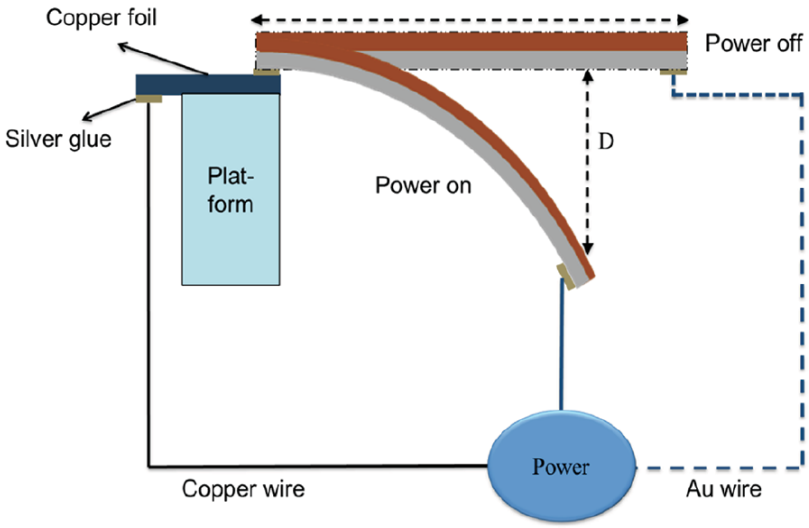

Figure 2.20: Experimental setup of bimorph actuator. Retrieved from: (50).

For a more understanding comparison, *Lou et al.* (51) studies a unimorph version and a bimorph version of the same actuator, a piezoelectric micro-machined ultrasonic transducer, composed of Aluminum Nitride (AlN) as the active layers and Molybdenum (Mo) in between them. The bimorph version forms a (Mo/AlN/Mo/AlN/Mo) structure, while the unimorph is obtained through Focused Ion Beam (FIB) post-processing, deactivating the upper (Mo/AlN), but maintaining the structural integrity.

Although the application of this actuator is off topic to the work realized, the results are still important, as it is clear that the bimorph configuration outperforms the other in approximately the double, reaching 140 nm, while the unimorph version reaches 70 nm. This is because in the unimorph version, only one AlN layer is activated while the other, being deactivated, works a resistance to deformation. On the other hand, in the bimorph configuartion, both AlN layers are activated, meaning both generate structural deformation.

Table 2.4 lists all the actuators mentioned in Chapter 2, and compares the main characteristics and achieved performance in terms of tip deflection and force (blocked force or force exerted).

Table 2.4: Comparison of actuators mentioned, their characteristics and performance.

Paper	**Actuator Configuration**	**Materials**	**Displacement**	**Force**
(47)	Unimorph	P(VDF-TrFE-CTFE) Scotch tape (passive) Spunned Electrodes	25 MV/m-17 k (Curvature radius)	3 mN (30 MV/m)
(45)		P(VDF-TrFE-CTFE) Stainless Steel	$\pm$ 250μm (300 Hz 50 MV/m)	N/A
(42)		P(VDF-TrFE) Passive Substrate	2.06 mm (20 MV/m)	0.0077-0.023 N (20 MV/m)
(48)		P(VDF-TrFE) Gold PEDOT-PSS electrodes	4.9 μm 100 V	N/A
(51)		AlN Mo	70 nm	N/A
(43)	Bimorph	Nickel electrodes Piezoelectric Brass	$\pm$ 1mm	$\pm$ 0.35 N
(44)		P(VDF-TrFE-CTFE) AgNW	N/A	1.92 mN

(49)		Polypyrrole Gold	5.4 mm (1.3 V 1 Hz)	1 mN
(50)		PVDF Graphene Paper	14 mm (13.0 V)	N/A
(51)		AlN Mo	140 nm	N/A

In conclusion, the foreseeable market for soft EAP actuators includes every field that would benefit from soft, lightweight, noiseless, cost and energy efficient EAP actuators, enabling economically and environmentally friendly solutions to the current heavy and hard options available at the moment.

3 Methods and Methodology

After reflecting on the scientific context of the study and introducing the theoretical concepts needed for its comprehension, this chapter intends to present and describe all the materials, procedures and equipment utilized in the experimental analysis of this work. It is comprised of two topics:

- The fabrication of the sample actuators, experimental set-up and equipment used, the tests performed, as well as all the initial conditions and parameters. To electromechanically characterize the actuator, a set of tests were performed:
  - Tensile tests: experimentally obtain the elastic modulus of each material present in the actuator and evaluate the electrostriction of the P(VDF-TrFE-CTFE);
  - Bending tests: measure the tip displacement, blocking force and bending stiffness of the actuator;
  - Displacement test monitored with a camera: evaluate the displacement of the actuator with the use of a laser sensor and a camera.
- The analytical model of the actuator in question is deducted and presented. With this model, which is based on the classical beam theory (52; 53), the author intends to validate the actuator in study as geometrically and mechanically similar to a multilayer cantilever beam, therefore, its behavior can be modelled as such.

3.1. Experimental Testing on the PVDF-based Electroactive Actuator

3.1.1. Fabrication of Samples

The actuator used for this study is unimorph asymmetric and it is comprised of five layers (Figure 3.1):

- An electroactive polymer in the center – P(VDF-TrFE-CTFE) film;
- Two aluminum electrodes – one on each side of the film;
- Two passive layers also one on each side of the electrodes:
  - A Kapton tape;
  - An adhesive tape, made of polyethylene.

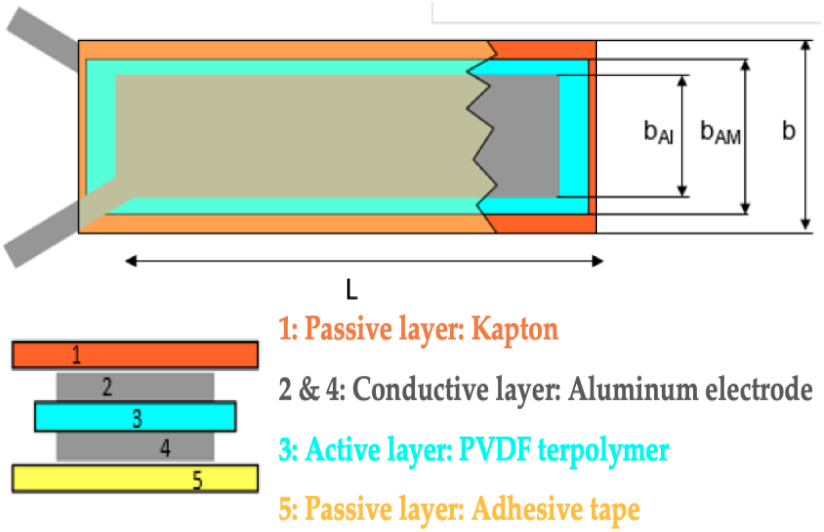

Figure 3.1: Representation of the actuator and respective legend of each layer.

It is important to note that, besides what was mentioned previously about the advantages of the multilayer structure, in this case, the passive layers serve to change the contraction of the polymer into a bending, due to the difference between the Young's Modulus of both passive layers. This is why it is an asymmetric actuator, because the outer layers are different. Therefore, keeping in mind that there are several ways of classifying an actuator, it can be considered an/a:

- Electrical actuator, since it uses an electrical input;
- Linear actuator, since it produces a motion in a straight line;
- Soft actuator, because the active material used is an EAP, that in recent literature is included in the soft materials list, which are materials that respond to some sort of stimuli (pH, chemical, electricity, heat, light) by changing their size and/or shape (54).

In order to study and explore the influence of specific parameters of this actuator, three different samples were fabricated, with the following dimensions:

Table 3.1: Dimensions of the samples used for study.

Sample	PVDF-TrFE-CTFE Thickness (μm)	Kapton Width (mm)	Polyethylene Width (mm)	Electrodes Width (mm)
60PVDF	60	15	15	14
60PVDFHalf	60	8	8	7
130PVDF	130	15	15	14

These three samples, displayed in Figure 3.2, apart from their specific dimensions, were all fabricated following the same procedure. The terpolymer film (Solvene T P(VDF-TrFE-CTFE) is produced by Solvay Polymers (Italy), it is sandwiched between two aluminum tape electrodes – acting as the conductive layers - and two passive layers, a kapton tape and an adhesive tape are added, one on each side. The different elastic modulus of the passive layers in this stacking sequence comprise a 5-layer asymmetric unimorph actuator that, under an applied electric field, produces a bending of the structure in the axial direction, instead of a strain in the longitudinal axis that it would be obtain with just the actuated terpolymer film.

Figure 3.2: Final form of the fabricated samples used for study.

Previously, experiments were made to measure and prove the electrostriction capacity of the P(VDF-TrFE-CTFE).

3.1.2. Tensile Test for Measurement of the Experimental Elastic Modulus

By definition, a tensile test determines the strength and elongation properties of a material, by applying a tensile force on the specimen and studying its response to the stress caused (55). In this test, a specimen is clamped in its edges inside a machine that slowly pulls one of the edges, forcing the material to elongate and react to the forces being applied.

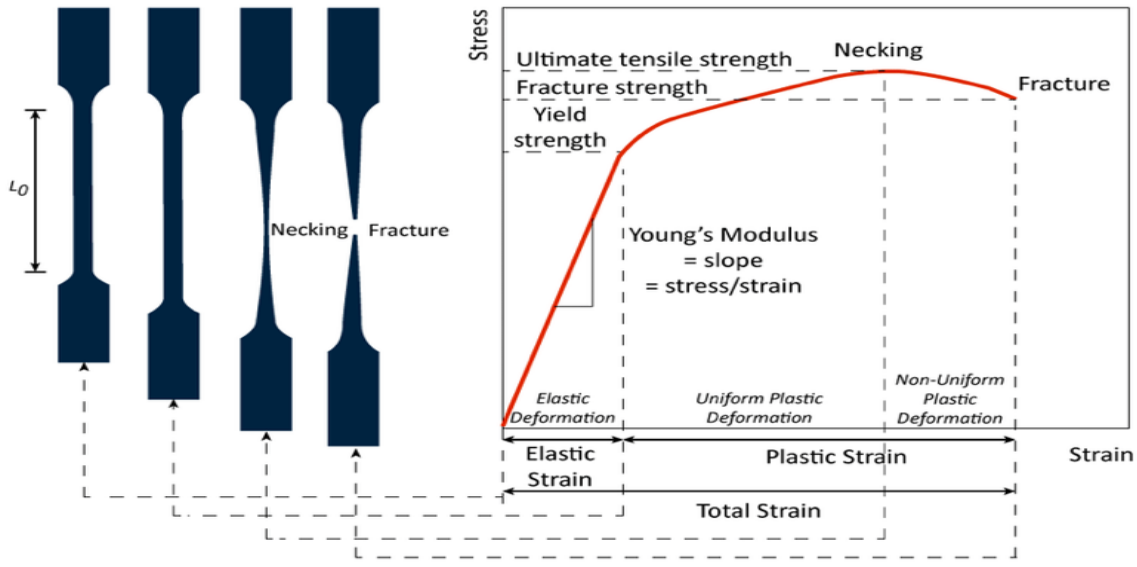

Figure 3.3: Different stages of a specimen during a tensile test. Retrieved from:(56).

The data obtained results in a stress/strain curve as plotted in Figure 3.3. From this plot it is possible to determine several tensile properties such as the elastic and plastic domain, ultimate tensile strength, yield strength, strain, ductility, the modulus of elasticity, among others.

As stated before, the objective in this test is to obtain the Young's Modulus of each material used, therefore the focus lies in the elastic strain part of the plot. Here the progress follows Hook's Law, meaning the elongation of the material increases linearly with the force applied to it. This relationship can be graphically represented by $\sigma/\varepsilon = E$, where σ is the stress, ε is the strain and E is the elastic modulus to be obtained.

In this case, the test instrument used was Instron^{TM}ElectroPuls E1000, equipped

with an Instron^{TM}static load cell 2527-129 (www.instron.us) that has a capacity of 2 kN. The set-up is completed with two clamps 3D-printed with ABS material that hold the edges of the samples as seen in Figure 3.4 .

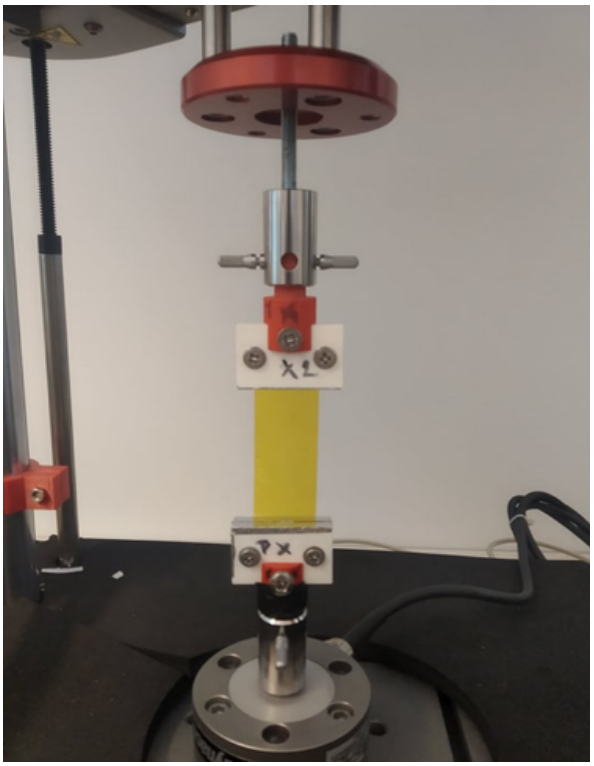

Figure 3.4: Experimental set-up for tensile tests.

This test was realized for Kapton, Polyethylene and the Aluminum Tape. In order to have more precision for the evaluation of the PVDF elastic modulus, a load cell with 5 N capacity (Instron 2530-5N with a sensitivity of 1.6-2.4 mV/V at a static rating) has been chosen. The tests were repeated three times for each material in order to eliminate any systematic errors present during the execution of each test.

The data was analysed, plotting a stress/strain graphic for each test, knowing that the slope of those graphs equals the elastic modulus. The average of the three tests was obtained and used as the experimental Young's Modulus of the actuator's materials (Figure 3.5). In the same order as the graph in Figure 3.5, the relative standard deviation is 2.5%, 17.5%, 14.6% and 3.4%.

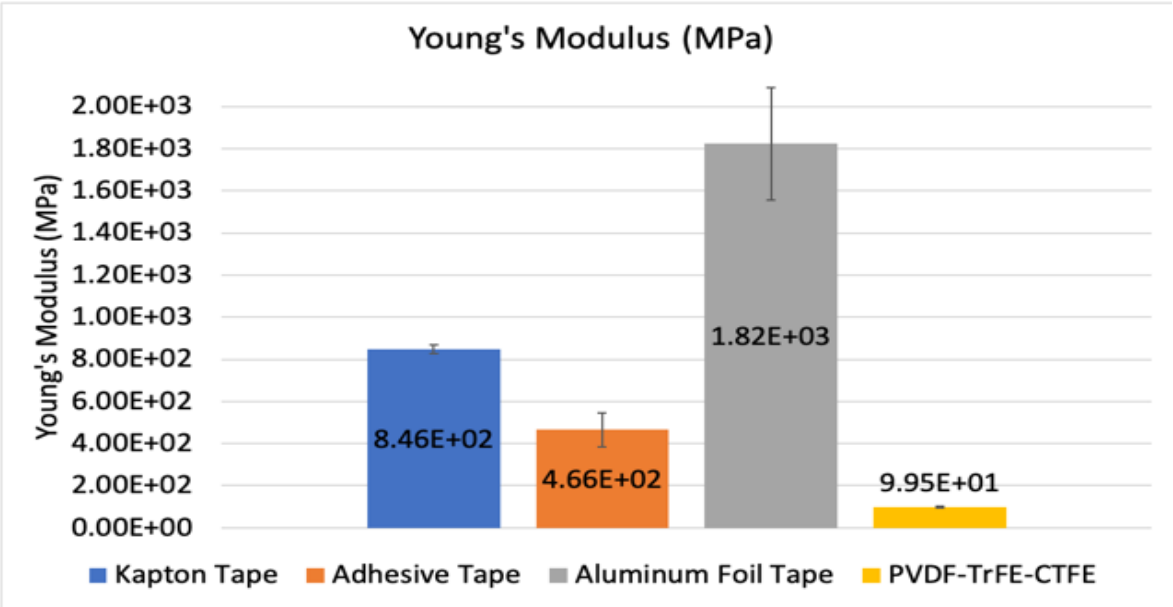

Figure 3.5: Graphic of the experimental Young's Modulus of the actuator's materials.

3.1.3. Bending Test for Measurement of Tip Displacement, Bending Stiffness and Blocking Force

With these tests, and through a deep and detailed analysis of the data acquired, it is possible to adequately evaluate the properties and characterize electromechanically this multilayered PVDF-based electroactive actuator, namely the tip displacement, bending stiffness and blocking force, as well as establish correlations between each other.

3.1.3.1. Measurement of Bending Stiffness

An experimental set-up such as the one displayed in Figure 3.6 was chosen. A specific 3-dimensional (3D)-printed support with Acrylonitrile Butadiene Styrene (ABS) material, designed to fit the machine for the bending test, was attached to it, and connected to the wires of a voltage amplifier (TREK 10/10B-HS) through crocodile plugs. The voltage amplifier itself was operated through an input waveform generator (RIGOL DG1022, www.rigolna.com).

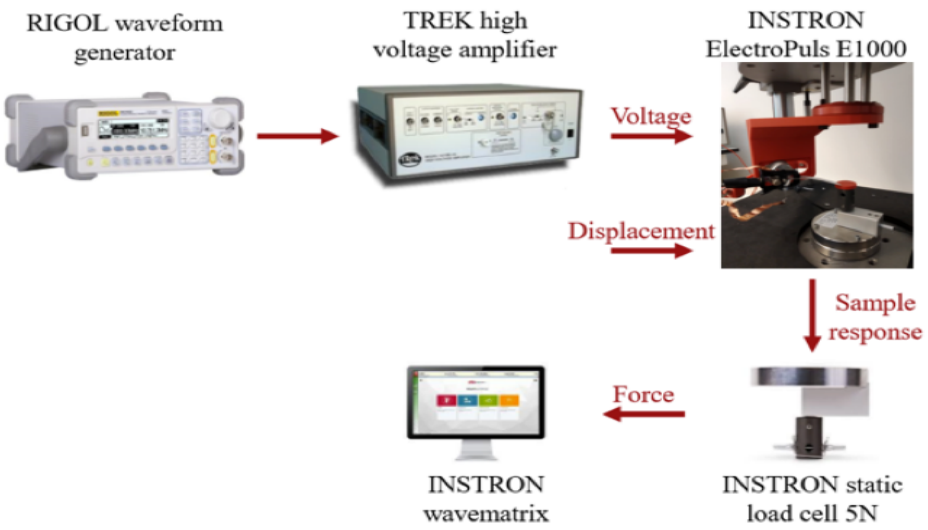

Figure 3.6: Measurement set-up for the tests.

The Instron static load cell 2530-5N (capacity: 5N, sensitivity: 1.6-2.4 mV/V at a static rating) was used. Also, this time the crocodile plugs were connect to the free extension of the aluminum layers, as it can be seen on (Figure 3.6).

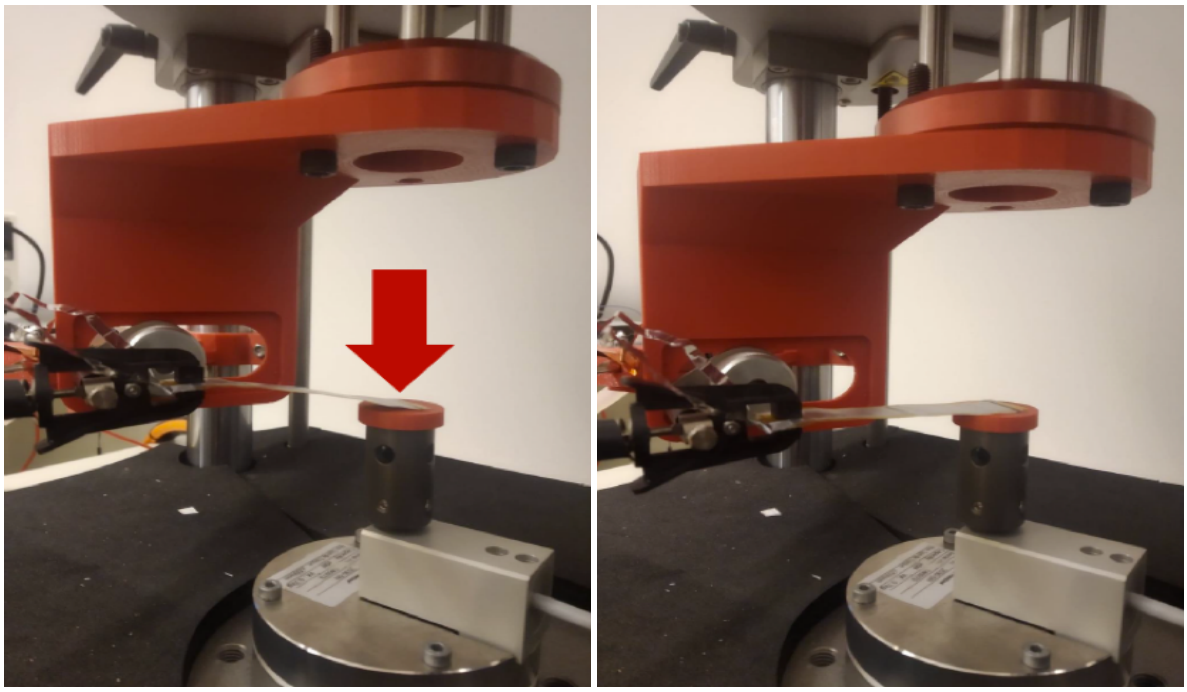

(a) Starting point. **(b)** Ending-point.

Figure 3.7: Measurement test set-up for the bending tests.

As it can be seen when comparing Figure 3.7a and Figure 3.7b, the linear motor controls the displacement of the actuator, allowing to calculate the tip blocking force

throughout the load cell at different values of displacement of the actuator. In this case, the displacement is seen as the vertical distance between the fixed tip of the actuator and the load cell, so the movement of the linear motor is 4 mm downwards, and the force values were measured in intervals of 0.5 mm. From the results of these tests, force-displacement graphics are constructed and analysed in Chapter 4.

For each sample, the test was repeated three times for four different values of voltage, as explained in the scheme of Figure 3.8, and the displacement was settled from 0 to 4 mm. The 130PVDF sample requires different values of voltage in order to obtain the same electric field for all samples in study: 8.33 MV/m, 11.67 MV/m and 15 MV/m.

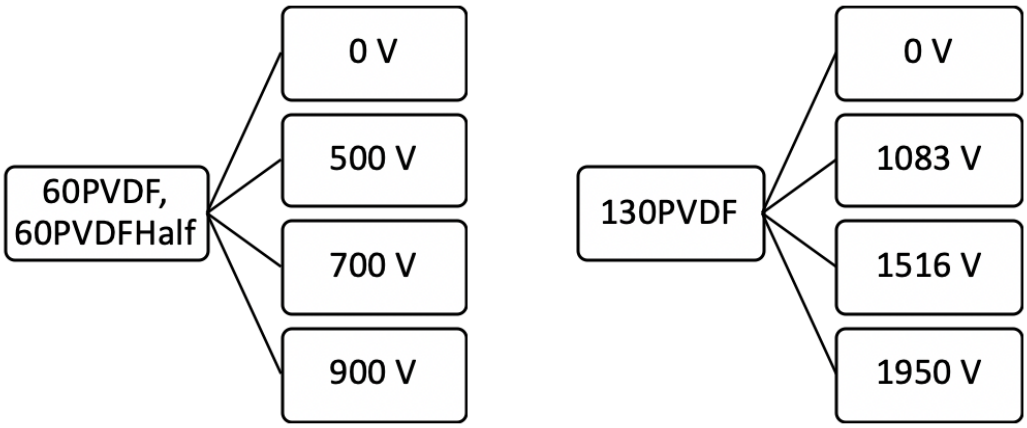

Figure 3.8: Procedure for bending tests.

3.1.3.2. Measurement of Blocking Force

The blocking force of an actuator is the maximum force that it can generate. This type of value can be measured in a set-up where the displacement is completely blocked, so that when the voltage is applied to the actuator, the force produced does not "dissipate" in the form of displacement, but is fully applied in the load cell that records the value.

The previous set-up was used also to evaluate the blocking force, although this time, the motor was maintained in a fixed position, recording the force produced by the tip of the actuator when different values of electric field were applied.

3.1.3.3. Measurement of Tip Displacement

Another experiment to accurately detect and measure the displacement of the actuator was realized. The ABS 3D-printed clamps fixed the samples on one side only, as a cantilever beam would be (picture of the set-up) with a camera vertically placed above the set-up to record the deflection. A MATLAB® script was used to convert the distance measured in pixels from the video, to millimeters and obtain a displacement value.

In this test, the voltages applied to each sample were the same as before, in Figure 3.8, except for the 0 V.

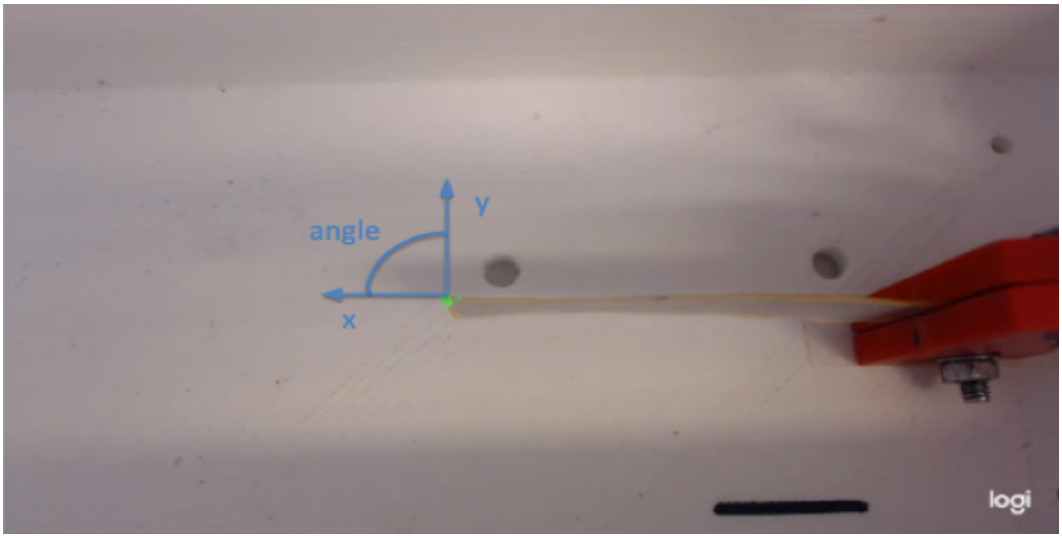

Figure 3.9: Experimental set-up for deflection tracking.

The MATLAB® script was comprised of the following steps:

a). Delimit the object's region of interest;

b). From the video data, make the pixel to mm conversion;

c). Extract the coordinates (x, y) and the angle of deflection, from the converted data;

d). Detect the points of interest.

The steps are resumed in Figure 3.10.

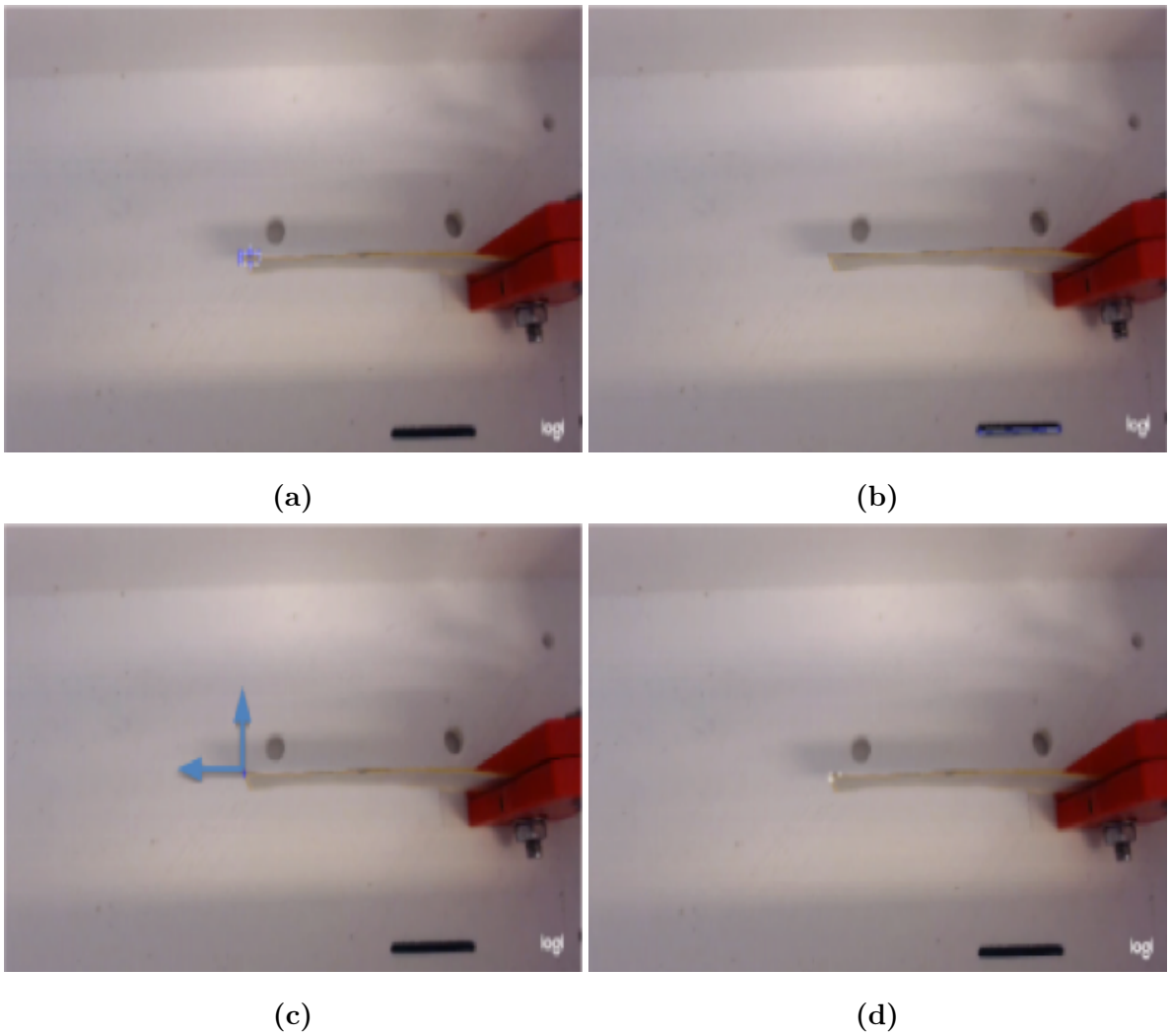

(a) **(b)**

(c) **(d)**

Figure 3.10: Script steps to convert the deflection tracking to the displacement measured on the test.

3.2. Analytical Mechanical Model – The Beam Theory

It is called the Euler-Bernoulli beam theory, classical beam theory or even engineer's beam theory and it is a simplification of the linear theory of elasticity, therefore providing a description of the relationship between the applied load and the beam's deflection.

It is based on three assumptions:

1. The beam's cross-section is infinitely rigid in its own plane;

2. The beam's cross-section remains plane after deformation;

3. The lines that are straight and perpendicular to the geometrical beam's axis remain straight and perpendicular during deformation.

With this theory, applying it with the necessary assumptions to fit this model, the intent is to calculate the neutral axis, the bending moment of this actuator and the caused deflection.

Starting with the simplest concept: a beam is every structure that has one axial dimension much bigger than the other two, so already with this premise, the actuator in question can be considered a beam.

One can define our actuator as a cantilever multilayered beam, because the actuator is fixed only at one end in the set-up used, it has five different layers and it is also possible to state that it is in pure bending (53).

Table 3.2: Legend of parameters used in the theoretical model.

Symbol	**Legend**	**Symbol**	**Legend**
L	Length of the beam	$\mathbf{E_i}$	Young's Modulus of the ith layer
$\mathbf{A_i}$	Cross-section area of the ith layer	$\mathbf{h_i}$	Thickness of the ith layer
ω_i	Width of the ith layer	υ_i	Poisson's Ratio of the ith layer
ρ_i	Density of the ith layer		

This is the analytical model constructed for the actuator in question. The end objective is to estimate the Young's Modulus theoretically, in order to obtain the theoretical value of the strain of the actuator.

If the widths are all 5x longer than the thicknesses, the Young's Modulus E_i is substituted by the effective Young's Modulus $\widehat{E}_i$, according to Equation 3.1:

$$\widehat{E}_i = \begin{cases} E_i & ,\omega_i < 5h_i \\ \frac{E_i}{1-\upsilon_i^2} & ,\omega_i \geq 5h_i \end{cases} \tag{3.1}$$

Table 3.3: Values of the thickness, width and Poisson's ratio of all the layers.

Material	$\mathbf{h_i}$ (mm)	ω_i (mm)	$5h_i$ (mm)	υ_i
Aluminum Foil (L2=L4)	0.055	14	0.275	0.33
P(VDF-TrFE-CTFE) (L3)	0.060	15	0.300	0.33
Kapton (L1)	0.057	15	0.285	0.34
Adhesive Tape (L5)	0.050	15	0.250	0.46

Considering the height of the bottom, z_0, as 0 and the height of the ith layer as z_i. Equation 3.2 calculates:

$$z_i = \Sigma_{j=1}^{i} h_i \tag{3.2}$$

Table 3.4: Values of Young's modulus (theoretical), cross-section area, density of each layer and total length.

Material	$\mathbf{E_i}$ (MPa)	$\mathbf{A_i}$ ($\mathbf{mm^2}$)	L (mm)	ρ_i ($\mathbf{g/cm^3}$)
Aluminum Foil (L2=L4)	1.82 E+3	2.86	52	2.7
P(VDF-TrFE-CTFE) (L3)	9.95 E+1	3.12		1.7
Kapton (L1)	8.46 E+2	2.964		1.42
Adhesive Tape (L5)	4.66 E+2	2.6		0.92

Table 3.3 and Table 3.4 sum up the relevant values of each layer, and Table 3.5 shows the results of these two equations when applied to the actuator in question.

Table 3.5: Values of z_i and $\widehat{E}_i$ for each layer.

ith **Layer**	z_i **(mm)**	$\widehat{E}_i$ **(MPa)**
z_5 **(Adhesive Tape)**	0.277	5.905 E+2
z_4 **(Alum. Foil)**	0.227	2.047 E+3
z_3 **(P(VDF-TrFE-CTFE)**	0.172	1.116 E+2
z_2 **(Alum. Foil)**	0.112	2.047 E+3
z_1 **(Kapton)**	0.057	9.570 E+2

With these values, it is possible to calculate the neutral axis of the actuator, based on the theory of multilayered beams (52), that is expressed as:

$$z_c = \frac{\Sigma_{i=1}^{n} \widehat{E}_i \omega_i (z_i^2 - z_{i-1}^2)}{2\Sigma_{i=1}^{n} \widehat{E}_i \omega_i (z_i - z_{i-1})} \tag{3.3}$$

The calculations go as follows in Table 3.6 (values were used in Pa and mm, respectively):

Table 3.6: Calculations to obtain the value of z_c.

ith **Layer**	$\widehat{E}_i\omega_i(z_i^2 - z_{i-1}^2)$ **(1)**	$\sum$**(1)**	$\widehat{E}_i\omega_i(z_i - z_{i-1})$ **(2)**	$\sum$**(2)**	z_c **(mm)**
z_5	2.232 E+8	1.194 E+9	4.429 E+8	4.514 E+9	0.132
z_4	6.288 E+8		1.576 E+9		
z_3	2.854 E+7		1.005 E+8		
z_2	2.663 E+8		1.576 E+9		
z_1	4.664 E+7		8.182 E+8		

The next step is to calculate the moment of inertia of the *ith* layer, with respect to the neutral axis of the actuator z_c, through Equation 3.4:

$$I_i = \int_i (z - z_c)^2 dA_i = \frac{1}{3}\omega_i[(z_i - z_c)^3 - (z_{i-1} - z_c)^3] \tag{3.4}$$

The moment of inertia is needed to calculate the bending stiffness $\overline{EI}$ - Equation 3.5 - and linear density $\overline{\rho A}$ – Equation 3.6 - of the actuator, here considered as a beam for the sake of simplicity.

$$\overline{EI} = \Sigma_{i=1}^{n} \widehat{E}_i I_i \tag{3.5}$$

$$\overline{\rho A} = \Sigma_{i=1}^{n} \rho_i A_i \tag{3.6}$$

As before, all the results from Equations 3.4, 3.5 and 3.6 were gathered in Table 3.7.

Table 3.7: Values of I_i, $\widehat{E}_i I_i$ and $\rho_i A_i$ for each layer. Value of the linear density and bending stiffness of the actuator.

ith **Layer**	I_i **(mm⁴)**	$\widehat{E}_i I_i$ **(Pa mm⁴)**	$\overline{EI}$ **(Pa mm⁴)**	$\rho_i A_i$ **(g/mm)**	$\overline{\rho A}$ **(g/mm)**
z_5	1.092 E-2	6.447 E+6	2.703 E+7	2392	2.730 E+4
z_4	3.680 E-3	7.531 E+6		7722	
z_3	3.561 E-4	3.976 E+4		5304	
z_2	1.947 E-3	3.986 E+6		7722	
z_1	9.429 E-3	9.024 E+6		4208.88	

As explained in Chapter 2, the Maxwell Stress effect is thought to be predominant in this dynamic. With equation 3.7 the Maxwell Stress S_m (%), is calculated, and subsequently with equation 3.8 the maximum stress on the x axis, σ_x can be obtained. From σ_x, the force exerted on the x axis by the active layer can be determined, using equation 3.9.

$$S_m = \frac{1}{2Y} \epsilon_0 \epsilon E^2 \tag{3.7}$$

$$\sigma_x = Y S_m \tag{3.8}$$

$$F_x = \sigma_x A \tag{3.9}$$

Based on the principles of mechanics of pure bending, the longitudinal stress σ_x, which is the maximum stress, relates to the bending momentum M on the y axis through the following equation 3.10:

$$\sigma_x = \frac{M z_c}{I} \Leftrightarrow M = \frac{\sigma_x I}{z_c} \tag{3.10}$$

With the value of M and with equation 3.11, it is possible to determine the maximum force exerted on the y axis, F_y.

$$F_y = \frac{M}{L} \tag{3.11}$$

Assuming a voltage of 700 V, which means an applied electric field of 11.67 MV/m:

Table 3.8: Obtained values for S_m , σ_x and, respectively, F_x.

S_m (%)	σ_x ($\mathbf{N/m^2}$)	$F_x = \sigma_x A$ (N)	M (N m)	F_y (N)
0.0545	5.420 E+4	1.690 E-1	1.080 E-5	2.080 E-4

From the literature, in a cantilever beam fixed on one side and with a force being applied at the tip of the beam, the value of the maximum deflection can be calculated through:

$$z_m = \frac{WL^3}{3EI} \tag{3.12}$$

4 Results and Discussion

4.1. Load-Displacement Graphics

This Chapter reports the experiments' results and focuses on the experimental validation of the model, as described in Chapter 3.

For each sample (60PVDF, 60PVDFHalf and 130PVDF), three series of tests with four different voltages were realized. The results are showed in Figure 4.1. Since the load was measured in intervals of 0.5 mm in a displacement of 4 mm, each test is composed by 8 points (load, displacement). All the points obtained for 0 MV/m, 8.33 MV/m, 11.67 MV/m and 15 MV/m were approximated by linear regression lines.

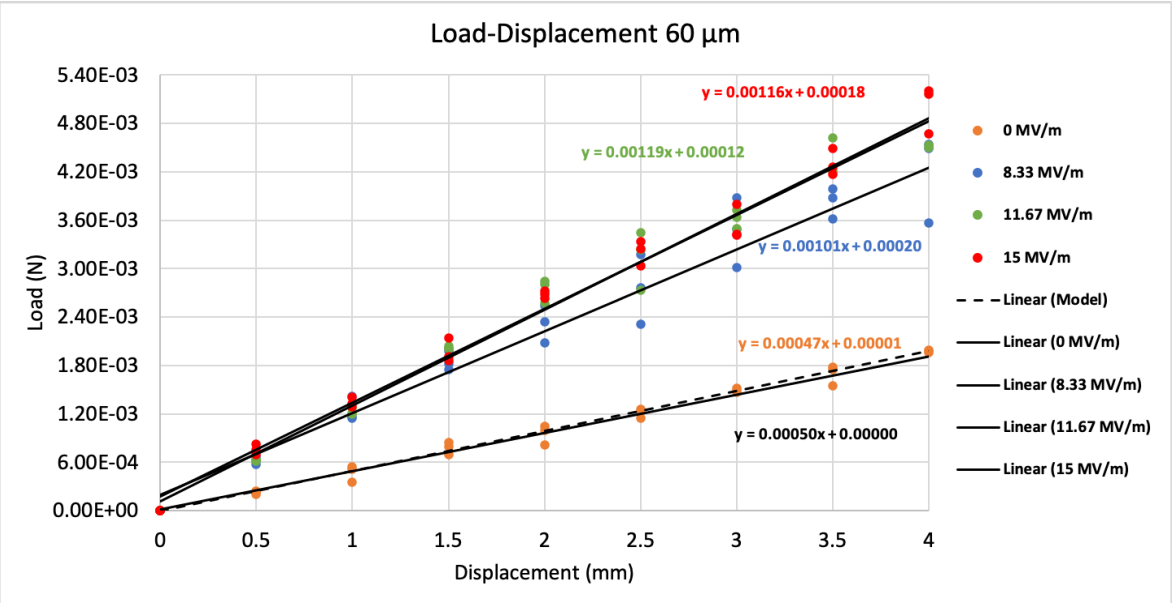

(a)

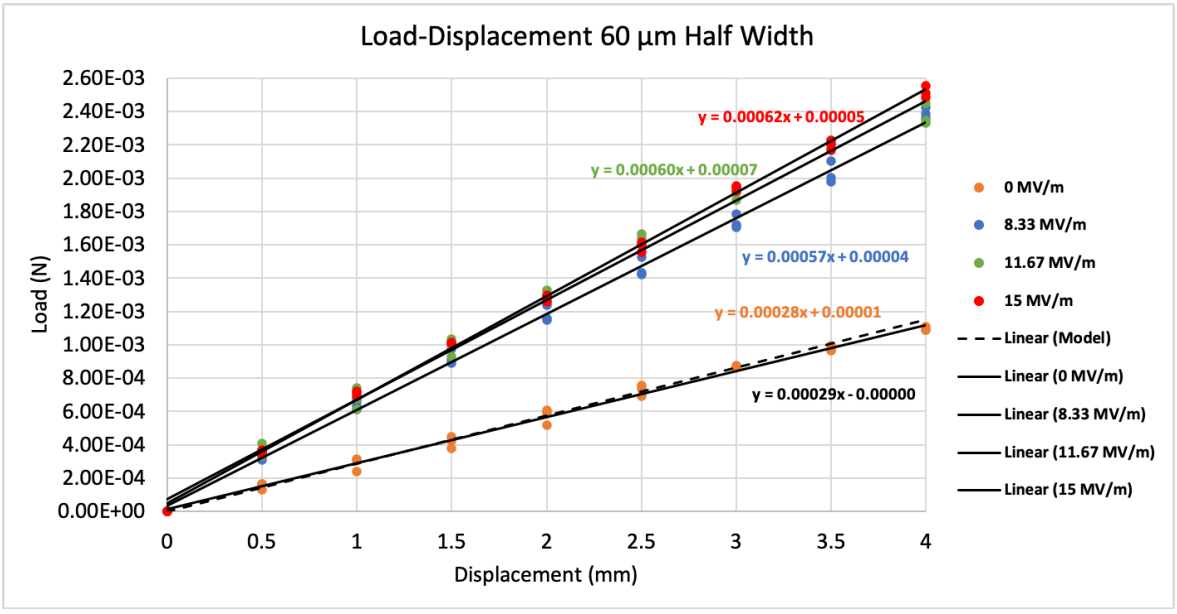

(b)

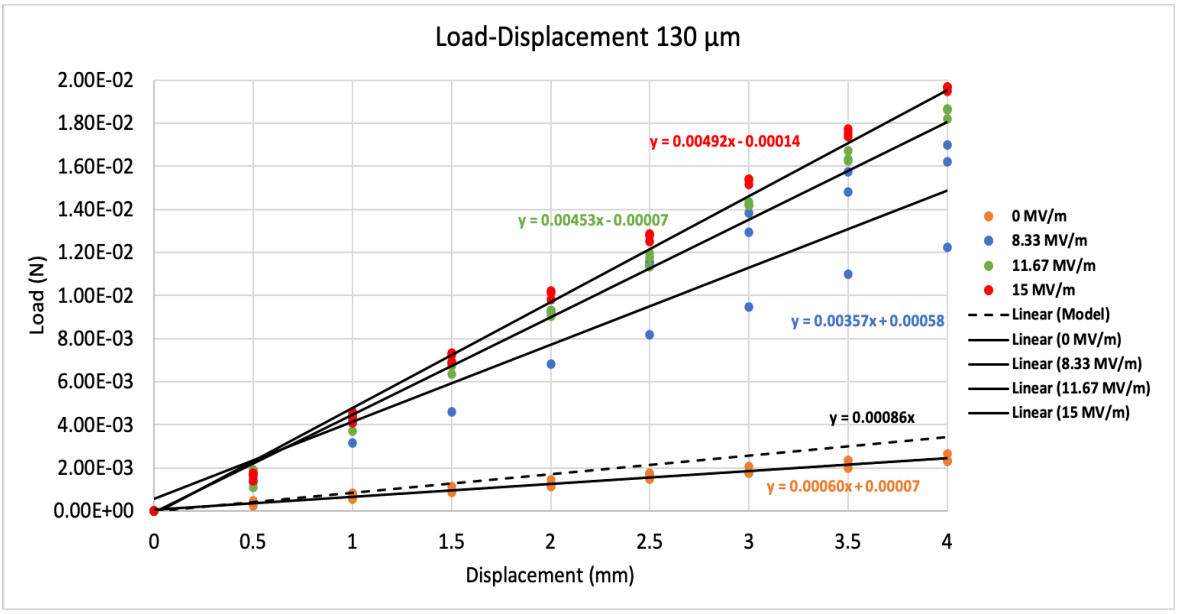

(c)

Figure 4.1: Load-Displacement graphic of the three tests for each voltage value. a) 60 μm. b) 60 μm Half Width. c) 130 μm.

Linear regression lines follow the general equation:

$$y = mx + b \tag{4.1}$$

In which the (x, y) points are known, m is the slope value, and b is the value of y in the origin, that is $(0, b)$. Table 4.1, Table 4.2 and Table 4.3 indicate the values of these coefficients for each case.

Table 4.1: m and b coefficients for the linear regression lines in sample 60PVDF.

Voltage	m	b	R^2
Model	5.00 E-4	0	1
0 V	4.70 E-4	1.00 E-5	0.9940
500 V	1.01 E-3	2.00 E-4	0.9924
700 V	1.19 E-3	1.20 E-4	0.9944
900 V	1.16 E-3	1.80 E-4	0.9955

Table 4.2: m and b coefficients for the linear regression lines in sample 60PVDFHalf.

Voltage	m	b	R^2
Model	2.90 E-4	0	1
0 V	2.80 E-4	1.00 E-5	0.9989
500 V	5.70 E-4	4.00 E-5	0.9991
700 V	6.00 E-4	7.0 E-5	0.9973
900 V	6.20 E-4	5.0 E-5	0.9994

Table 4.3: m and b coefficients for the linear regression lines in sample 130PVDF.

Voltage	m	b	R^2
Model	8.60 E-4	0	1
0 V	6.00 E-4	7.00 E-5	0.9973
500 V	3.57 E-3	5.80 E-4	0.9837
700 V	4.53 E-3	-7.00 E-5	0.9942
900 V	4.92 E-3	-1.40 E-4	0.9962

Comparing equation 3.12 from Section 3.2 with the Load-Displacement graphics and rearranging the equation, it is possible to infer that **the value of the Bending Stiffness (EI) can be obtained from the slope m (Figure 4.2)**.

Since the Model plot was taken from the theoretical model deducted in Section 3.2, this means that **the actuator samples can be represented as cantilever beams.**

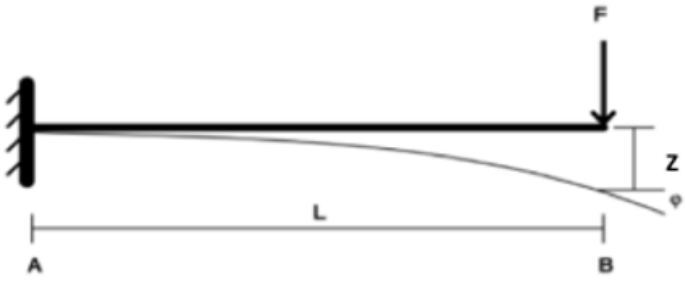

$$z = \frac{FL^3}{3EI} \Leftrightarrow F = \frac{3EI}{L^3} z$$

Figure 4.2: Scheme and equation of the relation between the displacement and the force produced.

If these actuators behave like a cantilever beam, the load produced is a reaction to the displacement. This means that if there is no displacement ($x = 0$) the reaction load should be also be zero. Therefore, the straight lines in Figure 4.1 shifted downwards of a quantity equal to parameter b, now passing through the origin. Figure 4.3 shows the results.

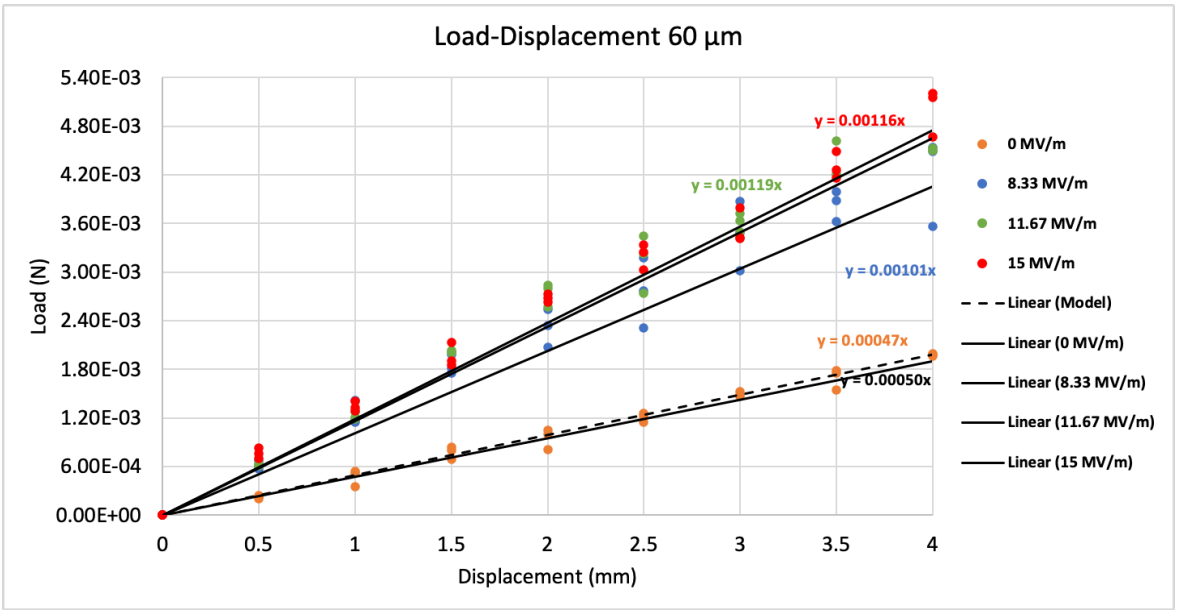

(a)

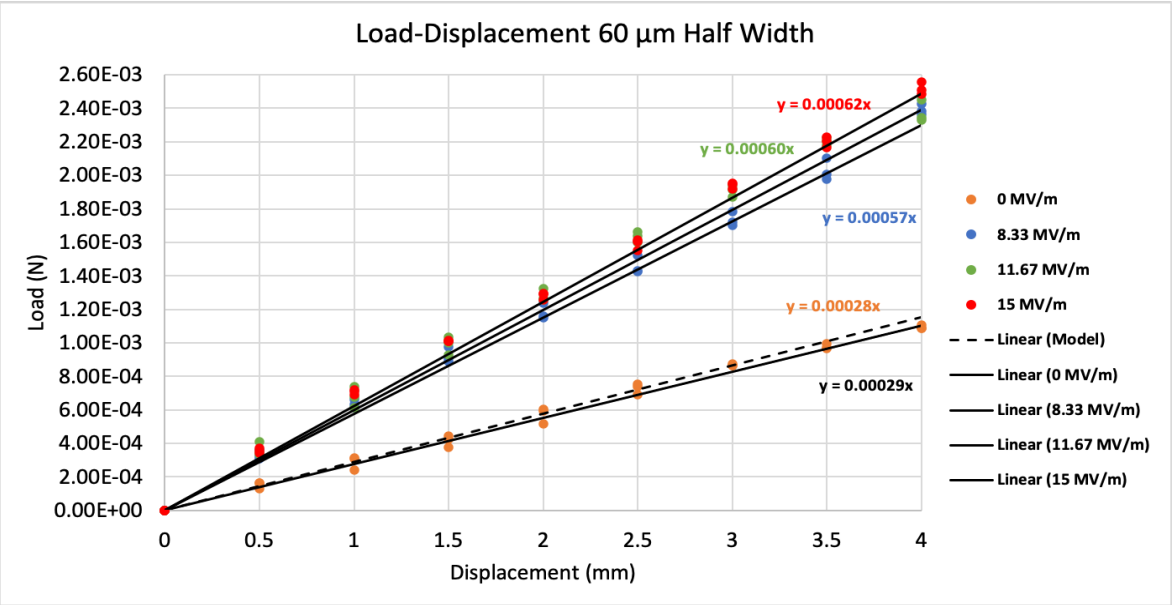

(b)

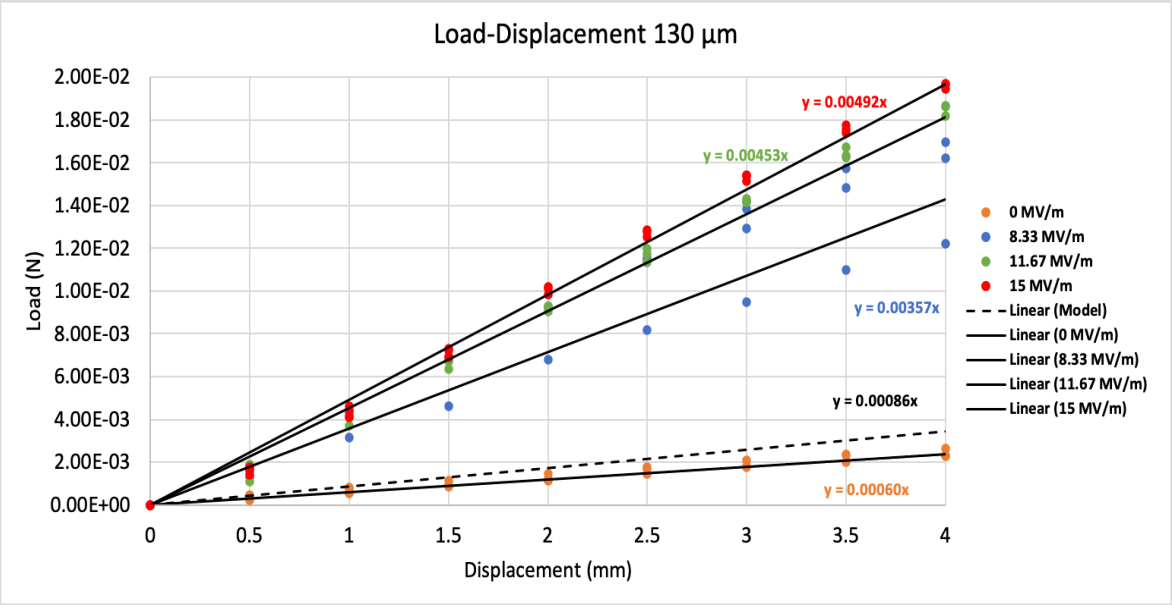

(c)

Figure 4.3: Load-Displacement graphic of the three tests for each voltage value with the respective linear regression lines shifted of a quantity equal to the corresponding b quantity. a) 60 μm. b) 60 μm Half Width. c) 130 μm.

The 0 MV/m plot (orange) matches the Model plot (dashed) for all samples, except in the 130PVDF sample were the discrepancy is more significant. This can be due to an imperfection in the layering of this sample or in the preparation of the test. Therefore, **the samples can be validated as cantilever beams**.

With this in mind, analyzing the individual plots from the three samples, the slopes increase with a higher electric field, meaning **the EI increases with an increase of the electric field (Table 4.4).**

Table 4.4: Bending Stiffness values corresponding to 0 MV/m, 8.33 MV/m, 11.67 MV/m and 15 MV/m for the three samples.

Sample	**0 MV/m [N/mm]**	**8.33 MV/m [N/mm]**	**11.67 MV/m [N/mm]**	**15 MV/m [N/mm]**
60PVDF	4.70 E-4	1.01 E-3	1.19 E-3	1.16 E-3
60PVDFHalf	2.80 E-4	5.70 E-4	6.00 E-4	6.20 E-4
130PVDF	6.00 E-4	3.57 E-3	4.53 E-4	4.92 E-3

Table 4.5: Percent of stiffness increase of the three samples, with respect to the stiffness of each sample at 0 V.

	ΔStiffness [500 V/0 V[	**ΔStiffness [700 V/0 V[**	**ΔStiffness [900 V/0 V[**
60PVDF	+114.89%	+153.19%	+146.81%
60PVDHalf	+103.57%	+114.28%	+114.29%
	ΔStiffness [1083 V/0 V[	**ΔStiffness [1516 V/0 V[**	**ΔStiffness [1950 V/0 V[**
130PVDF	+495%	+655%	+720%

The stiffening properties of an actuator are evaluated analyzing the difference in the slope of load-displacement plots between a 0 V test and a test with applied voltage. Comparing these three samples, the 60PVDF and 60PVDFHalf perform similarly, while **the 130PVDF sample, for the applied electric field, produces a load at least 3x higher.**

A statistical analysis of the results was also realized: the average load of each point and the corresponding standard deviation were calculated, by means of Excel® formulas, and the results are plotted in Figure 4.4.

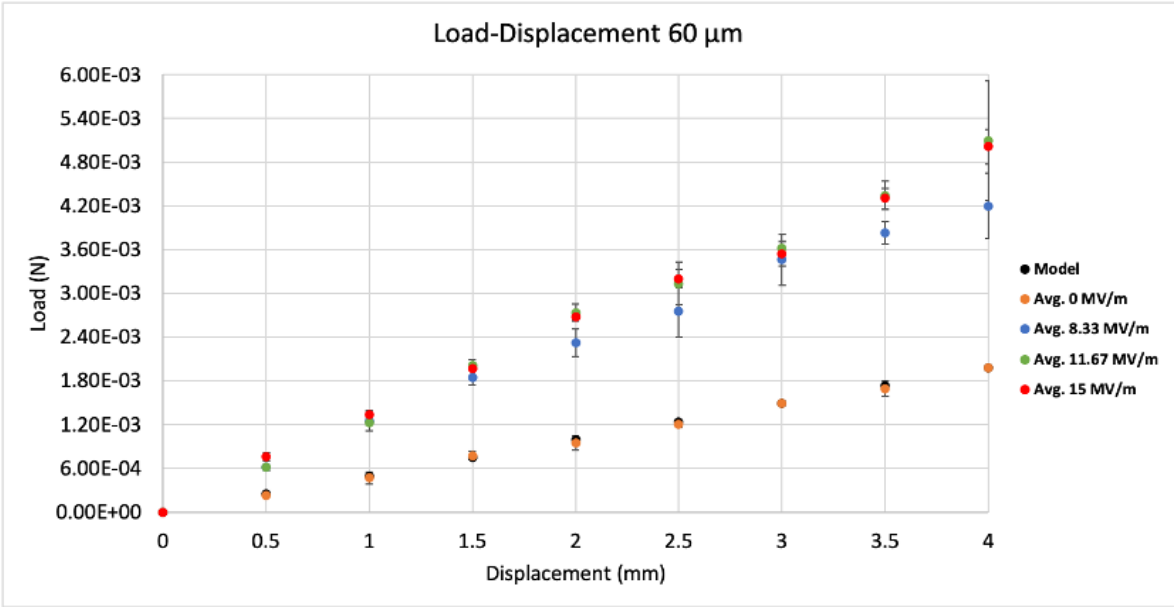
Load-Displacement 60 µm
Load (N)
6.00E-03
5.40E-03
4.80E-03
4.20E-03
3.60E-03
3.00E-03
2.40E-03
1.80E-03
1.20E-03
6.00E-04
0.00E+00
0
0.5
1
1.5
2
2.5
3
3.5
4
Displacement (mm)
Model
Avg. 0 MV/m
Avg. 8.33 MV/m
Avg. 11.67 MV/m
Avg. 15 MV/m

(a)

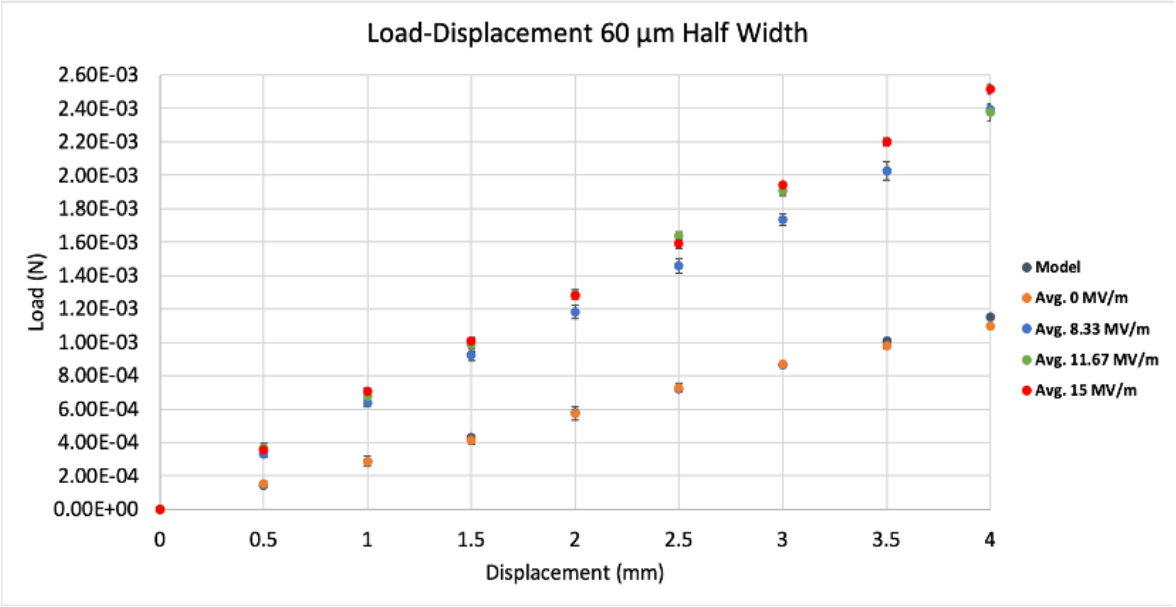
Load-Displacement 60 µm Half Width
Load (N)
2.60E-03
2.40E-03
2.20E-03
2.00E-03
1.80E-03
1.60E-03
1.40E-03
1.20E-03
1.00E-03
8.00E-04
6.00E-04
4.00E-04
2.00E-04
0.00E+00
0
0.5
1
1.5
2
2.5
3
3.5
4
Displacement (mm)
Model
Avg. 0 MV/m
Avg. 8.33 MV/m
Avg. 11.67 MV/m
Avg. 15 MV/m

(b)

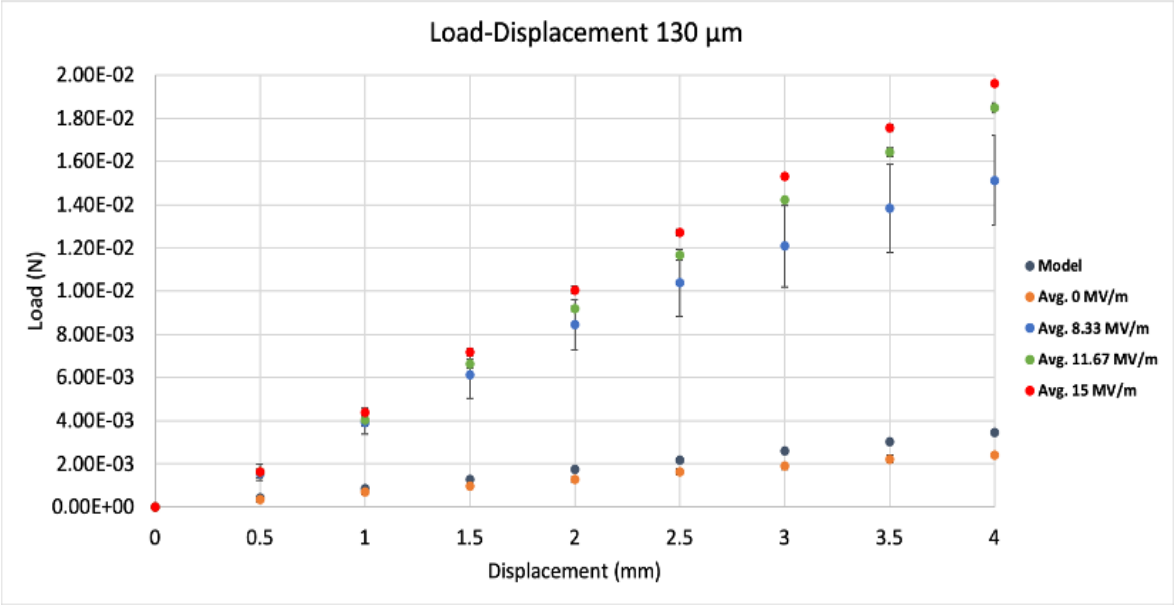

(c)

Figure 4.4: Calculated average load of each point with corresponding standard deviation. a) 60 μm. b) 60 μm Half Width. c) 130 μm.

From this, it is clear **the thickness of the active material plays a major influence on the load produced by the actuator, increasing it, at least twofold**.

However, it is expectable that this relationship would reach an optimal point (57). The electric field is calculated by $E = V/d$, in which V is the voltage value and d is the thickness value. If there is a need to increase the load produced, doing it by increasing the thickness means applying a higher voltage in order to not decrease the electric field. This is not doable for a human-friendly device.

4.2. Electric Field vs. Tip Displacement

In the deflection tracking test, the data from the video was converted and filtered and the final results are presented in the form of displacement-time plots (Figure 4.5). A total of 9 tests were performed, 8.33 MV/m, 11.67 MV/m and 15 MV/m for each sample. Note that the remaining plots of the deflection tracking tests that are not presented here, can be found in the appendix I.

The plots presented some noise in the beginning due the time the samples take to stabilize after activation, so the graphics were corrected. Therefore, the accuracy in reasonable but the general behavior is coherent with the load-displacement tests, **meaning the displacement increases with a higher electric field applied**.

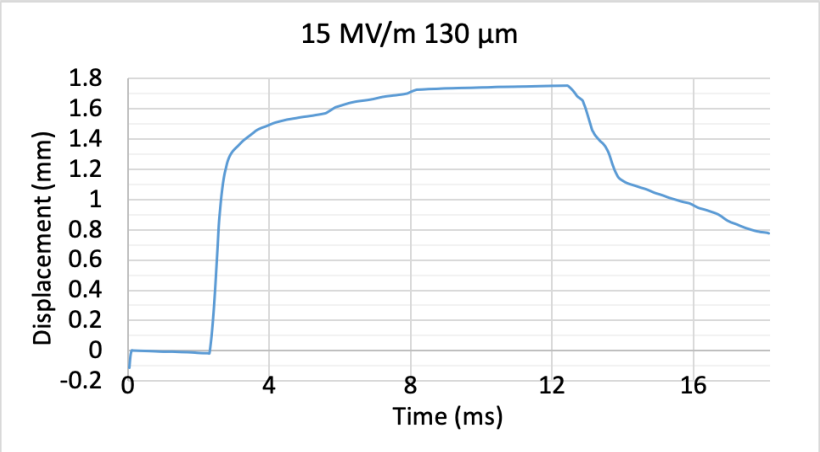

Figure 4.5: Displacement-time plot for the 130PVDF sample under a 15 MV/m electric field.

For instance, the maximum displacement values, determined with the "MAX()" formula from Excel®, also confirm this influence of the electric field (Table 4.6). Moreover, it is also possible to highlight the **dominance of the 130PVDF sample, with values, at least, 2 times greater.**

Table 4.6: Maximum deflection values obtained from the deflection tracking tests.

Maximum Displacement (mm)	**60PVDF**	**60PVDFHalf**	**130PVDF**
8.33 MV/m	0.676mm	0.461mm	1.221mm
11.67 MV/m	0.704mm	0.606mm	1.277mm
15 MV/m	0.738mm	0.727mm	1.752mm

4.3. Blocking Force vs. PVDF Thickness

To measure the blocking force in this test, a square signal of different voltages (Figure 4.6) was applied consecutively for 10 seconds with a few seconds of interval in

between, as exemplified in Figure 4.7. In some tests, the signal resulted in 5 peaks, while in others resulted in 4 peaks.

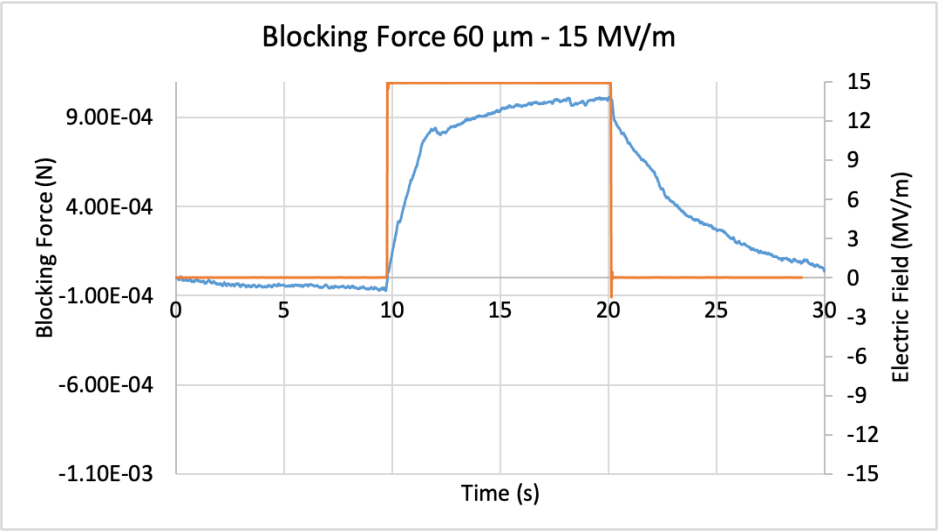

(a) 60PVDF at 15 MV/m.

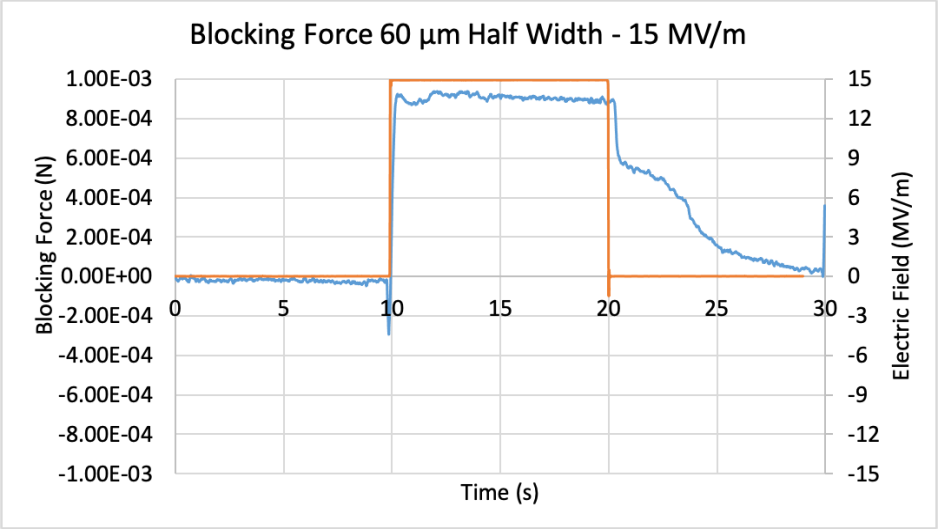

(b) 60PVDFHalf at 15 MV/m.

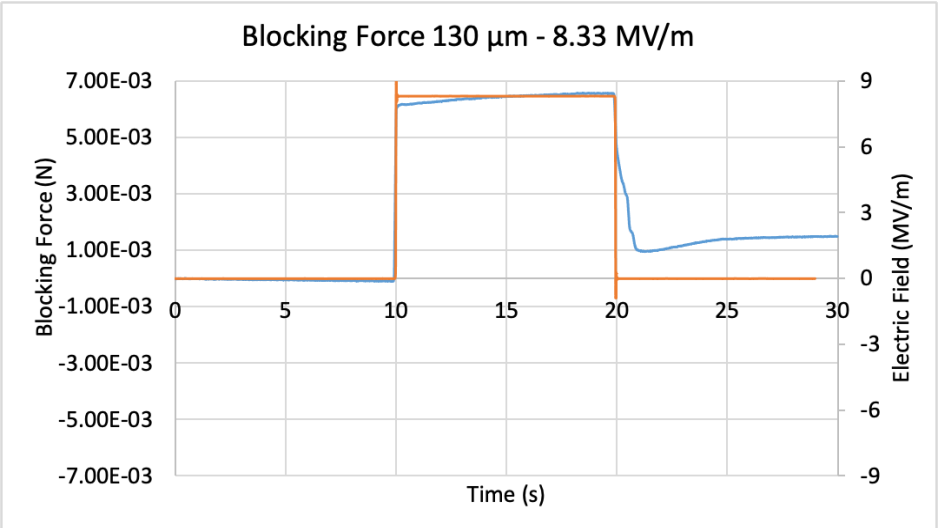

(c) 130PVDF at 8.33 MV/m.

Figure 4.6: Single Blocking Force test.

The remaining graphics of the blocking force tests can be found in the appendix.

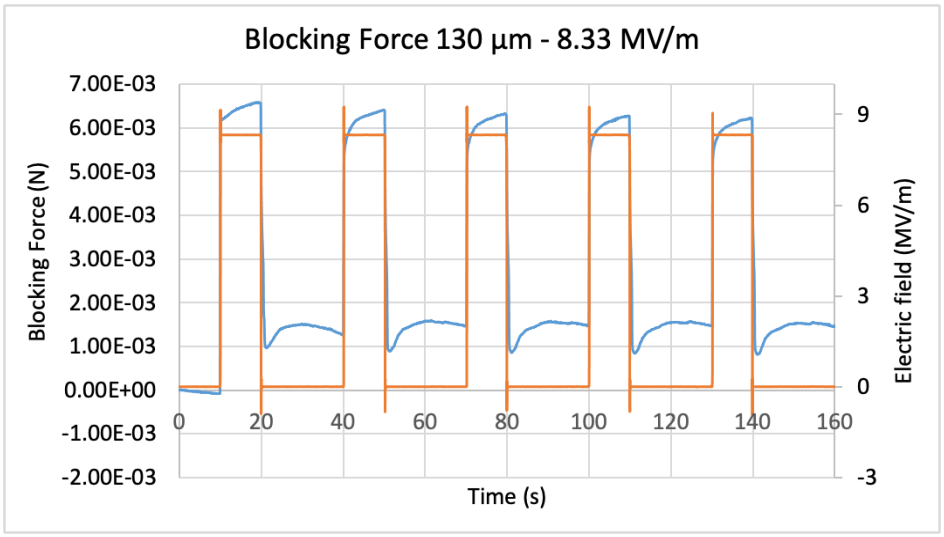

Figure 4.7: Data recorded from a blocking force test, with the 130PVDF sample.

With this type of test is it possible to showcase repeatability, meaning the electroactive behavior of the PVDF can be further validated. However, not all the peaks are similar with the first one always being higher than the others, which can be due to a threshold the actuator breaks upon the initial activation, and in the following peaks the blocking force values do not reach zero even without the electric signal, that can be a result of the hysteresis present in the material, from its nonlinear behavior.

The following procedure was performed in Excel®, and was applied to each blocking force data set:

1. Get the maximum value of each of the 4 or 5 peaks;
2. Obtain the average of these 4 or 5 values;
3. Plot and rearrange for voltage applied, for each sample actuator.

The resulting graphics are in Figure 4.8.

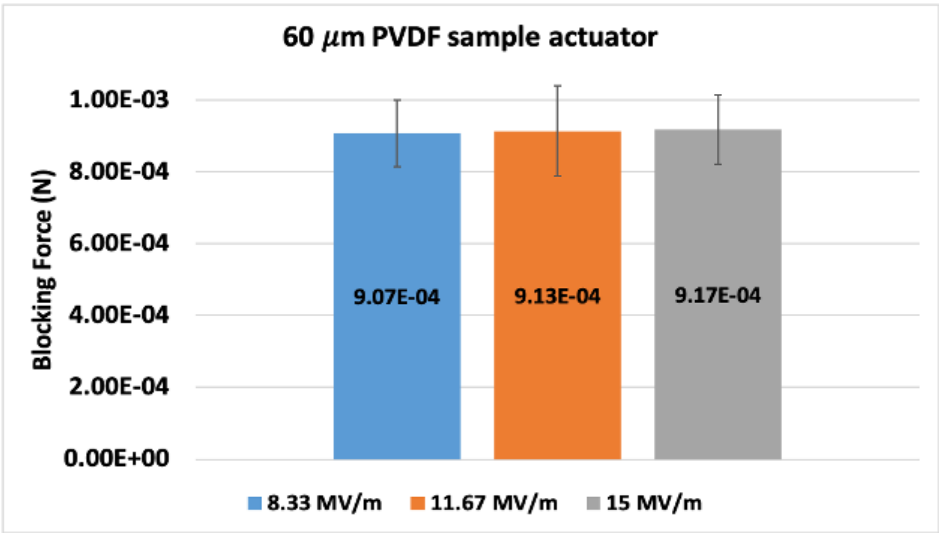

(a)

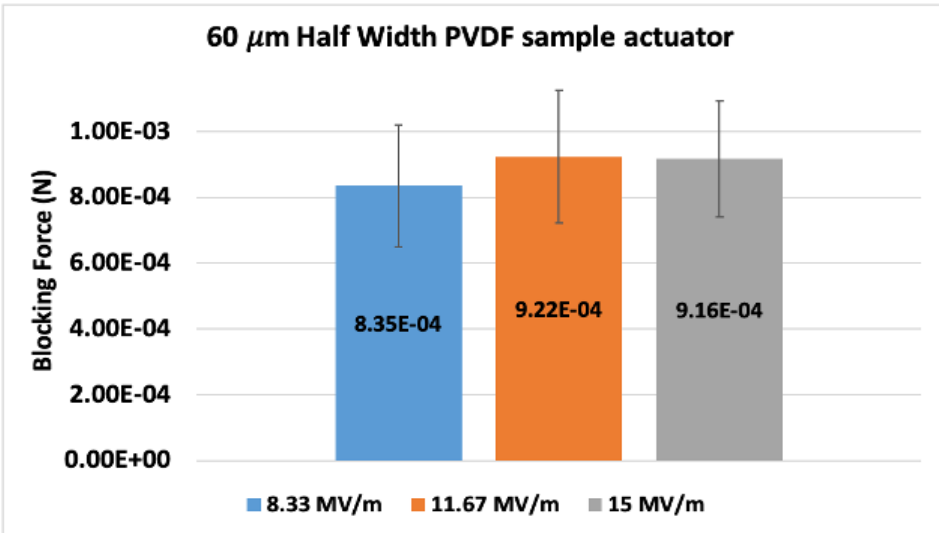

(b)

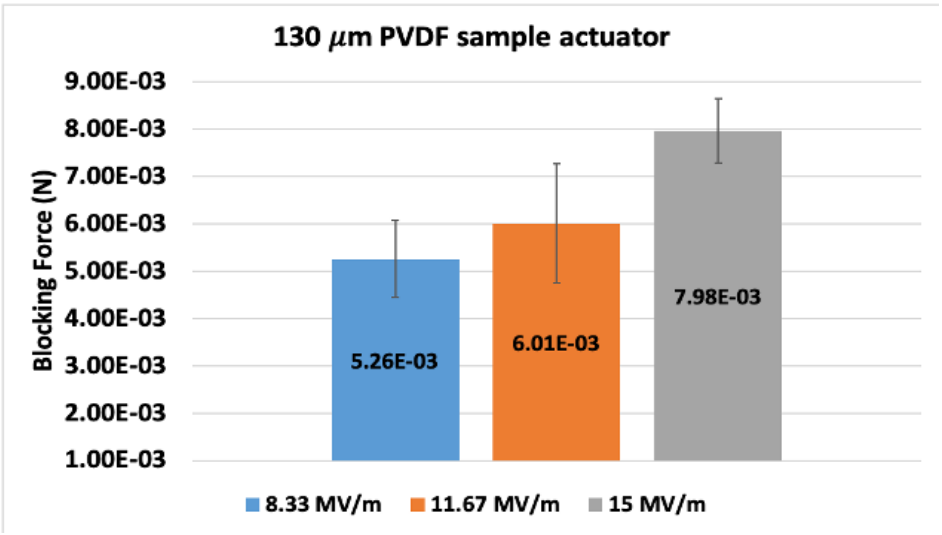

(c)

Figure 4.8: Graphics of the average blocking force of the 3 actuators and corresponding standard deviations. a) 60 μm. b) 60 μm Half Width. c) 130 μm.

The linear relationship between electric field and force is once again confirmed with **all the samples obtaining a higher blocking force with an increase in the electric field applied.**

Similarly to the results from the load-displacement graphics, the 60PVDF and 60PVDFHalf behave almost in the same way, which leads to the conclusion that **the width of the actuator itself does not influence the final performance.** Moreover, the difference between the 60μm samples and the 130μm sample is clear, with the latter having a blocking force an order of magnitude greater. All the relative standard deviations are presented below, in Table 4.7:

Table 4.7: Relative standard deviation of the blocking force tests.

Relative Standard Deviation (%)	**8.33 MV/m**	**11.67 MV/m**	**15 MV/m**
60PVDF	4.40%	12.75%	3.18%
60PVDFHalf	38.64%	12.75%	3.18%
130PVDF	15.42%	20.97%	8.50%

5 Simulation - COMSOL Multiphysics®

COMSOL Multiphysics® is a multi-purpose simulation software for modeling designs, devices and processes in all fields of engineering. Aside from the "platform product" which is the main interface of work, it offers a series of add-on modules of different physics such as Electromagnetics, Structural Mechanics, Acoustics, Chemical Engineering, Fluid Flow and Heat Transfer (www.comsol.com/products).

The programme includes infinite features, in terms of geometry, physics involved, materials used and other constraints of the experiment, to help recreate, as best as possible, several environments and set-ups where the actuator, in this case, is supposed to perform and allows an insight almost as accurate as a real test. Mainly, the software allows for a better understanding, prediction and optimization of behaviors and processes, enabling a total personalization of parameters like geometry, materials, constraints of the model, etc. Furthermore, it is compatible with MATLAB®, AutoCAD®, SolidWorks®, and others.

5.1. Objective

The simulation was built to predict and analyse the electromechanical behavior of the actuator. All the steps taken to construct a physically-correct simulation are described as well as all the parameters chosen. Moreover, taking full advantage of the software's potential, namely its ability to perform innumerous tests in various conditions without the worry of causing material damage or wear, certain parameters were changed to assess its influence in the material's behavior, such as thickness or Young's Modulus of the outer passive layers of the actuator.

5.2. The Model Builder

The user-friendly interface is comprised of a standardized model-builder to apply in every simulation: It starts with a *Model Wizard* to choose the dimension of the geometry, the physics interfering in the simulation and finally the type of study.

Three geometries were built in AutoCAD® with dimensions similar to Table 3.1 and the following remaining dimensions:

Table 5.1: Dimensions of actuator's geometry.

Material	Length (mm)	Thickness (mm)	Width (mm)
ABS - Clamps	10	10	15
Kapton Tape	62	0.057	15/8
Aluminum Foil		0.055	14/7
P(VDF-TrFE-CTFE)		0.060/0.130	15/8
Aluminum Foil		0.055	14/7
Adhesive Tape		0.050	15/8
ABS - Clamps	10	10	15

When imported to the simulation software the actuators would adopt this visual look, similar to Figure 5.1 .

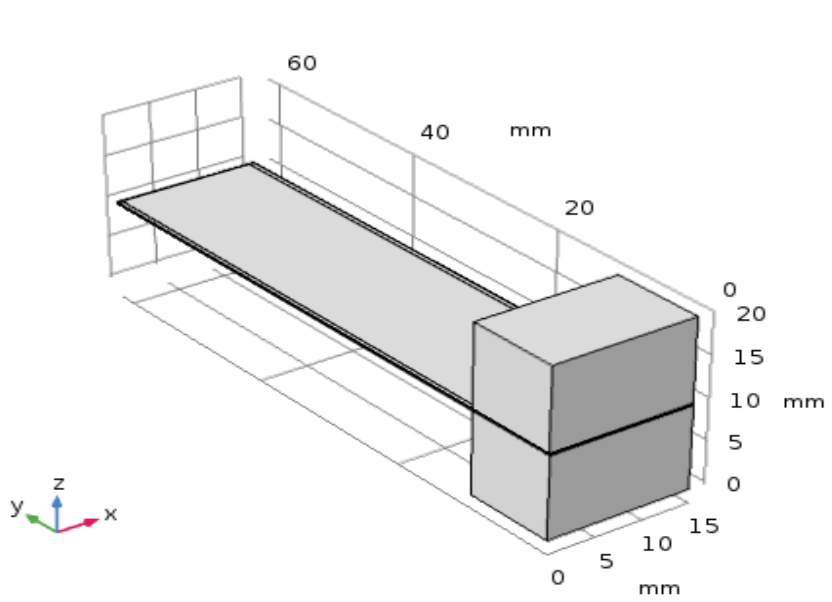

(a)

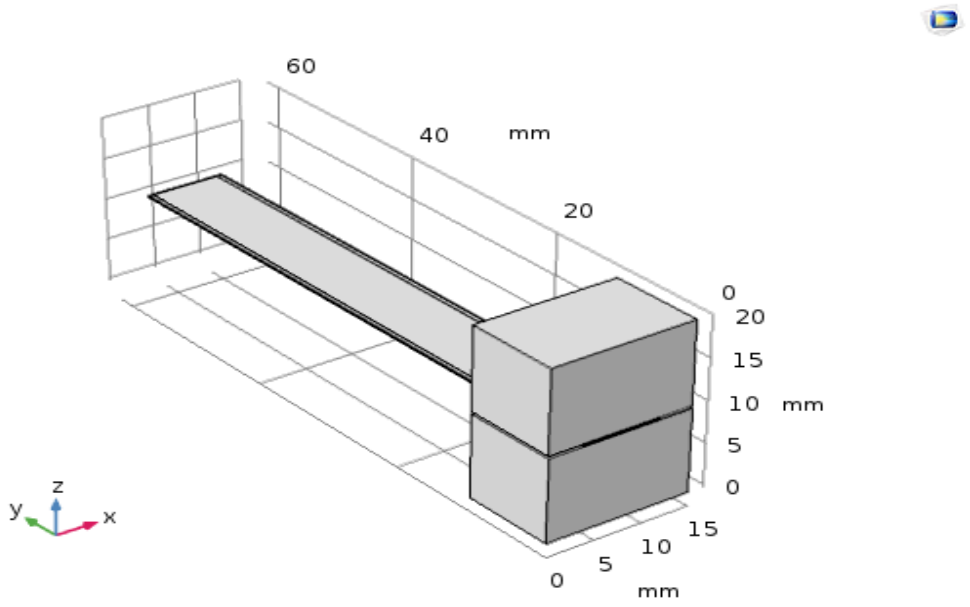

(b)

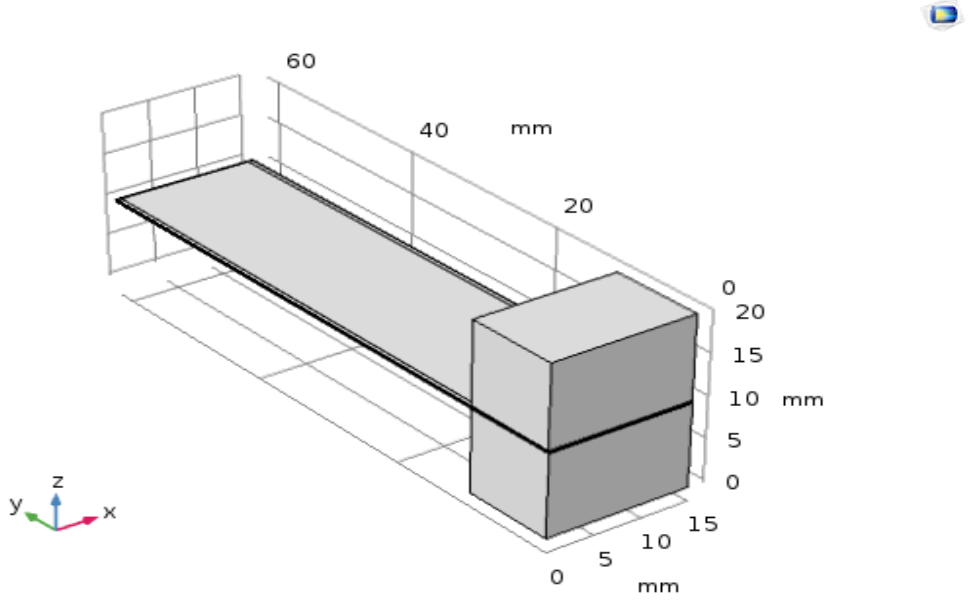

(c)

Figure 5.1: Sample's geometry imported to COMSOL Multiphysics.

In the next step, material properties were assigned to each of the five layers, directly from the material library included in the software. According to the physics chosen, certain properties must be defined, as shown in Table 5.1. However, for more accuracy, the Young's Modulus values were changed to the ones obtained experimentally, as explained in the previous section.

Table 5.2: Material properties of each component of the actuator.

Material	Density (g/cm3)	Young's Modulus (Pa)	Poisson's Ratio	Dielectric Constant
Kapton (Tape)	1.42	8.46E+08	0.34	3.5
Aluminum (Electrodes)	2.70	1.82E+09	0.33	10.3
PVDF P(VDF-TrFE-CTFE)	1.78	9.95E+07	0.33	45
Polyethylene (Adhesive Tape)	0.92	4.66E+08	0.46	1.2
ABS (Clamps)	1.11	2.05E+09	0.35	3.10

For this simulation, the physics chosen were *Solid Mechanics* and *Electrostatics*. When coupled together they create the *Multiphysics* node of *Electromechanical Forces*, meaning this simulation allows to study the behavior of the actuator when influenced by the interaction of these two physics.

In the *Solid Mechanics* node, besides from the default specifics (*Linear Elastic Material, Free, Initial Values*) that are automatically added, a *Fixed Constraint* was selected for the side faces of one end, which mimic the fixed end of the actuator. Nothing else was changed as the main features are already appropriate for the type of physics chosen.

Figure 5.2 displays the *Model Builder* showing the *Geometry* node with the imported geometry, the *Materials* node with each material assigned to the corresponding layer and the *Solid Mechanics* node with all the specifications already explained.

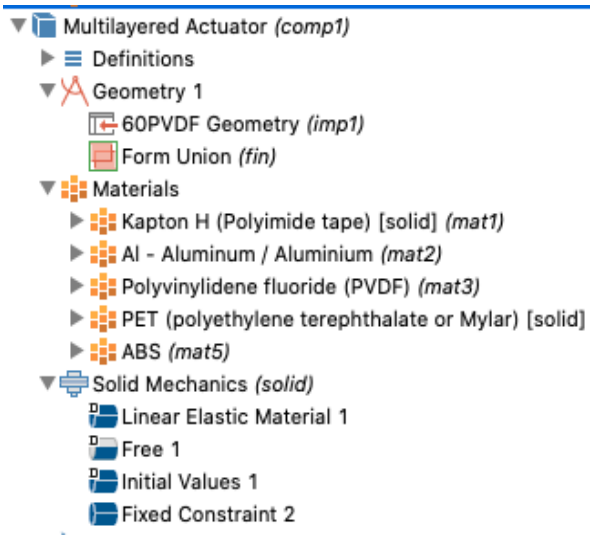

Figure 5.2: Segment of the model builder showing the Geometry node, Materials node and Solid Mechanics node.

For the *Electrostatics* node, a terminal node was added to each electrode present, one denominated as *Ground* and the other as *Terminal* 500 V, 700 V or 900 V, since the value is easily changed in the *Model Builder*. Aside from the default specifics (*Charge Conservation Solid, Zero Charge, Initial Values*) a *Charge Conservation Piezoelectric* was added and assigned only to the PVDF-TrFE-CTFE layer.

Although the *Piezoelectric Material* and *Charge Conservation Piezoelectric* node duo is used together and usually coupled with the *Piezoelectric Effect Multiphysics* node, for this case, the *Electromechanical Forces* node was used instead in the Multiphysics, and the *Piezoelectric Material* node was not added in the *Solid Mechanics* node. This forces the simulation to assume the PVDF layer as normal dielectric, rather than a piezoelectric, which is correct since PVDF-TrFE-CTFE is not piezoelectric.

The *Mesh* node is what enables the simulation software to discretize the geometry in question into small elements using the Finit Elements theory, allowing for a better analyse of the behavior of the actuator, throughout the whole geometry. In this case, a physics-controlled finer mesh was chosen, which consists of a free tetrahedral geometry.

A stationary study was performed, meaning only the results showed only the final displacement value.

Figure 5.3 displays the *Model Builder* with the *Electrostatics* node, the *Multiphysics* node, the *Mesh* node and the *Study* node showing all the specifics mentioned earlier.

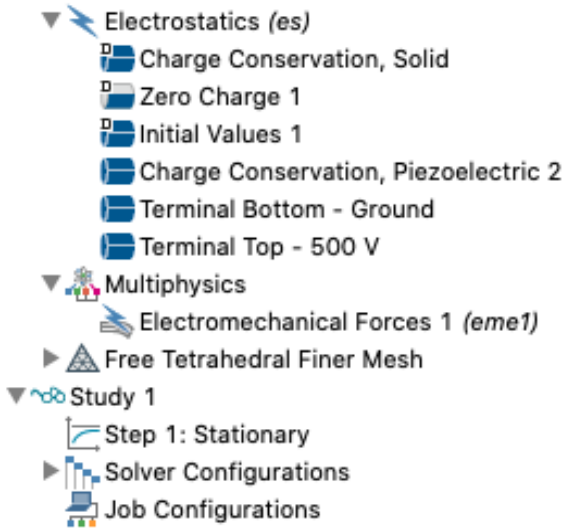

Figure 5.3: Segment of the model builder showing the Electrostatics node, Multiphysics node, Mesh node and the Study node.

The simulation was then executed with the 60PVDF and 60PVDFHalf sample for 500 V, 700 V and 900 V, while with the 130PVDF sample, the values of voltage used were 1083 V, 1516 V and 1950 V.

With this in mind, the end objective is to compare the values of displacement obtained with the simulation and experimental tests and draw conclusion on the validation of the model built.

5.3. Simulation Results

The three samples (60PVDF, 60PVDFHalf, 130PVDF) were simulated and Figure 5.4. shows the graphic result of the simulation, were the maximum displacement value is defined and a color scale is presented, enabling a better understanding of the impact of the electric field throughout the whole geometry, **confirming, in fact, the bending of the structure.**

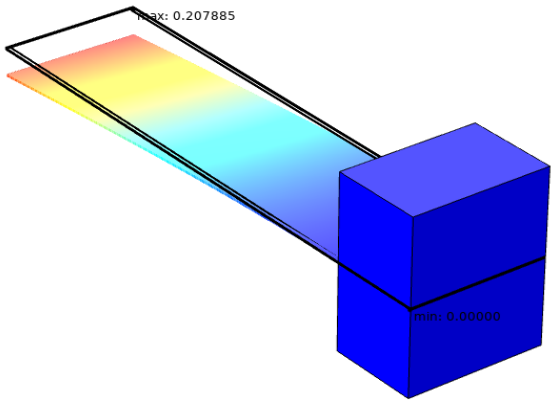

Figure 5.4: 3D Graphic result of the simulation.

In order to compare and observe the influence of the electric field in the deflection of the actuator, Figure 5.5 shows the simulated deflection along the actuator's length for different values of voltage. The data was taken from the results obtained with the simulation.

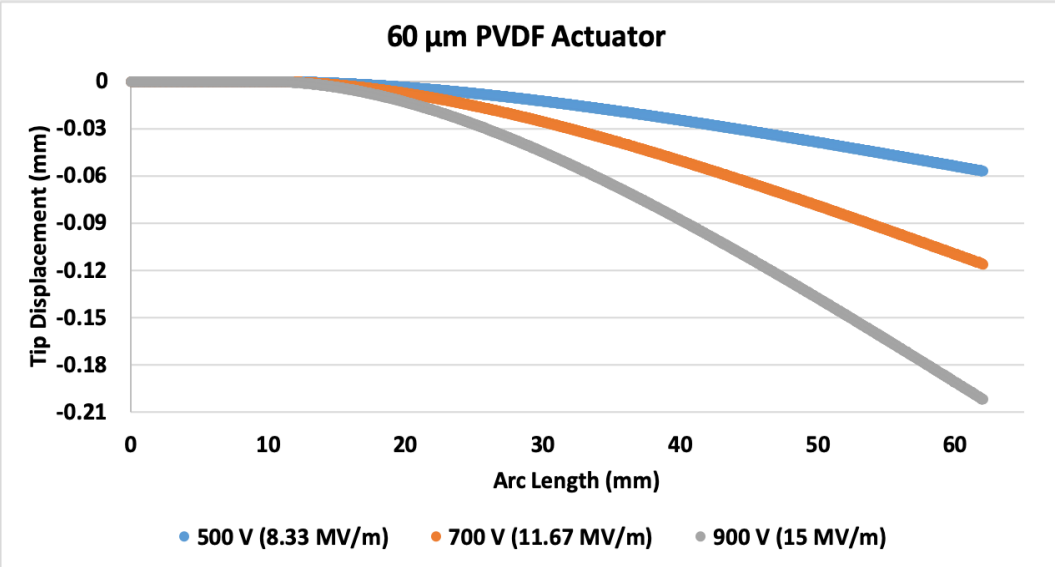

(a)

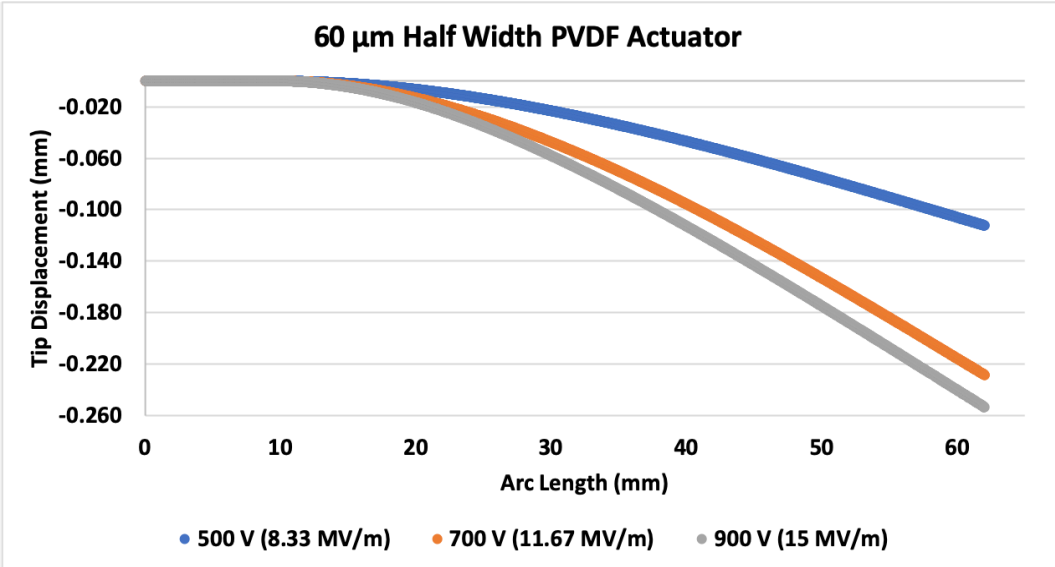

(b)

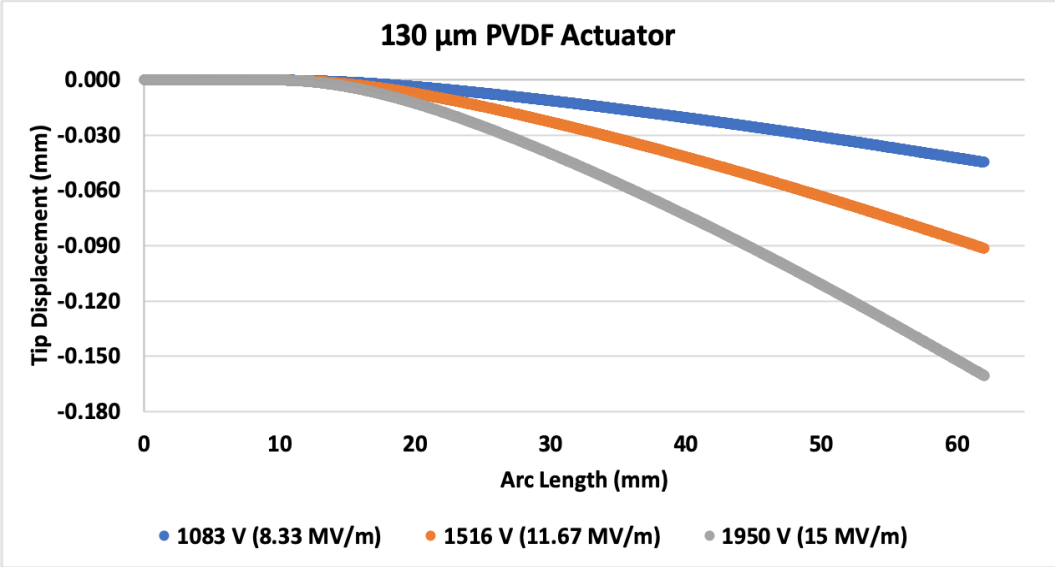

(c)

Figure 5.5: Simulated deflection along the actuator for electric fields of 8.33, 11.67 and 15 MV/m. a) 60 μm. b) 60 μm Half Width. c) 130 μm.

The final values of displacement under a certain voltage (500 V, 700 V and 900 V or 1083 V, 1516 V and 1950V) are shown in Table 5.3. Moreover, **the model is coherent in the increasing of displacement with the increase of electric field applied.**

Table 5.3: Obtained values of maximum displacement in COMSOL Multiphysics simulation.

	500 V	**700 V**	**900 V**
60PVDF	0.0569 mm	0.1160 mm	0.2019 mm
60PVDFHalf	0.1122mm	0.2283 mm	0.2533 mm
	1083 V	**1516 V**	**1950 V**
130PVDF	0.0446 mm	0.0914 mm	0.1605 mm

In order to validate the simulation, the author compared the results obtained with the deflection tracking test and the simulation. Figure 5.6 displays the comparison between the two tests, in all three actuators.

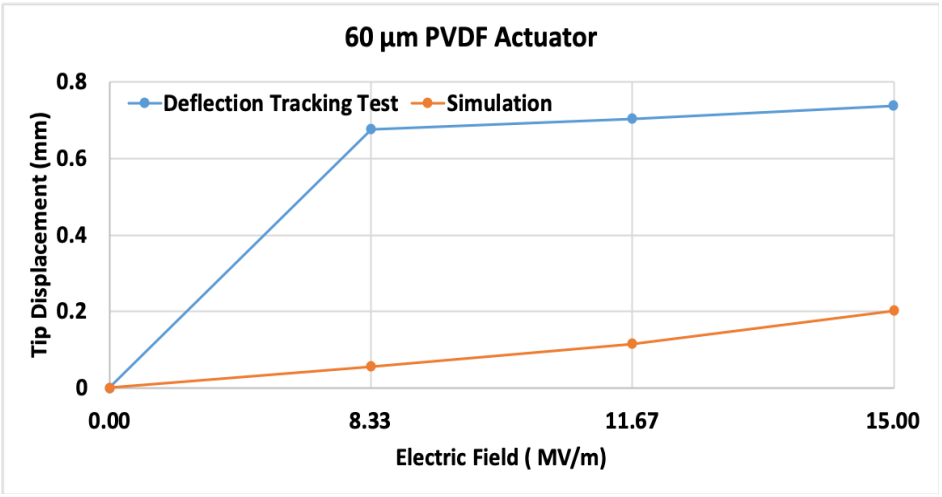

(a)

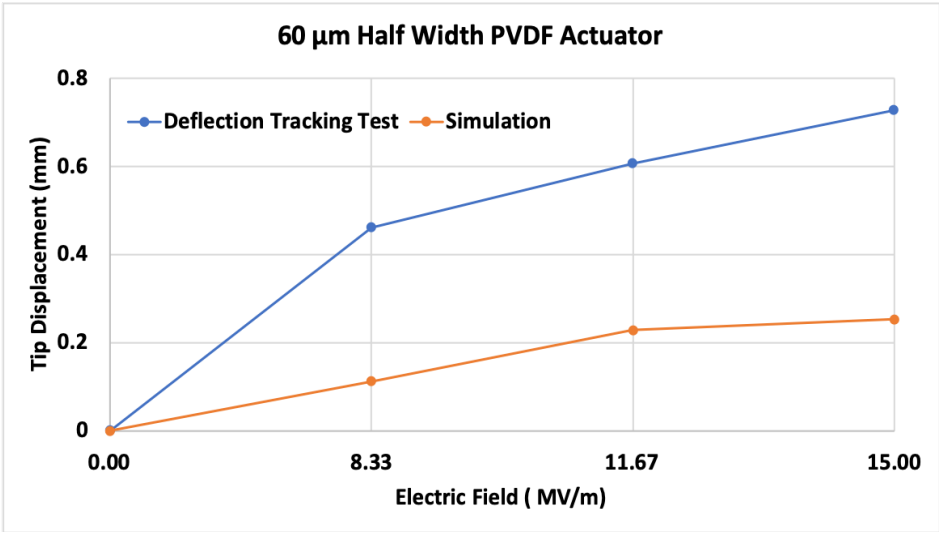

(b)

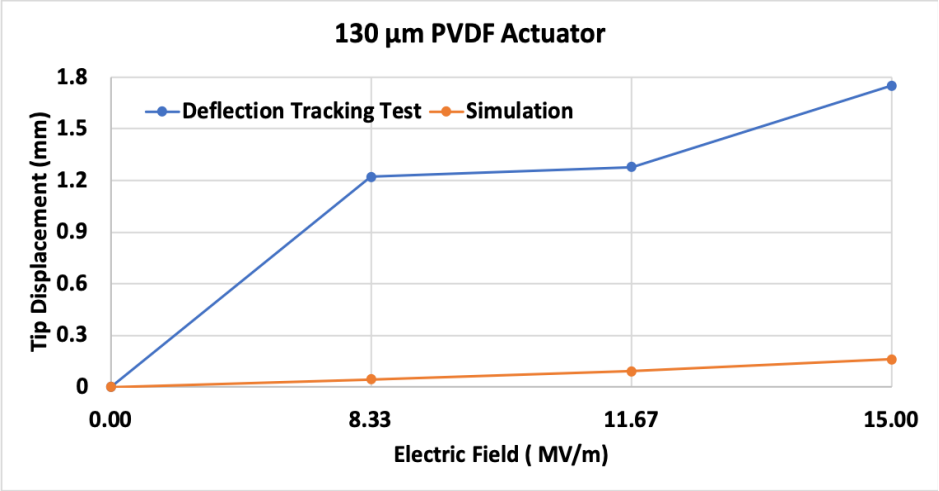

(c)

Figure 5.6: Comparison plot between the simulation and deflection tracking results. a) 60 μm. b) 60 μm Half Width. c) 130 μm.

The discrepancies between the simulation values and the values obtained with the deflection tracking test are justified by the limitations of reproducing accurately the simulation. The simplification of the electrodes' connection, the absence of the environmental conditions such as temperature and pressure, and the assuming a linear material in the actuator, therefore not accounting for the viscoelasticity and electrostrictive properties of the material.

Moreover, in the 130 μm simulation, the results are signicantly lower than in the deflection tracking test. A possible reason for this, can be due to the electrostriction effect that increases its contribution, however this will be analysed in future works.

Nevertheless, the general behavior of the actuators is coherent in both the experiment and the simulation, increasing the displacement with an increase in the applied electric field.

From Figure 5.7, it is possible to see that the values of maximum displacement of each simulation, fit a polynomial trending line. The fitting resembles the Maxwell Stress equation (2.2), meaning the simulation is correct.

Therefore, it is possible to validate the simulation built in COMSOL Multiphysics® for the electromechanical characterization of the PVDF-based electroactive actuator.

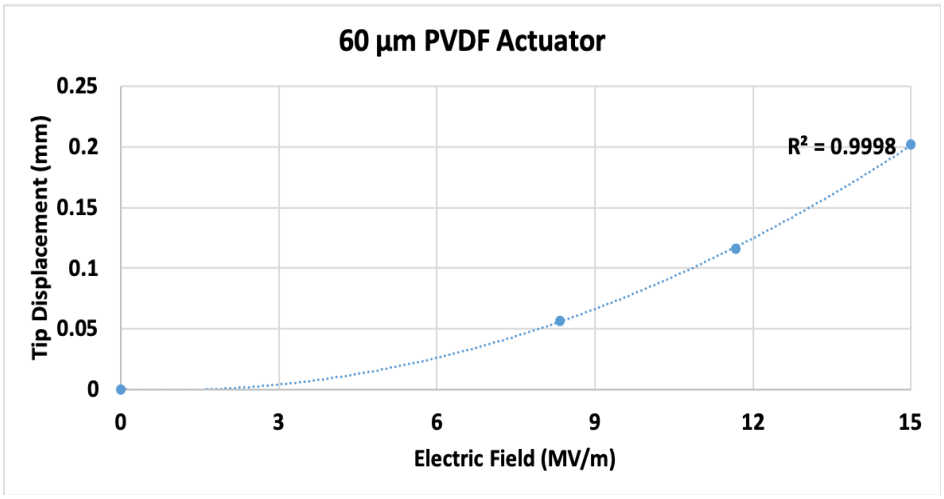

(a)

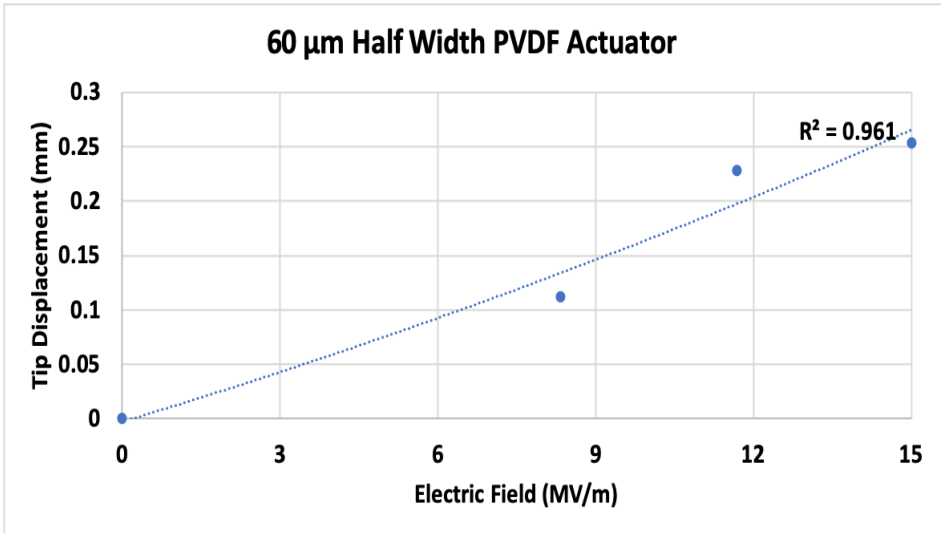

(b)

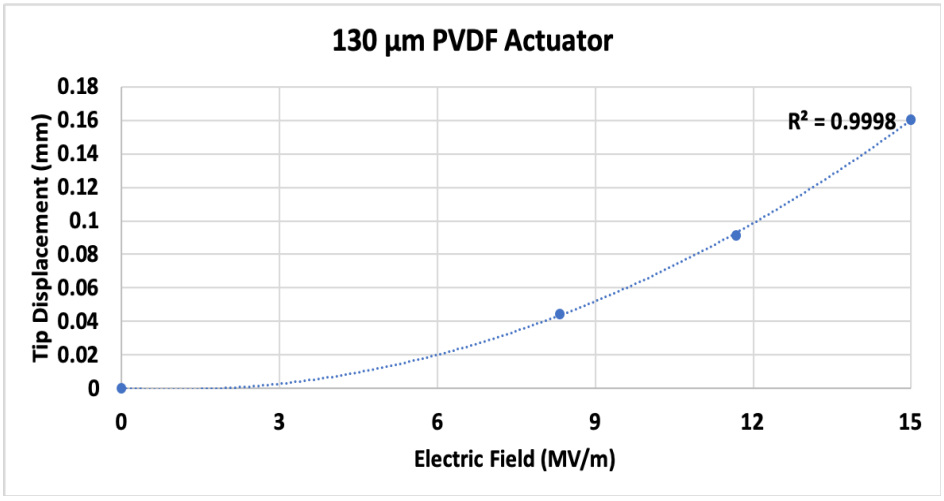

(c)

Figure 5.7: Polynomial fitting of the maximum displacement results of the simulations. a) 60 μm. b) 60 μm Half Width. c) 130 μm.

6 Conclusions and Future Challenges

In this chapter, the author intends to focus on the conclusions that can be drawn from the analysis that has taken place in Chapter 4 and Chapter 5.

Three actuator samples were designed to evaluate the influence of the width and thickness of the active material's layer, in the overall performance. Moreover, a virtual model was built in COMSOL Multiphysics® to develop a more efficient approach when evaluating the behavior of a multilayered unimorph actuator. The values of Blocking Force, Displacement and Bending Stiffness obtained for the 3 actuators are summarized in Table 6.1.

Table 6.1: Displacement, Blocking Force and Bending Stiffness values of the 3 actuators.

Actuator	**Displacement (mm)**	**Blocking Force (N)**	**Bending Stiffness (N/mm)**
60PVDF	0.676 - 0.738	9.07E-4 - 9.17E-4	4.70E-4 - 1.16E-3
60PVDFHalf	0.461 - 0.727	8.35E-4 - 9.22E-4	2.80E-4 - 6.20E-4
130PVDF	1.22 - 1.75	5.26E-3 - 7.98E-3	6.00E-4 - 4.92E-3

When it comes to actuators, what is defined by better performance depends on the function it is supposed to tackle on. Consequently, this function is closely related to the application and what is the priority: force, tip deflection, the range of values for the electric field, among other parameters.

Focusing on force and displacement, which are usually the leading characteristics when evaluating the performance of an actuator, it is evident that the ones that can produce greater forces and/or displacements will encounter a wider range of applicability (Figure 6.1).

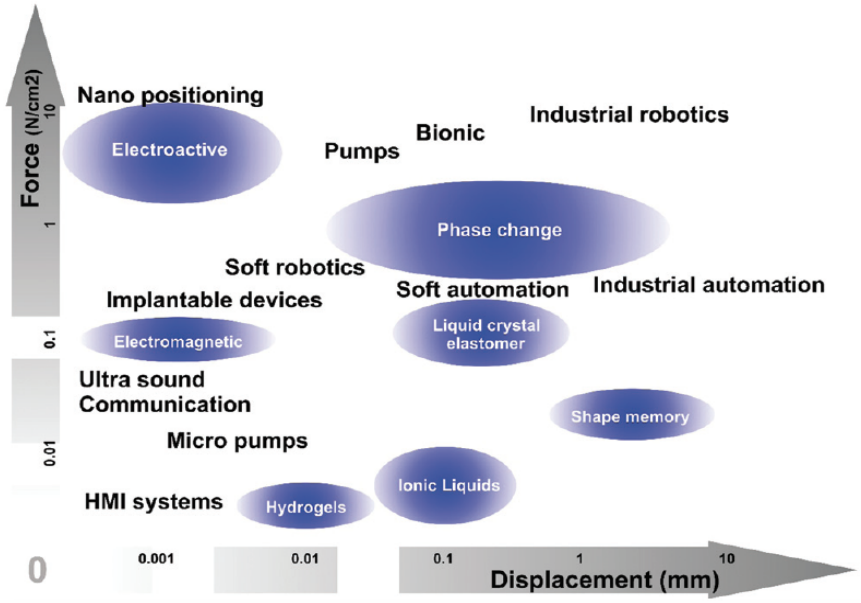

Figure 6.1: Graphical distribution of actuator types (blue circles) considering force in function of displacement and the relation with application areas. Retrieved from: (12).

It is possible to position the actuators studied in Figure 6.1, calculating the Force (N/cm^2) from the Blocking Force values and knowing the 60PVDF and 130PVDF actuator's area is 9.3 cm^2 and 4.96 cm^2 for the 60PVDFHalf. Figure 6.2 shows how they position themselves in comparison with other actuation technologies.

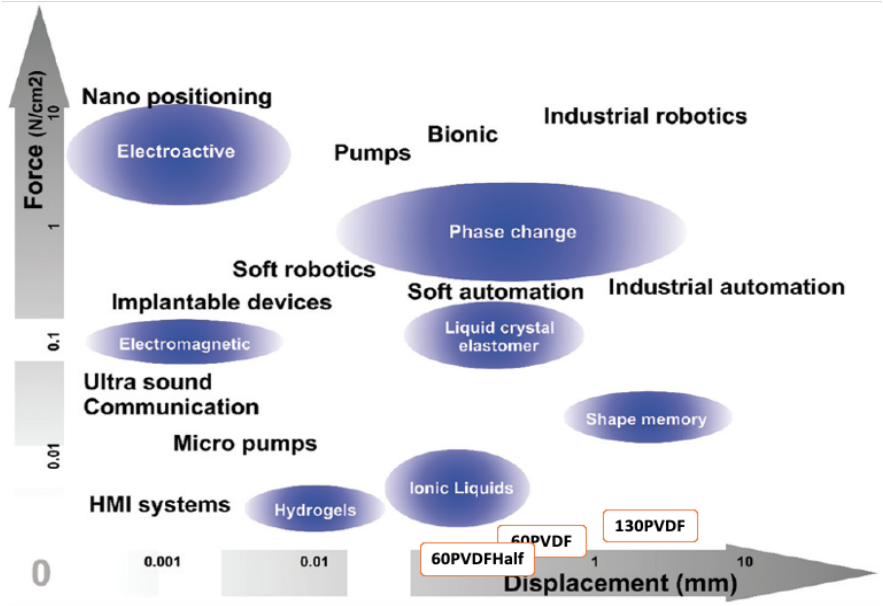

Figure 6.2: Positioning of the 3 actuators. Adapted from: (12).

Comparing, specifically with other electroactive technologies, **the range of displacements obtained with these actuators are significantly higher.** However, they fall short when the issue is **Force, revealing values, at least, 3 orders of magnitude lower** than the existing electroactive technologies presented in the graphic.

All in all, the results conclude that:

1. **Increasing the thickness of the active material's layer, the actuator produces more force.** This happens because the active material within the actuator is the one responsible for producing force when under an applied voltage, while the remaining layers are denominated passive layers for their support role, and the electrodes are required to apply the electric field. While from this test, it is not possible to infer on the evolution of the displacement/tip deflection of the actuator, from equation (12) in Chapter 3, it is natural to presume that a higher force produced, consequently results in a higher tip deflection. However, *Tiwari et al.* (58) state that a decrease of thickness is accompanied by an increase in the tip deflection. Therefore, the author believes that there is an optimal point of thickness of active material that maximizes the force, and subsequently the tip deflection, for the reasons explained in section 4.1.

2. **The width of the actuator does not play a major influence in the overall performance of the actuator.** The differences in performance observed between the 60PVDF sample and the 60PVDFHalf are minimal compared to the magnitude of the values, which deems them neglectable, although the tendency is observed as a decrease in force and deflection when the width decreases.

3. **An increase in the applied electric field is followed by a greater deflection of the tip of the actuator.** As explained before, any mechanical reaction of the actuator is caused by the electrical stimulation, and since the actuator possesses two passive layers of different Young's Modulus, this mechanical reaction translates into a bending. Therefore, a higher electric field applied caused a greater bending, and consequently a greater tip deflection.

4. **A higher blocking force value is achieved with greater thickness of the active material present in the actuator.** From this set of tests, it was

concluded there were no significant differences in the 60PVDF and 60PVDFHalf samples, neither concerning the electric field applied, neither between them, seen has the blocking force values of these two samples vary only a few hundredths with an increase of the electric field, and also all the six values are within a 0.90E-04 N range difference of each other. Nonetheless, the 130PVDF sample exhibited blocking force values of an order of magnitude greater than the 60 μm samples. Furthermore, while this was not noted in the other samples, the increase of electric field actually induced a higher blocking force value, exhibiting a step of, at least, 1.00E-03 N.

5. **The simulation built is valid for multilayered unimorph actuators**. Hence, confirming the linear relationship between the displacement value and the electric field applied, therefore it can be used as a pre-assessment of the geometry's performance.

In a concluding note, these results also confirm and support the tunability and versatility of polymer actuators in easily changing their specifics. With this in mind, some future challenges arise. In order to refine this study, other parameters can be changed:

1. Experiment with different passive layers to widen the Young's Modulus' gap and, consequently, the displacement;

2. Focus on the electrode's material, study its influence and evaluate alternatives, such as sputtered-gold layers;

3. Experiment with a sample of a thickness of the PVDF layer over 130 μm to validate the theory of an optimal (force, displacement) point;

4. Optimization of the simulation model: perfect the geometry to better mimic the actuator and the connection with the electrodes. In the simulation it was assumed a linear elastic material for the layers, however, accounting for the viscoelasticity and electrostriction of the material should improve accuracy;

5. Dynamic study with the simulation model: only a static study was conducted and a dynamic approach can give valuable information on the evolution of the actuator's behavior.

Actuator-based technology still has a long way to overcome to match nature, and although a lot of progress has been made, as the literature shows, research has only scratched the surface on the potential of EAP actuators. In 20 years the evolution is remarkable, one can only hope and dream of what another 20 years will accomplish.

References

[1] S. Ashley, "Artificial Muscles," *Scientific American*, vol. 289, no. 4, pp. 52–59, 2003.

[2] Y. Bar-Cohen and C. Breazeal, *Biologically Inspired Intelligent Robots*. SPIE PRESS, 2003.

[3] C. Lee, M. Kim, Y. J. Kim, N. Hong, S. Ryu, H. J. Kim, and S. Kim, "Soft robot review," *International Journal of Control, Automation and Systems*, vol. 15, pp. 3–15, feb 2017.

[4] L. N. Awad, J. Bae, K. O'donnell, S. M. De Rossi, K. Hendron, L. H. Sloot, P. Kudzia, S. Allen, K. G. Holt, T. D. Ellis, *et al.*, "A soft robotic exosuit improves walking in patients after stroke," *Science translational medicine*, vol. 9, no. 400, 2017.

[5] N. Vitiello, S. Mohammed, and J. C. Moreno, "Guest editorial wearable robotics for motion assistance and rehabilitation," *IEEE Transactions on Neural Systems and Rehabilitation Engineering*, vol. 25, no. 2, pp. 103–106, 2017.

[6] Y. Bar-Cohen, "Electroactive polymers as artificial muscles," in *Compliant Structures in Nature and Engineering*, no. March, pp. 69–81, WIT Press, sep 2005.

[7] J. Madden, N. Vandesteeg, P. Anquetil, P. Madden, A. Takshi, R. Pytel, S. Lafontaine, P. Wieringa, and I. Hunter, "Artificial Muscle Technology: Physical Principles and Naval Prospects," *IEEE Journal of Oceanic Engineering*, vol. 29, pp. 706–728, jul 2004.

[8] K. Meijer, M. S. Rosenthal, and R. J. Full, "Muscle-like actuators? A comparison between three electroactive polymers," in *Smart Structures and Materials 2001:*

Electroactive Polymer Actuators and Devices (Y. Bar-Cohen, ed.), vol. 4329, p. 7, SPIE, jul 2001.

[9] tech. rep.

[10] Y. Bar-Cohen and I. A. Anderson, "Electroactive polymer (EAP) actuators—background review," *Mechanics of Soft Materials*, vol. 1, no. 1, p. 5, 2019.

[11] C. P. Chou and B. Hannaford, "Measurement and modeling of McKibben pneumatic artificial muscles," *IEEE Transactions on Robotics and Automation*, vol. 12, no. 1, pp. 90–102, 1996.

[12] P. Martins, D. Correia, V. Correia, and S. Lanceros-Mendez, "Polymer-based actuators: back to the future," *Physical Chemistry Chemical Physics*, vol. 22, no. 27, pp. 15163–15182, 2020.

[13] Y. Bar-cohen and J. P. L. Caltech, "Nanotechnology Using Electroactive Polymers as Artificial Muscles," *Jet Propulsion*, vol. 3, no. June, pp. 45–46, 2001.

[14] L. Hines, K. Petersen, G. Z. Lum, and M. Sitti, "Soft Actuators for Small-Scale Robotics," apr 2017.

[15] W. C. Röentgen, "Ueber die durch Electricität bewirkten Form- und Volumenänderungen von dielectrischen Körpern," *Annalen der Physik und Chemie*, vol. 247, pp. 771–786, jan 1880.

[16] M. Eguchi, "XX. On the permanent electret," *The London, Edinburgh, and Dublin Philosophical Magazine and Journal of Science*, vol. 49, pp. 178–192, jan 1925.

[17] H. Kawai, "The Piezoelectricity of Poly (vinylidene Fluoride)," *Japanese Journal of Applied Physics*, vol. 8, pp. 975–976, jul 1969.

[18] E. Fukada, "Piezoelectricity of Wood," *Journal of the Physical Society of Japan*, vol. 10, pp. 149–154, feb 1955.

[19] R. G. Kepler and R. A. Anderson, "Piezoelectricity and pyroelectricity in polyvinylidene fluoride," *Journal of Applied Physics*, vol. 49, pp. 4490–4494, aug 1978.

[20] Y. Wada and R. Hayakawa, "Piezoelectricity and Pyroelectricity of Polymers," *Japanese Journal of Applied Physics*, vol. 15, pp. 2041–2057, nov 1976.

[21] R. Baughman, "Conducting polymer artificial muscles," *Synthetic Metals*, vol. 78, pp. 339–353, apr 1996.

[22] A. J. Lovinger, "Ferroelectric Polymers," *Science*, vol. 220, pp. 1115–1121, jun 1983.

[23] R. H. Baughman, "Carbon Nanotube Actuators," *Science*, vol. 284, pp. 1340–1344, may 1999.

[24] R. Pelrine, "High-Speed Electrically Actuated Elastomers with Strain Greater Than 100%," *Science*, vol. 287, pp. 836–839, feb 2000.

[25] Y. Bar-Cohen, S. Sherrit, and S.-S. Lih, "Characterization of the Electromechanical Properties of EAP materials," tech. rep., 2001.

[26] Y. Bar-Cohen, "Electroactive polymers as artificial muscles - Reality and challenges," in *19th AIAA Applied Aerodynamics Conference*, American Institute of Aeronautics and Astronautics Inc., 2001.

[27] R. D. Kornbluh, R. Pelrine, H. Prahlad, and R. Heydt, "Electroactive polymers: an emerging technology for MEMS," in *MEMS/MOEMS Components and Their Applications* (S. W. Janson and A. K. Henning, eds.), vol. 5344, p. 13, SPIE, jan 2004.

[28] Y. Bar-Cohen, "Transition of EAP material from novelty to practical applications: are we there yet?," in *Smart Structures and Materials 2001: Electroactive Polymer Actuators and Devices*, vol. 4329, p. 1, 2001.

[29] Y. Bar-Cohen, "Biomimetic actuators using electroactive polymers (eap) as artificial muscles," 2006.

[30] V. Bharti, Y. Ye, T.-B. Xu, and Q. M. Zhang, "Correlation Between Large Electrostrictive Strain and Relaxor Behavior with Structural Changes Induced in P(VDF-TrFE) Copolymer by Electron Irradiation," *MRS Proceedings*, vol. 541, p. 653, feb 1998.

[31] Z. Y. Cheng, V. Bharti, T. B. Xu, H. Xu, T. Mai, and Q. M. Zhang, "Electrostrictive poly(vinylidene fluoride-trifluoroethylene) copolymers," *Sensors and Actuators, A: Physical*, vol. 90, no. 1-2, pp. 138–147, 2001.

[32] S. Zhang, C. Huang, R. J. Klein, F. Xia, Q. M. Zhang, and Z.-Y. Cheng, "High Performance Electroactive Polymers and Nano-composites for Artificial Muscles," *Journal of Intelligent Material Systems and Structures*, vol. 18, pp. 133–145, feb 2007.

[33] K. Uchino, *Advanced piezoelectric materials*. Woodhead Publishing Limited, 2010.

[34] F. Bauer, E. Fousson, and Q. M. Zhang, "Recent advances in highly electrostrictive P(VDF-TrFE-CFE) terpolymers," *IEEE Transactions on Dielectrics and Electrical Insulation*, vol. 13, no. 5, pp. 1149–1153, 2006.

[35] F. Bauer, "Review on the properties of the ferrorelaxor polymers and some new recent developments," *Applied Physics A*, vol. 107, pp. 567–573, jun 2012.

[36] R. M. Habibur, U. Yaqoob, S. Muhammad, A. I. Uddin, and H. C. Kim, "The effect of rgo on dielectric and energy harvesting properties of p (vdf-trfe) matrix by optimizing electroactive β phase without traditional polling process," *Materials Chemistry and Physics*, vol. 215, pp. 46–55, 2018.

[37] R. Kornbluh, R. Pelrine, J. Eckerle, and J. Joseph, "Electrostrictive polymer artificial muscle actuators," in *Proceedings. 1998 IEEE international conference on robotics and automation (Cat. No. 98CH36146)*, vol. 3, pp. 2147–2154, IEEE, 1998.

[38] F. Carpi and E. Smela, *Biomedical Applications of Electroactive Polymer Actuators*. 2009.

[39] D. Damjanovic and R. Newnham, "Electrostrictive and Piezoelectric Materials for Actuator Applications," *Journal of Intelligent Material Systems and Structures*, vol. 3, pp. 190–208, apr 1992.

[40] B. Qiao, X. Wang, S. Tan, W. Zhu, and Z. Zhang, "Synergistic effects of maxwell stress and electrostriction in electromechanical properties of poly (vinylidene

fluoride)-based ferroelectric polymers," *Macromolecules*, vol. 52, no. 22, pp. 9000–9011, 2019.

[41] J. Shintake, V. Cacucciolo, D. Floreano, and H. Shea, "Soft Robotic Grippers," jul 2018.

[42] M. I. Frecker and W. M. Aguilera, "Analytical modeling of a segmented unimorph actuator using electrostrictive P(VDF-TrFE) copolymer," *Smart Materials and Structures*, vol. 13, pp. 82–91, feb 2004.

[43] S. Zarif Mansour, R. J. Seethaler, Y. R. Teo, Y. K. Yong, and A. J. Fleming, "Piezoelectric bimorph actuator with integrated strain sensing electrodes," *IEEE Sensors Journal*, vol. 18, pp. 5812–5817, jul 2018.

[44] T. H. T. Fook, J. H. Jeon, and P. S. Lee, "Transparent Flexible Polymer Actuator with Enhanced Output Force Enabled by Conductive Nanowires Interlayer," *Advanced Materials Technologies*, vol. 5, p. 1900762, jan 2020.

[45] F. Bauer, J. F. Capsal, Q. Larcher, and F. D. Dos Santos, "Advances in relaxor ferroelectric terpolymer: New applications," in *2011 International Symposium on Applications of Ferroelectrics (ISAF/PFM) and 2011 International Symposium on Piezoresponse Force Microscopy and Nanoscale Phenomena in Polar Materials*, pp. 1–4, IEEE, jul 2011.

[46] F. Xia, S. Tadigadapa, and Q. Zhang, "Electroactive polymer based microfluidic pump," *Sensors and Actuators A: Physical*, vol. 125, pp. 346–352, jan 2006.

[47] S. Ahmed, Z. Ounaies, and E. A. F. Arrojado, "Electric field-induced bending and folding of polymer sheets," *Sensors and Actuators A: Physical*, vol. 260, pp. 68–80, 2017.

[48] P. Poncet, F. Casset, A. Latour, F. Domingues Dos Santos, S. Pawlak, R. Gwoziecki, A. Devos, P. Emery, and S. Fanget, "Static and dynamic studies of electro-active polymer actuators and integration in a demonstrator," in *Actuators*, vol. 6, p. 18, Multidisciplinary Digital Publishing Institute, 2017.

[49] S. K. Panda and D. Bandopadhya, "Bio-inspired underwater undulatory motion by using polypyrrole bimorph actuator," in *2019 IEEE International Conference on System, Computation, Automation and Networking (ICSCAN)*, pp. 1–6, 2019.

[50] P. Xiao, N. Yi, T. Zhang, Y. Huang, H. Chang, Y. Yang, Y. Zhou, and Y. Chen, "Construction of a fish-like robot based on high performance graphene/pvdf bimorph actuation materials," *Advanced Science*, vol. 3, no. 6, p. 1500438, 2016.

[51] L. Lou, H. Yu, M. T. X. Haw, S. Zhang, and Y. A. Gu, "Comparative characterization of bimorph and unimorph aln piezoelectric micro-machined ultrasonic transducers," in *2016 IEEE 29th International Conference on Micro Electro Mechanical Systems (MEMS)*, pp. 1090–1093, IEEE, 2016.

[52] X.-G. Guo, Z.-F. Zhou, C. Sun, W.-H. Li, and Q.-A. Huang, "A Simple Extraction Method of Young's Modulus for Multilayer Films in MEMS Applications," *Micromachines*, vol. 8, p. 201, jun 2017.

[53]

[54] J. Kim, J. W. Kim, H. C. Kim, L. Zhai, H.-U. Ko, and R. M. Muthoka, "Review of Soft Actuator Materials," *International Journal of Precision Engineering and Manufacturing*, vol. 20, pp. 2221–2241, dec 2019.

[55] "Tensile test." `www.instron.us/tensiletest`.

[56] D. Yalcin, ""how different specimen geometries affect tensilte test results?"." `https://www.researchgate.net/publication/319773789_How_do_different_specimen_geometries_affect_tensile_test_results`. Accessed: 2020-08-20.

[57] Cheng Huang, R. Klein, Feng Xia, Hengfeng Li, Q. Zhang, F. Bauer, and Z.-Y. Cheng, "Poly(vinylidene fluoride-trifluoroethylene) based high performance electroactive polymers," *IEEE Transactions on Dielectrics and Electrical Insulation*, vol. 11, pp. 299–311, apr 2004.

[58] V. Tiwari, R. Sharma, G. Srivastava, and R. Dwivedi, "Optimizing the design of polymer based unimorph actuator using comsol multiphysics," in *Proceedings of the 2012 COMSOL Conference in Banglore*, no. 1-5, 2012.

A Appendix I

A.1. Graphics of the results for the Deflection Tracking Tests

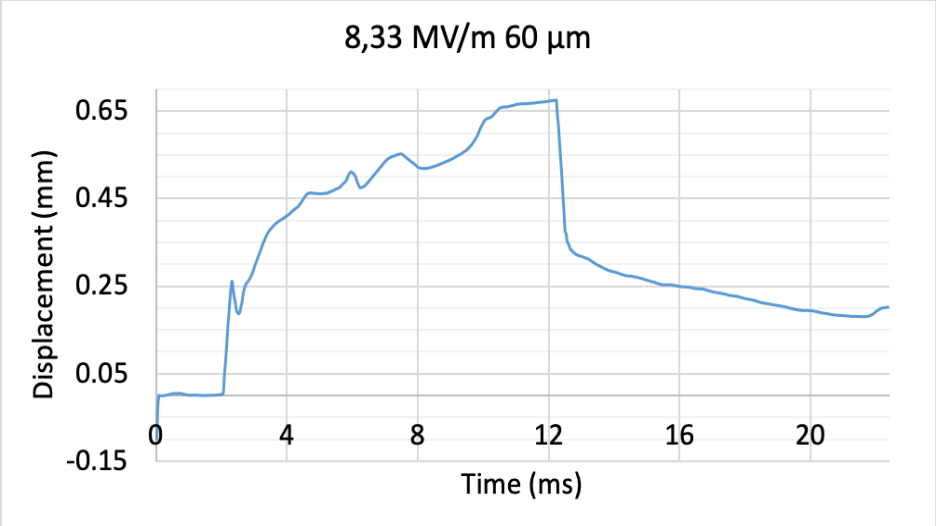

Deflection Tracking test for 60PVDF sample under 8.33 MV/m.

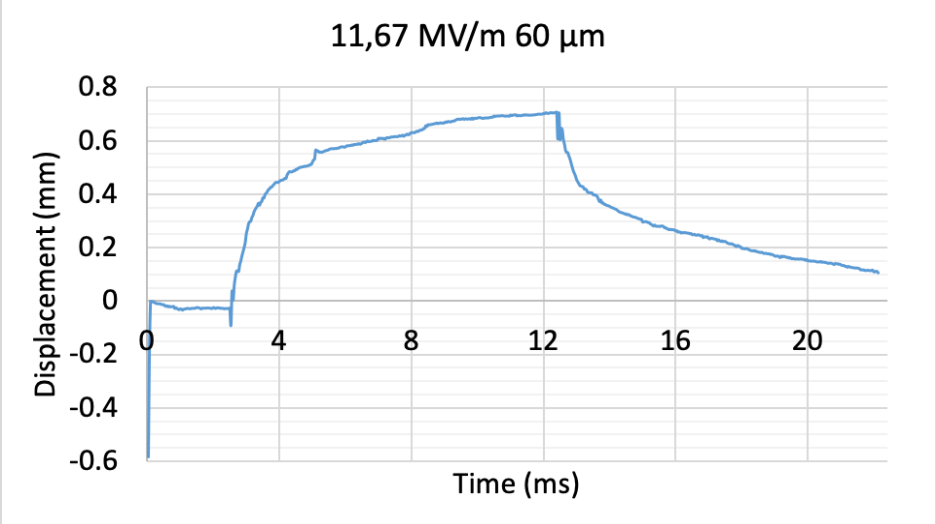

Deflection Tracking test for 60PVDF sample under 11.67 MV/m.

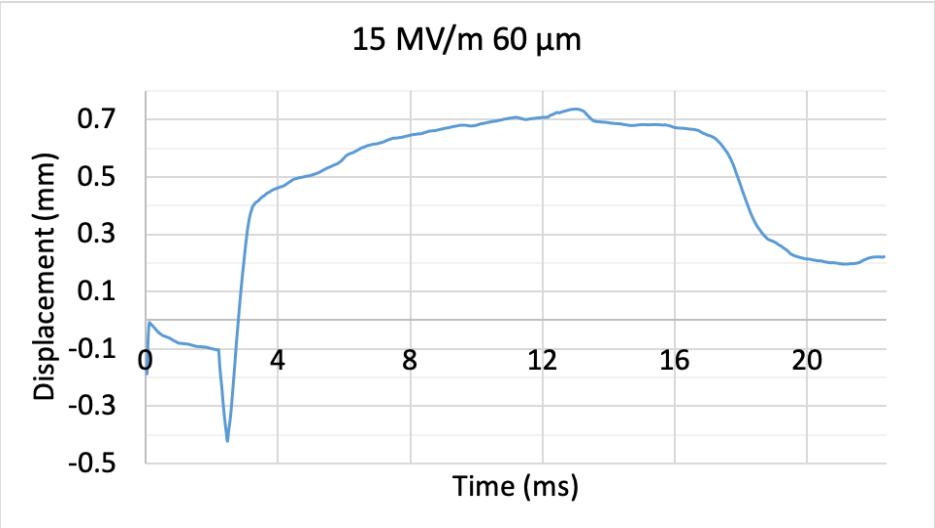

Deflection Tracking test for 60PVDF sample under 15 MV/m.

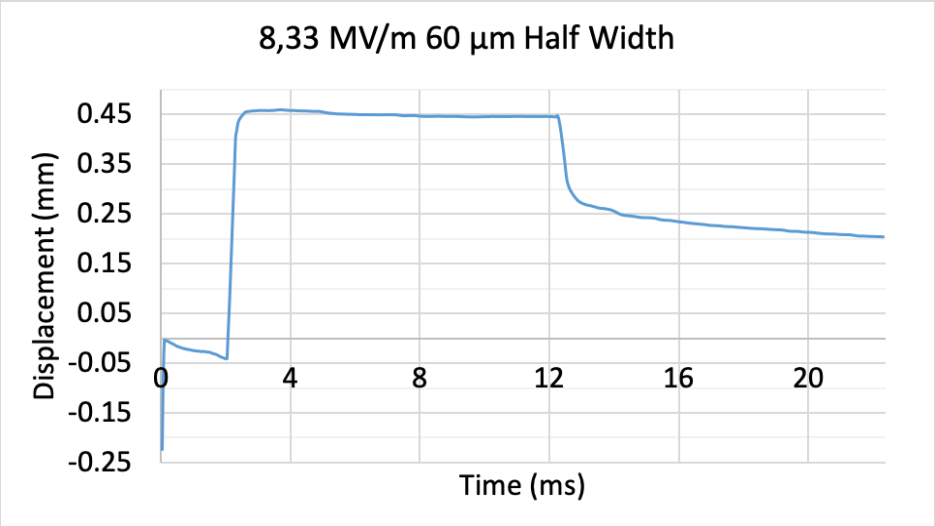

Deflection Tracking test for 60PVDFHalf sample under 8.33 MV/m.

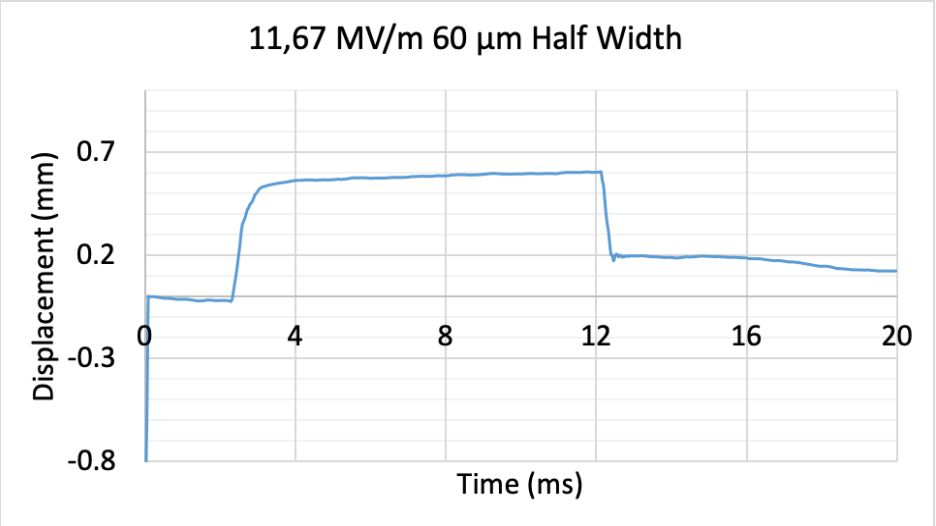

Deflection Tracking test for 60PVDFHalf sample under 11.67 MV/m.

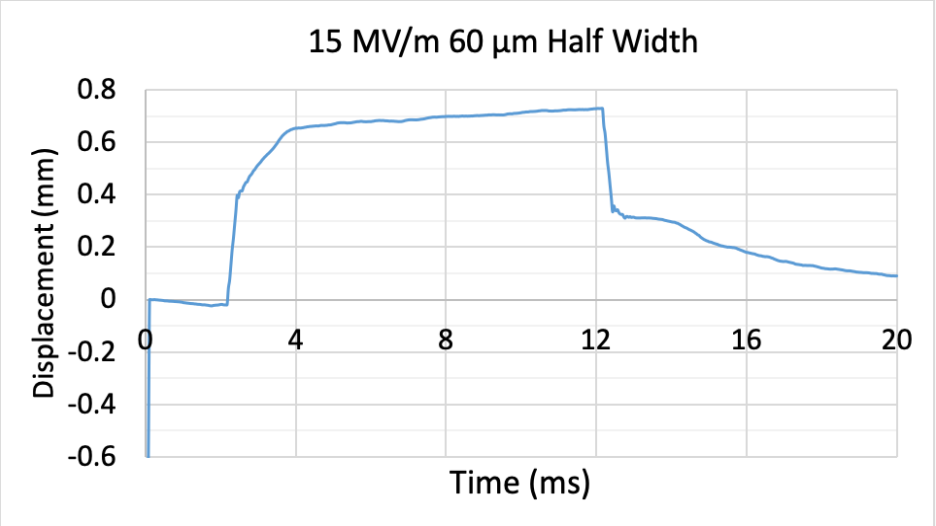

Deflection Tracking test for 60PVDFHalf sample under 15 MV/m.

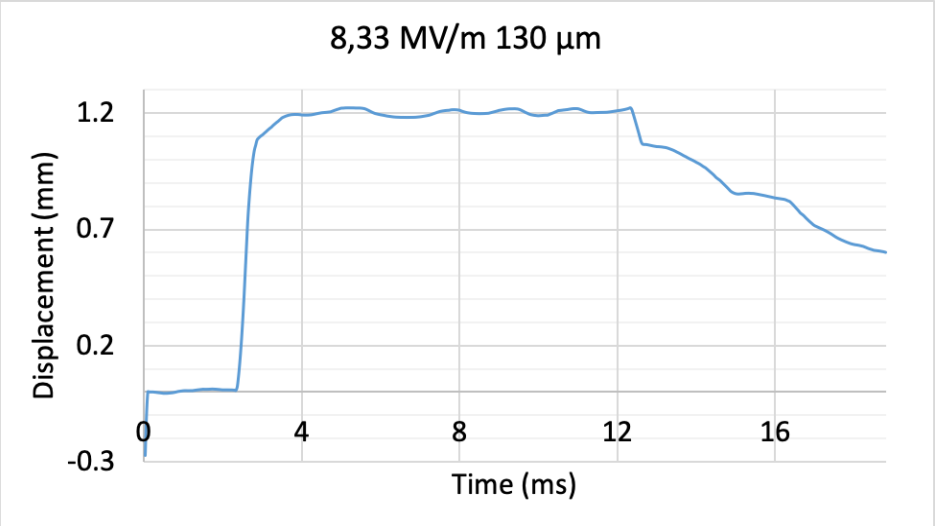

Deflection Tracking test for 130PVDF sample under 8.33 MV/m.

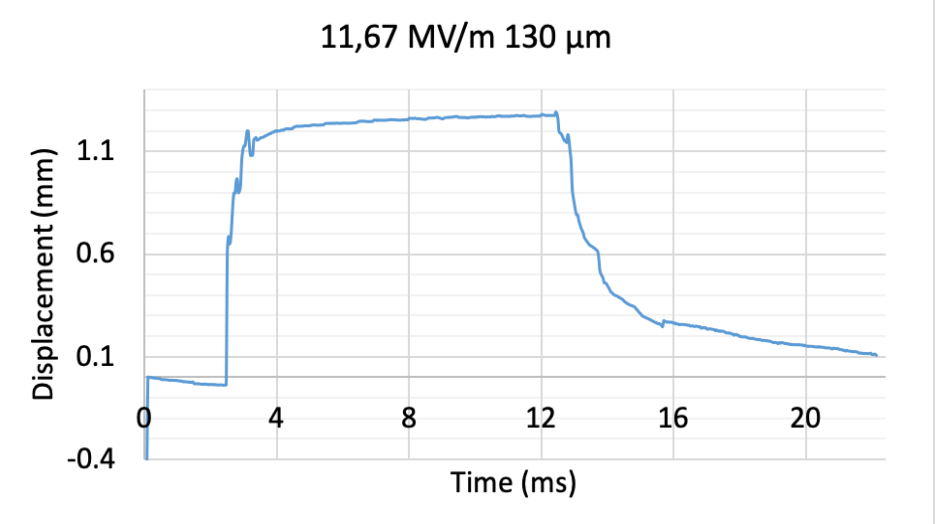

Deflection Tracking test for 130PVDF sample under 11.67 MV/m.

A.2. Graphics of the results for the Blocking Force Tests

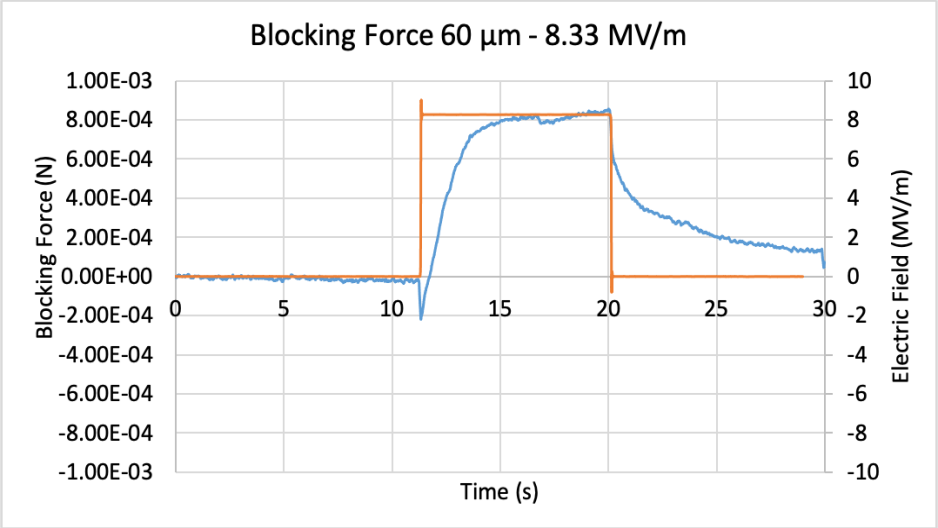

Single Blocking Force test for 60PVDF sample under 8.33 MV/m.

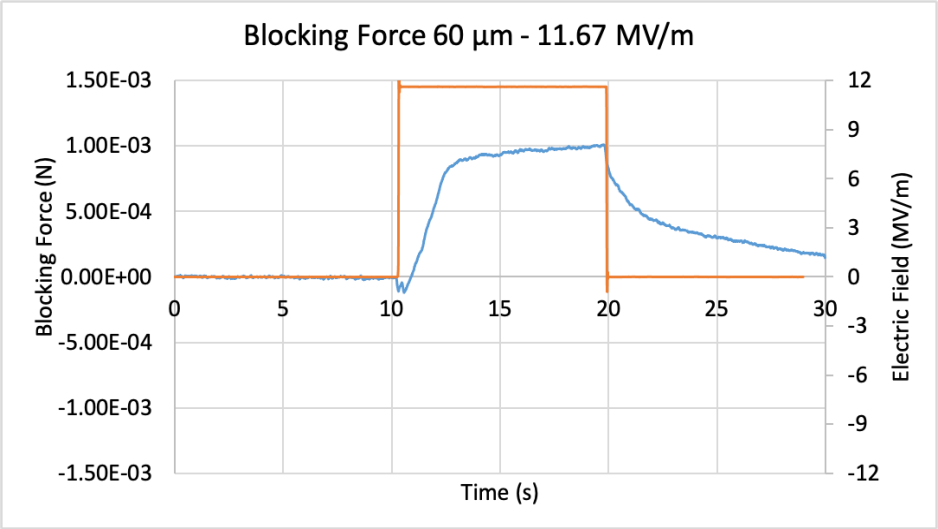

Single Blocking Force test for 60PVDF sample under 11.67 MV/m.

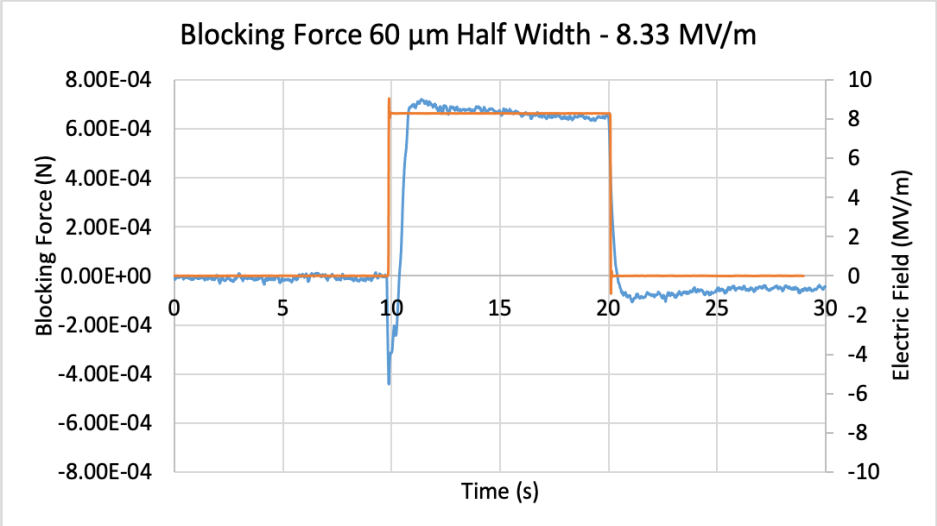

Single Blocking Force test for 60PVDFHalf sample under 8.33 MV/m.

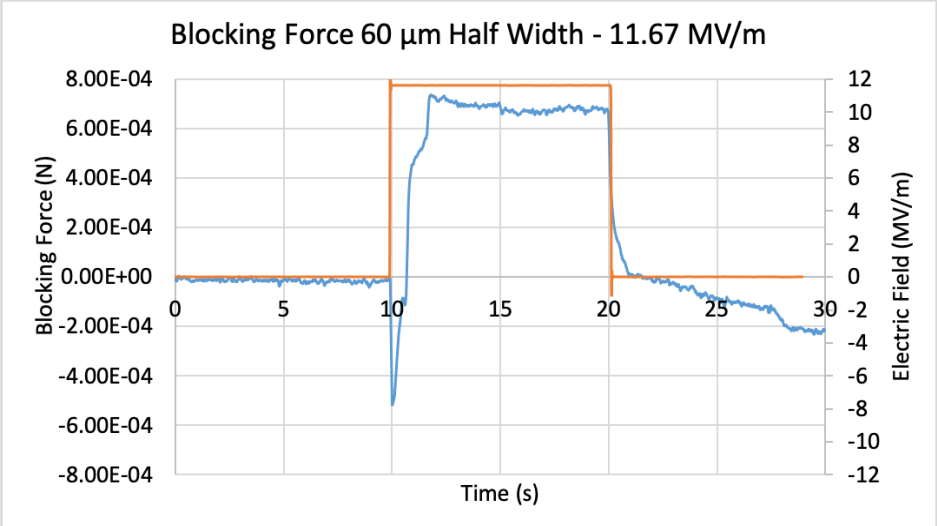

Single Blocking Force test for 60PVDFHalf sample under 11.67 MV/m.

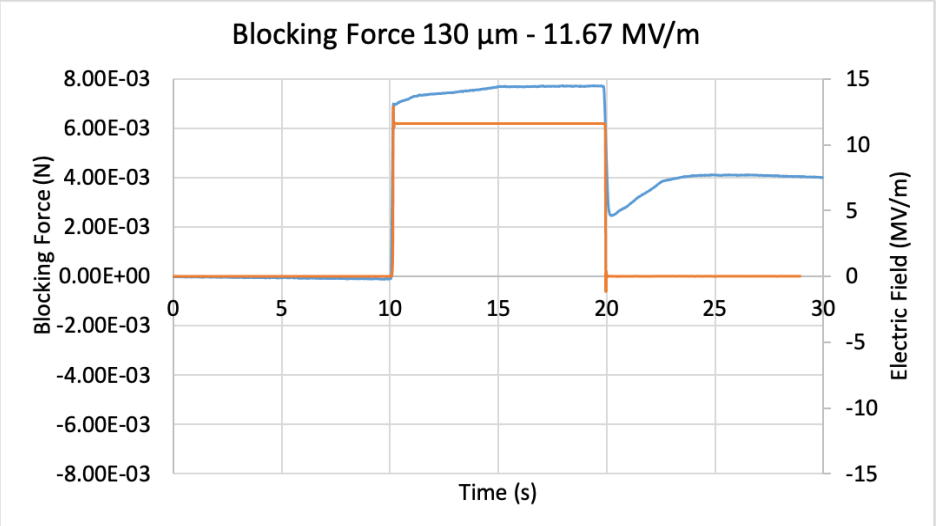

Single Blocking Force test for 130PVDF sample under 11.67 MV/m.

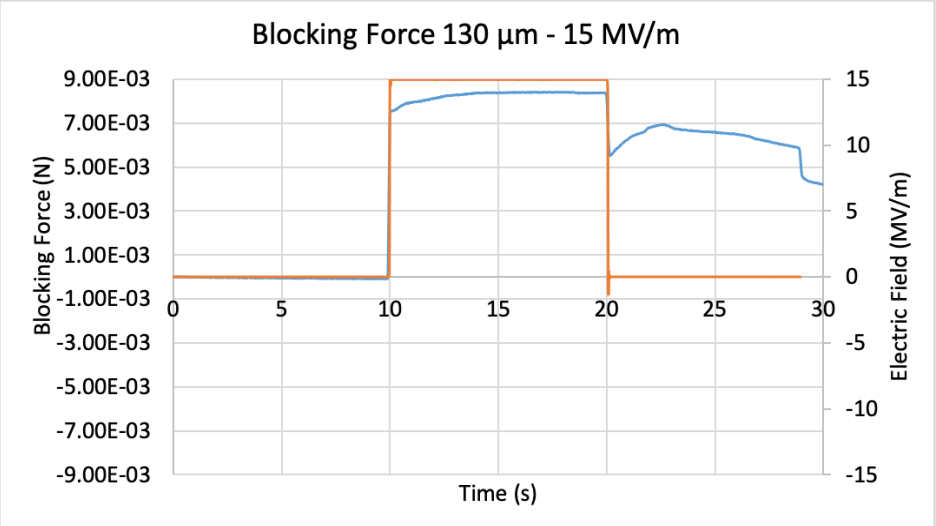

Single Blocking Force test for 130PVDF sample under 15 MV/m.

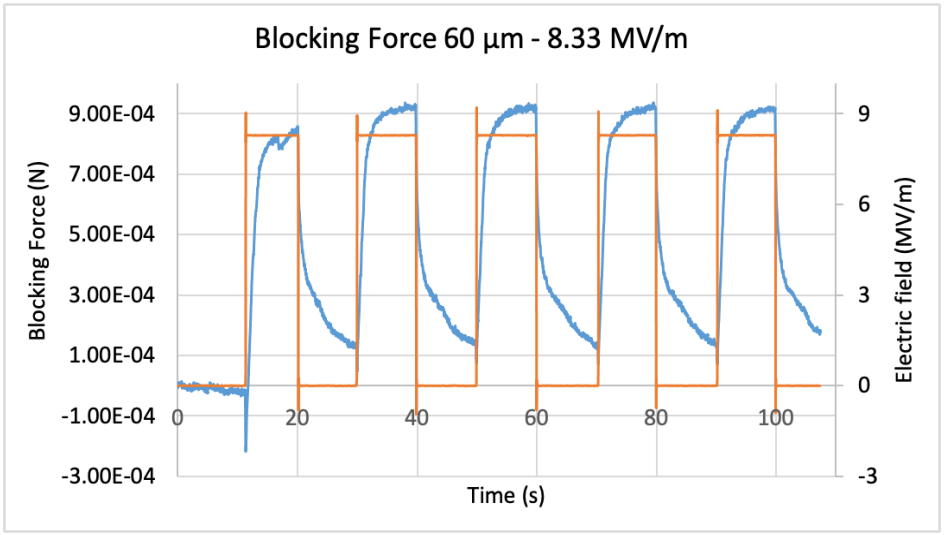

Repeated Blocking Force test for 60PVDF sample under 8.33 MV/m.

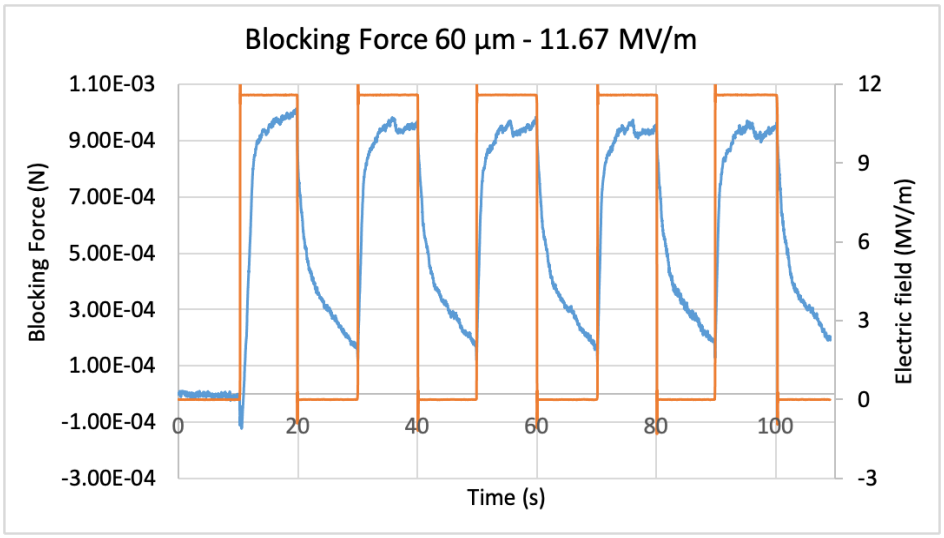

Repeated Blocking Force test for 60PVDF sample under 11.67 MV/m.

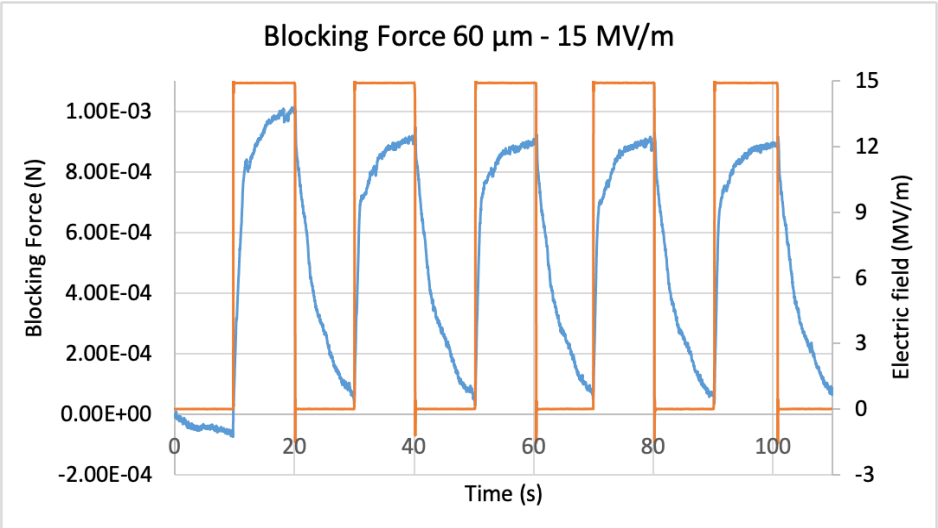

Repeated Blocking Force test for 60PVDF sample under 15 MV/m.

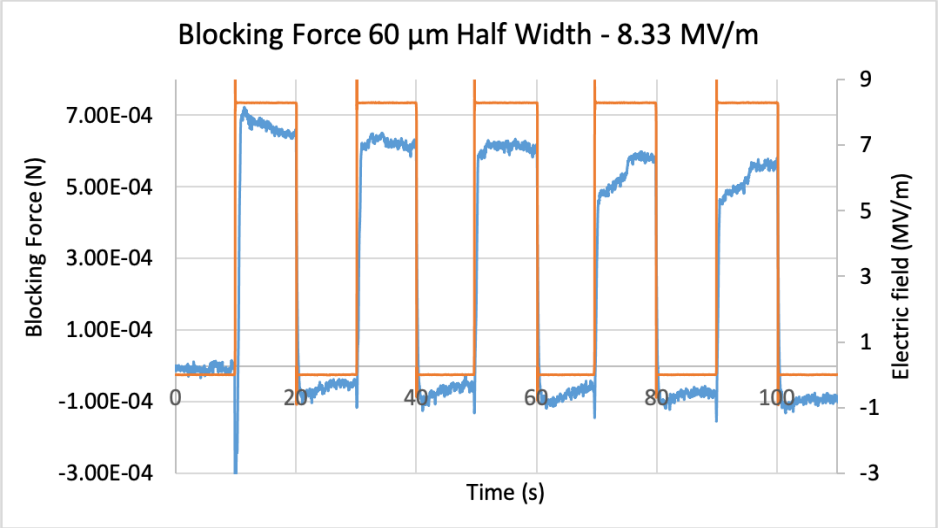

Repeated Blocking Force test for 60PVDFHalf sample under 8.33 MV/m.

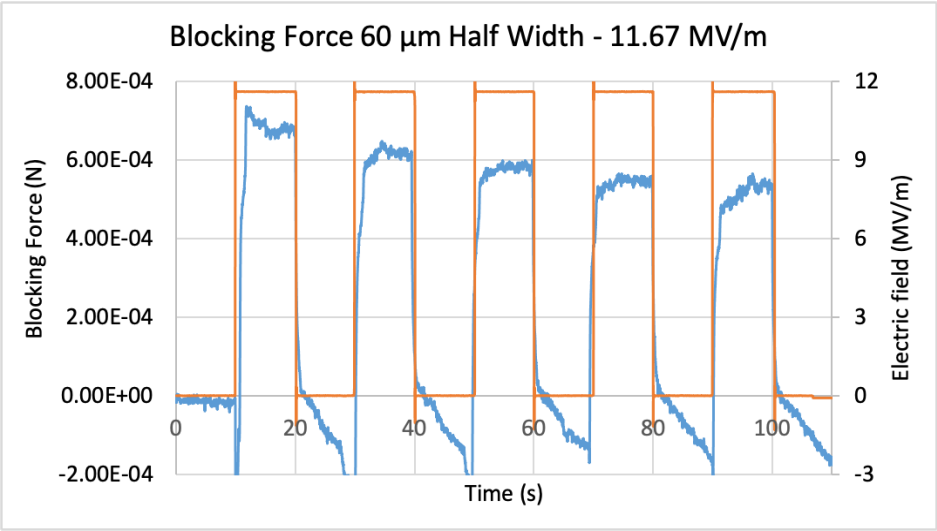

Repeated Blocking Force test for 60PVDFHalf sample under 11.67 MV/m.

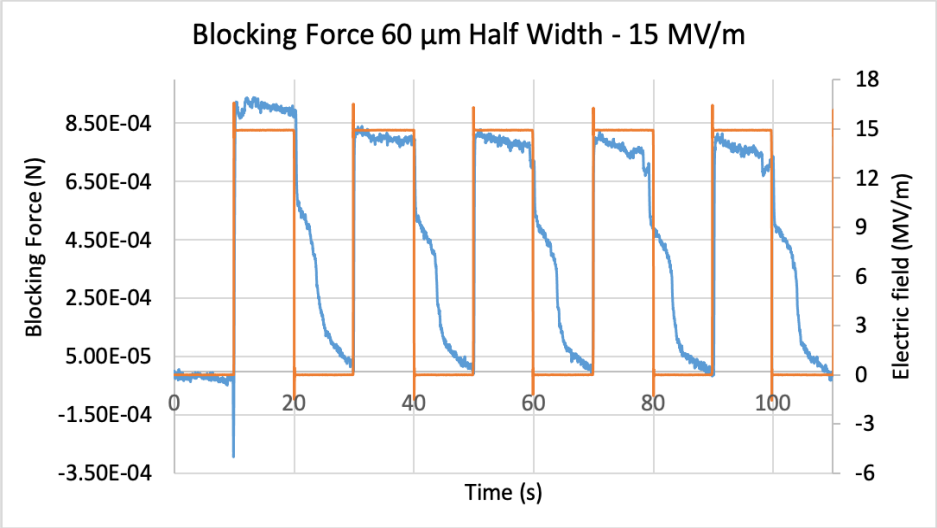

Repeated Blocking Force test for 60PVDFHalf sample under 15 MV/m.

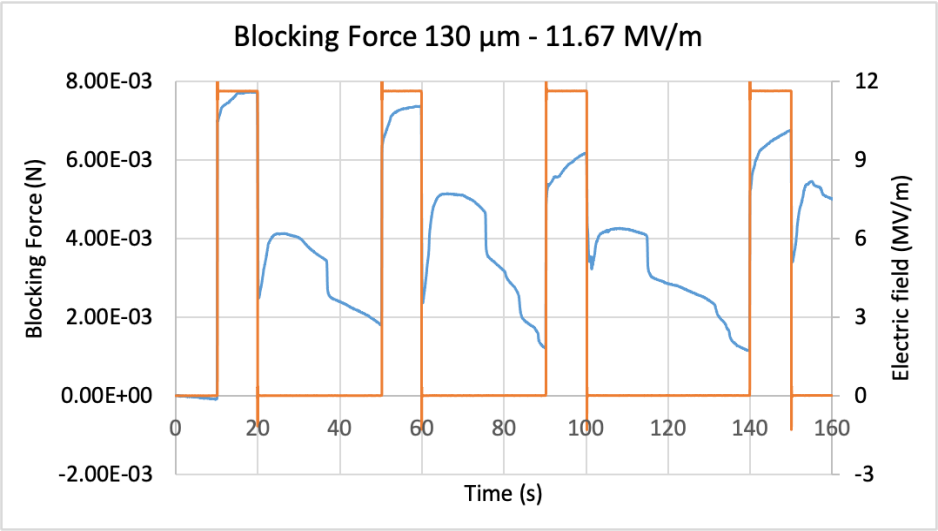

Repeated Blocking Force test for 130PVDF sample under 11.67 MV/m.

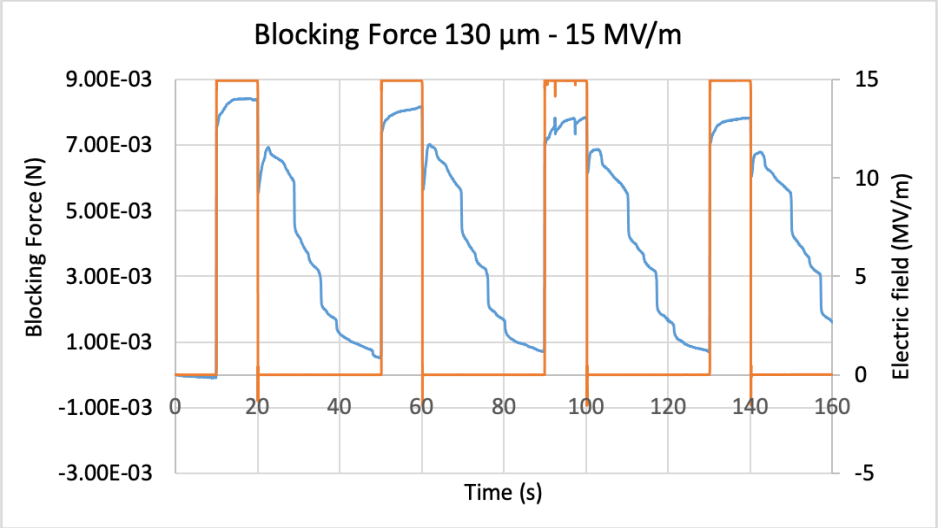

Repeated Blocking Force test for 130PVDF sample under 15 MV/m.